To the Graduate Council:

I am submitting herewith a dissertation written by Jia-Da Mo entitled "An Investigation on the Wake of a Cylinder with Rotational Oscillations." I have examined the final copy of this dissertation for form and content and recommend that it be accepted in partial fulfillment of the requirements for the degree of Doctor of Philosophy with a major in Aerospace Engineering.

J. M. Wu

J. M. Wu, Major Professor

We have read this dissertation
and recommend its acceptance:

A D. Vakili

R L Young

McReddy

Accepted for the Council:

Cew Minkel

Vice Provost
and Dean of the Graduate School

AN INVESTIGATION ON THE WAKE OF A CYLINDER WITH ROTATIONAL OSCILLATIONS

A Dissertation

Presented for the

Doctor of Philosophy

Degree

The University of Tennessee, Knoxville

Jia-Da Mo

May 1989

ACKNOWLEDGMENTS

The author gratefully acknowledges the help, encouragement and guidance he received over the years from Dr. J.M. Wu, supervisor and chairman of the doctoral committee. The author expresses his gratitude for the help and advice received from the other members of the committee, Drs. T.H. Moulden, K.C. Reddy, A.D. Vakili and R.L. Young.

Sincere thanks are also expressed to former Dean Harwell for providing him with an exchange student oportinuity, to the UTSI administration for their financial support and for permission to use the computer facilities and to the UTSI library personnel of their help towards finding numerous technical literature.

Thanks are extened to the author's son, his birth is a great encouragement for the final work.

Special thanks also goes to the author's wife for her constant support, encouragement and great sacrifices throughout this effort.

ABSTRACT

Analytical, numerical and experimental studies on a rotationally oscillating cylinder with or without a uniform flow have been performed. The analytical solutions were obtained for no on-coming stream. A Stokes layer and the curvature effect of the cylinder on the vorticity generation and diffusion were discussed. In the limit, the solution reduces to the classical oscillatory flat plat flow. For steady or oscillating cylinders in a uniform stream, the flow was numerically solved by taking the Navier-Stokes equation in the form of vorticity and stream function. Shedding of vorticies with or without external excitation of oscillation were discussed. Hydrodynamic forces were computed by integrating vorticity and its normal derivative over the cylinder surface. The results showed that forces acting on the cylinder strongly depend on the oscillation frequency and to a lesser degree with the amplitude. Flow visualization was conducted in a water tunnel for the above conditions. When the forcing frequency was near the natural vortex shedding frequency, the shed vortex in the wake became more organized which qualitatively agreed with the numerical prediction.

This study has proven that a rotational oscillation applied to a cylinder can significantly change the wake flow structure. A "resonant" flow state is reached when the forced frequency is that of the natural vortex shedding frequency. Both the unsteady lift and drag components reach their maximums when this resonance occur. The time averaged drag is also a maximum at such a state. Results indicated that no additional vorticity is created by the body but the vorticity distribution is altered due to the oscillation. The significant change to the wake flow and the mean values are attributed to the nonlinearity of convection in the wake flow.

TABLE OF CONTENTS

LIST OF FIGURES

LIST OF SYMBOLS

C_l, C_d	lift and drag coefficient
f_0, f_f, f_k	natural, forced and reduced frequency
I, J	computational grid numbers
$\vec{n}$	unit normal vector toward the body
p	static pressure
$q, \bar{q}$	complex velocity $(u - iv)$ and its conjugate
$r, \theta, \vec{r}$	physical cylindrical coordinate and its vector form
R_c	cylinder radius
Re	Reynolds number based on cylinder diameter
Rw	reduced Reynolds number
R, ϑ	location of stationary vortex pair
x, y	Cartisia coordinates
$\Delta\xi, \Delta\eta$	grid spacing in computational plane
S_t, S_f	natural and forced Strouhal number
$\vec{t}$	vector stress over body surface
$t, \Delta t$	time, time step
t_0	incipient time
t_s	flow separation time from starting
T	time when forced oscillation is applied
U, V	velocity components in computational plane
U_∞	free stream velocity
u_r, u_θ	radial and circumferential velocity component in physical plane
$\vec{v}$	local velocity vector
V_t	cylinder skin velocity

W	complex velocity potential function ($= \phi + i\psi$)
$z, \bar{z}$	complex plane coordinate ($= x + iy, or = re^{i\theta}$) and its conjugate
$z_1, \bar{z}_1$	stationary vortex position
λ	relaxation factor
Θ_A, Θ_k	oscillation amplitude and reduced amplitude
γ	circulation factor of potential stationary vortex
∂B_∞	outer boundary of computational domain
∂B	solid body boundary
β	grid size ratio=$\frac{\Delta\xi}{\Delta\eta}$
ζ	dimensionless vorticity
$\bar{\eta}$	Rayleigh variable
$\tilde{\eta}$	intermediate Rayleigh variable
ν	kinematic viscosity
$\vec{\tau}$	unit tangentant vector on the body
ξ, η	computational coordinates
ψ	streamfunction
$\bar{\psi}$	streamfunction in update iteration
$\vec{\sigma}$	vorticity flux
∇	nabla operator
	<u>Superscripts</u>
n	index for time step
k	index for iteration
	<u>Subscripts</u>
i, j	index for grid point
w	wall surface

CHAPTER I

INTRODUCTION

§1.1 Technical Background

Currently, several researchers are interested in studying the great potential of enhancing vortex lift by various unsteady excitations[1−11]. These excitations include mechanical means of wing or flap oscillations, periodic jet blowing or suction, acoustic, thermal excitation, and so on. A large body of work has been accumulated on this subject . It is worthwhile to emphasize that searching for super lift or control of shear flow by means of unsteady excitation lies in creating and controlling favorably generated vortices while avoiding and eliminating any unfavorable influences. Among many kinds of excitations, it is believed that probably the excitation by mechanical oscillation is most straightforward and effective[12−21].

The interaction between a moving body and the fluid includes the action of the body to the fluid and the reaction of the fluid on the body[22]. For conventional airfoils and wings, the underlying basic physical principles are established around inviscid flows. Hence the viscous flow effect is limited to the thin boundary layer and the subsequent narrow wake flow. Under the inviscid flow assumption, the periodic oscillation of flow to the first order does not contribute to the mean flow[23]. Nonlinearity is an intrinsic property of unsteady viscous flows, which is believed to be the key factor for producing the hysteresis effects in the flows. However man's understanding of them still remains shallow, and the field of unsteady and nonlinear aerodynamics is still in its infancy but has a potential of great practical applications in the future[24,25].

§1.2 Objectives of Present Work

As far as an unsteady pure shear interaction is concerned, the simplest and most direct boundary geometry is the flat plate. Historically, one of the very first unsteady viscous fluid mechanical problem was the Stokes oscillating plate, in which the Navier-Stokes equations were solved[26]. That problem illustrates the flow engendered by an oscillating boundary, in which an important flow phenomenon was found. That is, accompanying the unsteady motion of the flat plate, vorticity is constantly fed into the flowfield from the surface. Another problem is the sudden acceleration of a plate to a constant velocity in a quiescent fluid (or, a flat plate is suddenly placed in a uniform flow), in which an impulsive starting process is studied. As a solution to the above two classical problems, the latter indicates that the effect of plate motion diffuses slowly into the fluid at a rate proportional to the square root of the kinetic viscosity. However, for the former, the mathematical solution may be thought of as a damped viscous waves traveling away from the wall, but the physical process occurring is again viscous diffusion. The latter does not have a physical wave velocity, although one can trace, approximate, the depth of penetration of the diffusion effect as a function of time.

Although the above two problems show some important flow phenomena, they do not involve any body length scales. Furthermore, the large flow separation, which is one of the fundamental properties of unsteady viscous flow[27], is missing.

Practical flows, especially associated with flow separation and unsteadiness, are complicated. Consequently, in this work a simple geometry such as the circular cylinder is used to avoid the additional geometric-dependent complication. The cylinder problem requires minimum assumption, has only one characteristic length scale, and is free from geometrical singularities. Of course, the flow around a cylinder has obvious theoretical significance.

Flow around bodies have been manipulated through organized unsteady interactions by many authors. Under favorable flow condition, various features of viscous flows such as boundary layers, shear layers and transition may be controlled through selective periodic interactions. Often, perturbation with forcing frequencies equal to or in the neighborhood of natural characteristic frequencies are most effective. Therefore, successful interactions depend on the identification of the proper (length scale or) frequency and of a proper disturbance at the desired frequency.

The viscous flowfield around a cylinder is characterized by two length scales[28], one being associated to the properties of the boundary layer, and the other to the natural vortex shedding wavelength. These two length scales represent two frequencies which are relatively high for the former and low for the latter. We have limited this study to the low frequency interactions only.

The cylinder is a typical bluff body, and the flow around it contains separated and unsteady flows. Due to its symmetry, a simple shear interaction (which is produced by a circumferential rotary motion of the cylinder) can be separated from the more complicated motions. To our knowledge, from the existing literature survey, this is the first time this fundamental problem has been addressed.

§1.3 Outline of the Approaches

There is no doubt that the fully separated and unsteady flow is dominated by viscous effects. To understand the problem completely, solving the unsteady Navier-Stokes equations is a necessity. As it is well-known, due to the adherence condition, the action of a moving body on the fluid is factually a process of production of vorticity by the body. A direct solution of vorticity for the flow is considered to be proper. The stream function vorticity method has some attractive features. The pressure makes no appearance, and, instead of dealing with the continuity equation and two momentum equations, we need to solve only two equations to obtain the stream function and vorticity. Therefore the Navier-Stokes equation in stream function vorticity formulation is recognized for its suitability for the task at hand. However, even for the simple boundary geometry, this is still a challenging problem. The only way to attack the full problem is to generate the solution of the flow numerically by a high speed computer.

A complicated problem like the present one, however, can be attacked from different angles. For simplicity, the we made a two dimensinal flow assumption even though the general real flows are three dimensional. As shown in Figure 1-1(a), the general unsteady motion on an arbitrary body can be decomposed into normal and tangential components. Basically these two kind of interactions can be simply realized by a piston and an oscillating flat plate as shown in Figure 1-1(b). For one step deeper, from the geometrical point of view, the best extension is with a circular cylinder as shown in Figure 1-1(c). The flow around the cylinder is still too complicated to find the key mechanism of the interaction between the flow and the unsteady boundary. As shown in Figure 1-2, the flow around the cylinder can be separated as two cases with on-coming and without on-coming stream. The work included in this dissertation contains several branches of problem as shown in Figure 1-2, in which some of them are attacked by analytical methods and some of them by numerical computations.

For a numerical solution, it is generally believed that the finite difference method is better developed than the other numerical schemes[28−38]. It is well-known, however, that one disadvantage of the finite difference method is the possible error in satisfying boundary conditions because the geometric boundary is

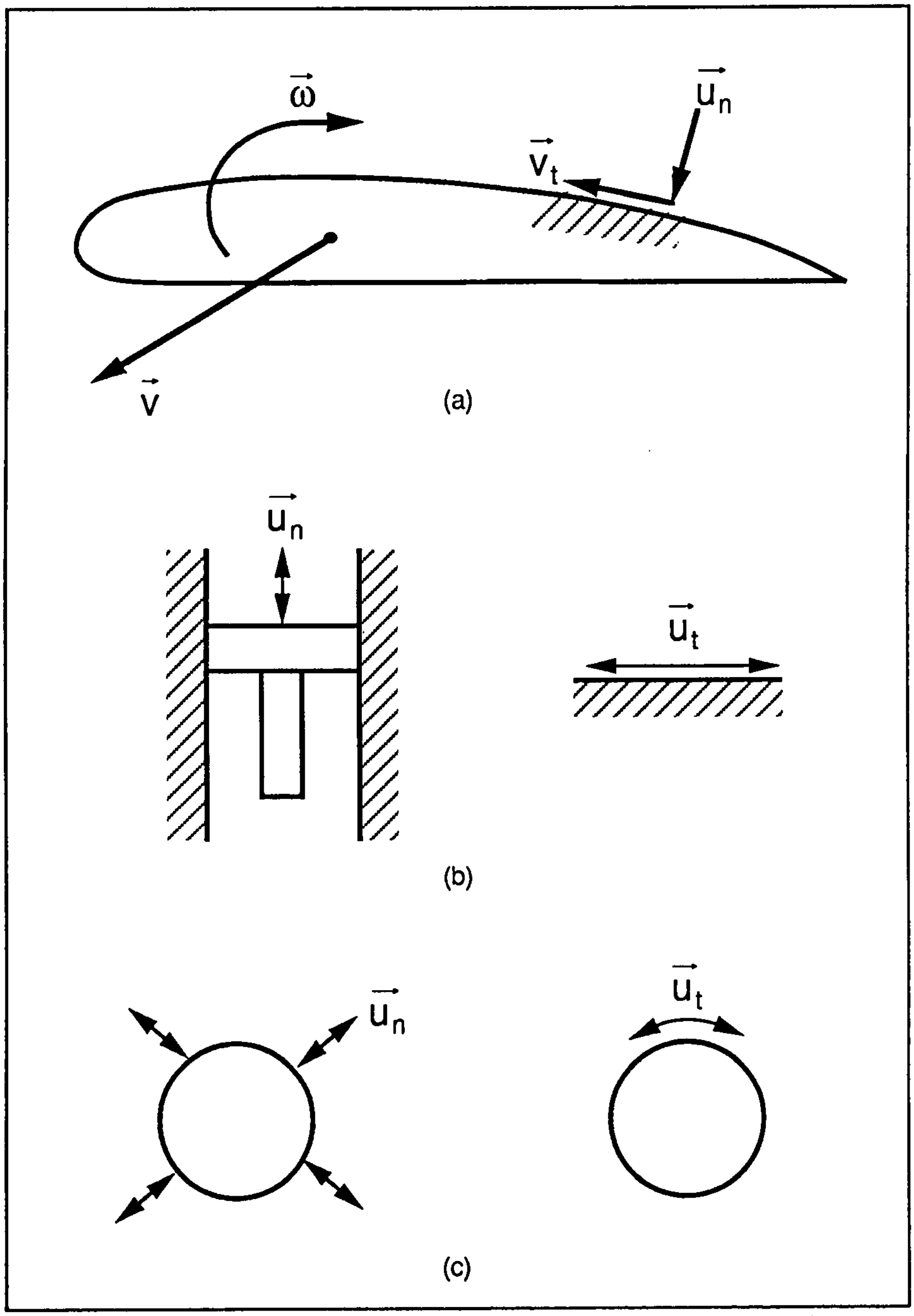

Fig. 1-1. General unsteady boundary geometry

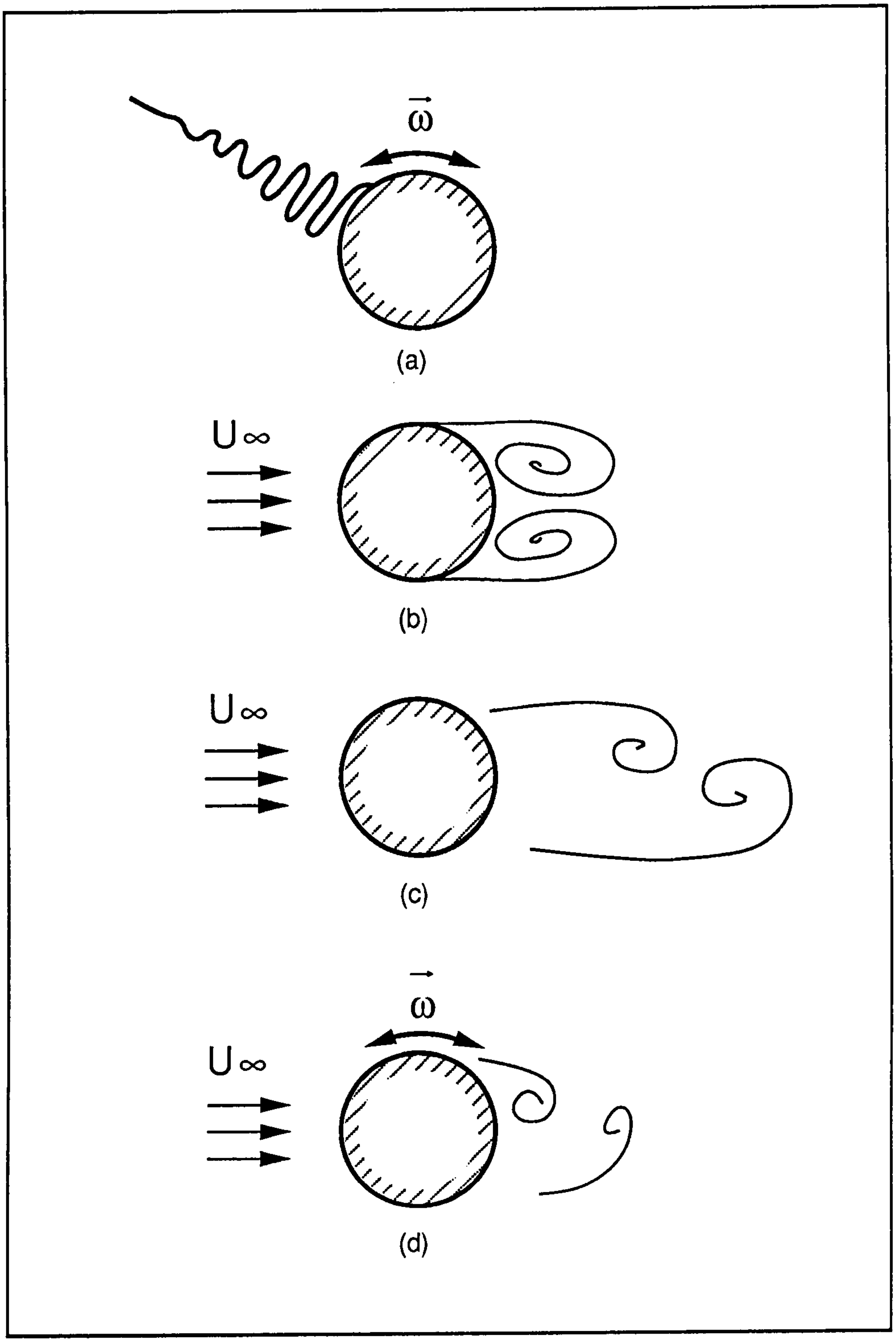

Fig. 1-2. Schematic of approaches

usually not on the grid point. Any extrapolation and interpolation will introduce errors. For the problem in hand, however, due to the simplicity of the geometrical shape, an analytical grid generation can be performed without increasing computational work. Therefore, the boundary condition is exactly satisfied on the boundary grid points. In addition, the Alternate Direction Implicit (ADI) scheme which is unconditionally stable and the over-relaxation factor in Successive Over-Relaxation method (SOR) which can be used to speed up the convergence of iteration are proposed to be used. A numerical solution by these two methods is applied to the branch of the problem when there is a uniform far-stream around both a steady and an oscillating cylinder.

Of course, a numerical approach does not help one to completely understand the physics of a problem, which can only be found by proper experimental simulations. A flow visualization experiment was conducted for the flow around an oscillating and stationary cylinder in the water tunnel. To view the flow pattern, both laser induced fluorescence and color dye techniques were employed.

Additionally, for such a complicated problem it is extremely helpful to obtain some key analytical results under proper assumptions, even locally or partially, which may shed some light on some general and important conclusions, unlike numerical solutions which only provide discrete conditions of the problem. An analytical analysis is conducted for several branches of the problem in Figure 1-2.

Theoretical, numerical and experimental approaches are complementary to each other. What is reported in this dissertation is only the preliminary step to understanding the problem. A turbulent flow approach for high Reynolds number flows and three dimensional consideration have more engineering significance. That will be the author's future work.

CHAPTER II

ANALYTICAL SOLUTIONS

In the last century, Stokes solved the flow problem generated by an oscillating infinite flat plate in a stationary medium. Naturally the flow generated by a rotatory oscillating cylinder in a stationary fluid is its extension problem as shown in Figure 1-2. From the view point of mechanics, the flow extracted by a cylinder not only has the geometric similarity to a flat plate, whose limiting geometry condition is a flat plate when its radius approaches to infinity, but a finite characteristic length has been introduced into the problem, making it more interesting than the original Stokes problem.

§2.1 Governing Equations

For convenience of analytical solution, the Navier-Stokes equation in primitive variables for incompressible, laminar flow is used. The governing equations in cylindrical coordinates, which is shown in Figure 2-1, may be written as following:

$$\frac{\partial u_r}{\partial t}+u_r\frac{\partial u_r}{\partial r}+u_\theta\frac{\partial u_r}{r\partial\theta}-\frac{u_\theta^2}{r}=\nu\left(\frac{\partial}{\partial r}(\frac{1}{r}\frac{\partial ru_r}{\partial r})+\frac{1}{r^2}\frac{\partial^2 u_r}{\partial\theta^2}-\frac{2}{r^2}\frac{\partial u_r}{\partial\theta}\right)-\frac{1}{\rho}\frac{\partial p}{\partial r} \quad (2.1)$$

$$\frac{\partial u_\theta}{\partial t}+u_r\frac{\partial u_\theta}{\partial r}+u_\theta\frac{\partial u_\theta}{r\partial\theta}-\frac{u_\theta u_r}{r}=\nu\left(\frac{\partial}{\partial r}(\frac{1}{r}\frac{\partial ru_\theta}{\partial r})+\frac{1}{r^2}\frac{\partial^2 u_\theta}{\partial\theta^2}+\frac{2}{r^2}\frac{\partial u_\theta}{\partial\theta}\right)-\frac{1}{\rho}\frac{\partial p}{r\partial\theta} \quad (2.2)$$

where u_r, u_θ are the velocity components in the radial and circumferential directions, p is the static pressure, ν the kinetic viscosity, ρ the density of the fluid and t is time.

For the present problem, the cylinder is only performing a purely circumferential motion and there is no oncoming stream, it is reasonable to make a symmetry assumption for the flow, that is, all physical quantities in the flow are a function

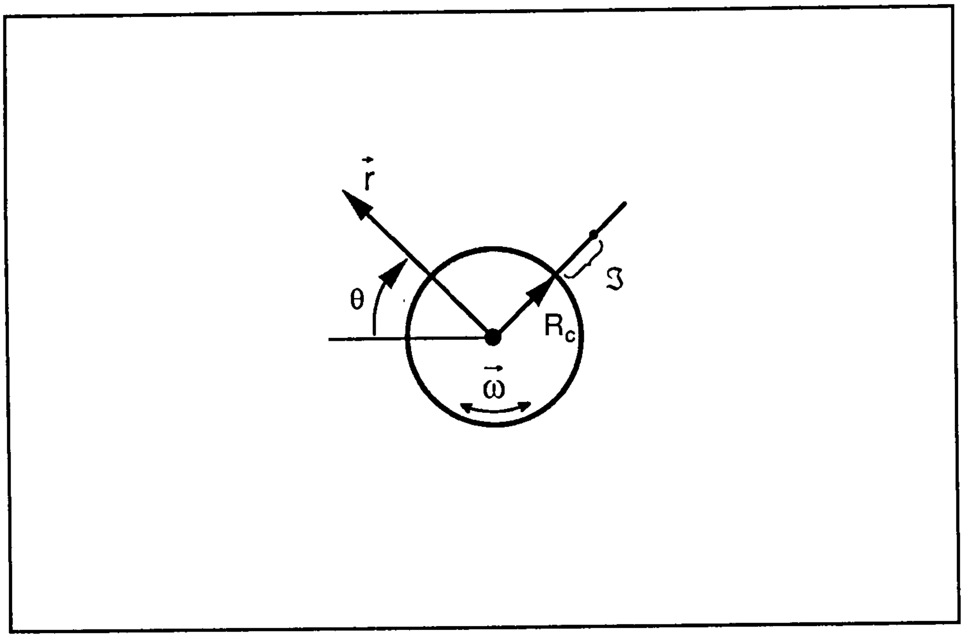

Fig. 2-1. Physical geometry and coordinate of cylinder Stokes problem

of radial coordinate r. From the continuity equation, the radial velocity component vanishes, i.e.,

$$\frac{\partial}{\partial\theta} = 0, \qquad u_r = 0$$

so the problem is simplified and the equations to solve are:

$$\frac{u_\theta^2}{r} = \frac{1}{\rho}\frac{\partial p}{\partial r} \tag{2.3}$$

$$\frac{\partial u_\theta}{\partial t} = \nu\left(\frac{\partial^2 u_\theta}{\partial r^2} + \frac{1}{r}\frac{\partial u_\theta}{\partial r} - \frac{u_\theta}{r^2}\right) \tag{2.4}$$

There is no velocity component in the radial direction. The only contribution to the inertia force on the left side of Equation (2.3) is from the centripetal force which is simply balanced by the pressure gradient. At the same time, the unknowns u_θ and p are decoupled. Hence, u_θ can be solved from (2.4) first, then the pressure p can be integrated directly from (2.3).

The far boundary condition for the problem is zero velocity at infinity. On the cylinder surface the no-slip condition is applied. For the rotationally oscillating cylinder, its motion can be described by the angular velocity in general form

$$\Omega = \Omega_0 sin(\omega t) \tag{2.5}$$

where Ω is the angular velocity and ω is phase frequency of the oscillation. Therefore, the velocity at the cylinder surface is

$$u_\theta(r = R_c, t) = R_c\Omega_0 sin(\omega t) \tag{2.6}$$

in which R_c is the radius of the cylinder. The initial condition is

$$u_\theta(r, t = 0) = 0 \tag{2.7}$$

which means that there is a stationary medium around the cylinder initially, also the oscillation on the cylinder is applied with a zero initial velocity.

The solution for u_θ in Equation (2.4), with the conditions (2.6) and (2.7) and zero velocity at infinity, is obtained analytically in the following section.

§2.2 Analytical Solution

Under the restriction applied in this branch of the study, the governing equations have been simplified to the forms of (2.3) and (2.4), which are linear. So all the analytical solution procedures for linear differential equation can be applied. The stability as well as limiting flow trends can be analyzed as well.

From the boundary condition, we can suggest the complex number form of solution as

$$u_\theta(r,t) = e^{i\omega t} f(r) \tag{2.8}$$

Substituting this into (2.4), we have

$$wie^{i\omega t} f(r) = \nu(e^{i\omega t} f''(r) + \frac{1}{r} e^{i\omega t} f'(r) - \frac{1}{r^2} e^{i\omega t} f(r))$$

or

$$f''(r) + \frac{1}{r} f'(r) - (\frac{\omega}{\nu} i + \frac{1}{r^2}) f(r) = 0$$

Let $r' = \sqrt{\frac{w}{\nu}}$ r, we have

$$f''(r') + \frac{1}{r'} f'(r') - (i + \frac{1}{r'^2}) f(r') = 0 \tag{2.9}$$

This is a standard form of modified Bessel function. The general solution is[39]

$$f(r') = AI_1(\sqrt{i} r') + BK_1(\sqrt{i} r') \tag{2.10}$$

where A and B are two arbitrary constants. From the boundary condition at infinity, the first term in (2.10) is dropped. The solution becomes

$$f(r') = BK_1(\sqrt{i} r') \tag{2.11}$$

From mathematical tables and after performing some algbraic operations , the function K_1 can be written as

$$K_1(\sqrt{i}r') = K_{1r}(r') + i\ K_{1i}(r') \tag{2.12}$$

where

$$K_{1r}(r') = \frac{\sqrt{2}}{2r'} + \frac{r'}{4\sqrt{(2)}}\{\sum_{\substack{k=0\\even}}^{\infty} \frac{(-1)^{\frac{k}{2}}(\frac{r'}{2})^{2k}}{\Gamma(k+1)\Gamma(k+2)}\left(\sum_{m=1}^{1+k}\frac{1}{m} + \sum_{m=1}^{k}\frac{1}{m}\right)$$

$$-\sum_{\substack{k=1\\odd}}^{\infty} \frac{(-1)^{\frac{k-1}{2}}(\frac{r'}{2})^{2k}}{\Gamma(k+1)\Gamma(k+2)}\left(\sum_{m=1}^{1+k}\frac{1}{m} + \sum_{m=1}^{k}\frac{1}{m}\right)\}$$

$$+\frac{r'}{2\sqrt{2}}\{(a + ln\frac{r'}{2})\left(\sum_{\substack{k=0\\even}}^{\infty} \frac{(-1)^{\frac{k}{2}}(\frac{r'}{2})^{2k}}{\Gamma(k+1)\Gamma(k+2)} - \sum_{\substack{k=1\\odd}}^{\infty} \frac{(-1)^{\frac{k-1}{2}}(\frac{r'}{2})^{2k}}{\Gamma(k+1)\Gamma(k+2)}\right)$$

$$-\frac{\pi}{4}\left(\sum_{\substack{k=0\\even}}^{\infty} \frac{(-1)^{\frac{k}{2}}(\frac{r'}{2})^{2k}}{\Gamma(k+1)\Gamma(k+2)} + \sum_{\substack{k=1\\odd}}^{\infty} \frac{(-1)^{\frac{k-1}{2}}(\frac{r'}{2})^{2k}}{\Gamma(k+1)\Gamma(k+2)}\right)\}$$

$$K_{1i} = -\frac{\sqrt{2}}{2r'} + \frac{r'}{4\sqrt{(2)}}\{\sum_{\substack{k=0\\even}}^{\infty} \frac{(-1)^{\frac{k}{2}}(\frac{r'}{2})^{2k}}{\Gamma(k+1)\Gamma(k+2)}\left(\sum_{m=1}^{1+k}\frac{1}{m} + \sum_{m=1}^{k}\frac{1}{m}\right)$$

$$+\sum_{\substack{k=1\\odd}}^{\infty} \frac{(-1)^{\frac{k-1}{2}}(\frac{r'}{2})^{2k}}{\Gamma(k+1)\Gamma(k+2)}\left(\sum_{m=1}^{1+k}\frac{1}{m} + \sum_{m=1}^{k}\frac{1}{m}\right)\}$$

$$+\frac{r'}{2\sqrt{2}}\{\frac{\pi}{4}\left(\sum_{\substack{k=0\\even}}^{\infty} \frac{(-1)^{\frac{k}{2}}(\frac{r'}{2})^{2k}}{\Gamma(k+1)\Gamma(k+2)} - \sum_{\substack{k=1\\odd}}^{\infty} \frac{(-1)^{\frac{k-1}{2}}(\frac{r'}{2})^{2k}}{\Gamma(k+1)\Gamma(k+2)}\right)$$

$$+(a + ln\frac{r'}{2})\left(\sum_{\substack{k=0\\even}}^{\infty} \frac{(-1)^{\frac{k}{2}}(\frac{r'}{2})^{2k}}{\Gamma(k+1)\Gamma(k+2)} + \sum_{\substack{k=1\\odd}}^{\infty} \frac{(-1)^{\frac{k-1}{2}}(\frac{r'}{2})^{2k}}{\Gamma(k+1)\Gamma(k+2)}\right)\} \tag{2.13}$$

in which the constant $a = 0.57721566....$

By applying the boundary condition on the cylinder surface, we obtain that

$$u_\theta(r', t) = \frac{\Omega_0}{K_{1r}(r' = \sqrt{\frac{\omega}{\nu}} R_c)} \sqrt{K_{1r}^2 + K_{1i}^2} sin(\omega t + tg^{-1}(\frac{K_{1i}}{K_{1r}})). \qquad (2.14)$$

This is the exact solution. It can be seen that the flow is also oscillating, its amplitude is a function of the radial distance and there is a phase difference from the forced oscillation over the boundary. The above solution, however, is in the form of an infinite series and this series usually converges very slowly. So for more quantitative discussion purpose, an approximate solution of the problem is used. The approximate solution is in more compact form and convenient to discuss the involved physics.

From the solution of the original Stokes problem, we knew that the region of viscous effect in the normal direction is in the order of $O(\sqrt{\nu})$. Physically, the viscous region should be smaller in the cylinder case than in the Stokes problem, because the latter has an infinite moving boundary, while the cylinder has a finite length scale. So, it is reasonable to consider $O(\delta_c) \leq O(\sqrt{\nu})$, where δ_c is the effective thickness of the viscous layer in the present problem. This suggests seeking an approximate solution near the cylinder surface.

For Equation (2.4), we can introduce a new variable $\Im$ such that

$$r = R_c + \Im \qquad (2.14)$$

geometrically $\Im$ is the normal curvilinear coordinate, as shown in Figure 2-1. Obviously, $O(\Im) \leq O(\sqrt{\nu})$. Under the small $\Im$ assumption relative to R_c, the first order approximation of (2.4) is

$$\frac{\partial u_\theta}{\partial t} = \nu(\frac{\partial^2 u_\theta}{\partial \Im^2} + \frac{1}{R_c}\frac{\partial u_\theta}{\partial \Im} - \frac{u_\theta}{R_c^2}) \qquad (2.15)$$

In this equation, we have approximated the curvature of the thin viscous flow layer by the curvature of the cylinder surface. Physically, this is acceptable as long as a restriction of $O(R_c) = O(1)$ is satisfied. Now the problem is to solve (2.15) under the boundary conditions of (2.6) and (2.7).

Assuming the same form of solution as in the exact solution by letting

$$u_\theta(\Im, t) = f(\Im)e^{iwt} \tag{2.16}$$

substituting in (2.15) and canceling the common factor, we get an ordinary differential equation for $f(\Im)$

$$f'' + \frac{1}{R_c}f' - (\frac{1}{R_c^2} + \frac{\omega}{\nu}i)f = 0 \tag{2.17}$$

which is a second order constant coefficients differential equation. The general solution is

$$f(\Im) = Cexp\left(-\frac{1}{2R_c} \pm \frac{1}{2}\sqrt{\frac{1}{R_c^2} + 4(\frac{1}{R_c^2} + \frac{\omega}{\nu}i)\Im}\right)$$

where C is an arbitrary constant, and from the boundary condition at infinity the positive branch is removed. By the condition at the cylinder surface, we obtain the solution

$$u_\theta = Im(Cexp\left(-\frac{1}{2R_c} + \frac{1}{2}\sqrt{\frac{5}{R_c^2} + \frac{4\omega}{\nu}i\Im e^{i\omega t}}\right)\right) \tag{2.18}$$

or

$$\begin{aligned} u_\theta(\Im, t) = u_0 exp\left(-\frac{1}{2}[\frac{1}{R_c} + (\frac{25}{R_c^4} + \frac{16\omega^2}{\nu^2})^{\frac{1}{4}}cos(\frac{1}{2}tg^{-1}(\frac{4\omega R_c^2}{5\nu}))]\Im\right) \\ *sin[\omega t - \frac{1}{2}(\frac{25}{R_c^4} + \frac{16\omega^2}{\nu^2})^{\frac{1}{4}}sin(\frac{1}{2}tg^{-1}\frac{4\omega R_c^2}{5\nu})\Im] \end{aligned} \tag{2.19}$$

where $u_0 = R_c\Omega_0$, which is the oscillating velocity amplitude of the wall.

Equation (2.19) is the first order approximate solution of the cylinder performing a rotatory oscillation in a steady medium. At first, the limiting case is considered. That is, when the cylinder radius approaches infinity and keeping u_0 fixed to compare with the Stokes problem. Then the solution (2.19) reduces to

$$\lim_{\substack{R_c \to \infty \\ u_0 fixed}} u(\Im, t) = u_0 e^{-\frac{\sqrt{2}}{2}\sqrt{\frac{\omega}{\nu}}\Im} sin(\omega t - \frac{\sqrt{2}}{2}\sqrt{\frac{\omega}{\nu}}\Im) \tag{2.20}$$

This is also exactly the solution of the classic Stokes problem as expected physically.

For convenience to discuss the effect of radius R_c quantitatively, in which the R_c is the representative length scale, the reduced Reynolds number is introduced. We define

$$R_\omega = \frac{(\omega R_c)R_c}{\nu} = \frac{\omega R_c^2}{\nu}.$$

Then, the solution (2.19) can be represented by

$$u_\theta(\Im, t) = u_0 exp\left(-\frac{[1+(25+16R_\omega^2)^{\frac{1}{4}}]\sqrt{1+\sqrt{1+\frac{16}{25}R_\omega}}}{2\sqrt{2R_\omega}(1+\frac{16}{25}R_\omega^2)^{\frac{1}{4}}} \frac{\Im}{\sqrt{\frac{\nu}{\omega}}} \right)$$

$$*sin\{\omega t - \sqrt{\frac{5}{8}} \frac{\sqrt{\sqrt{1+\frac{16}{25}R_\omega^2}-1}}{\sqrt{R_\omega}} \frac{\Im}{\sqrt{\frac{\nu}{\omega}}}\}. \tag{2.21}$$

The time dependent velocity profiles for a reduced Reynolds number $R_\omega = 50$, which is roughly of the experimental value to be discussed in chapter IV, are shown in Figure 2-2(a). The velocity profiles for different R_ω are shown in Figure 2-2(b). Obviously, the viscous diffusion decays away from the body, which means the velocity oscillation amplitudes decrease as the normal coordinate increases. The amplitude and phase decay more quickly if the reduced Reynolds number is lower. In addition, with setting up of the flowfield extracted by the cylinder surface oscillation, a vorticity field is found, in which the vorticity is diffused from the surface. The details about this is discussed in chapter V.

In addition, the effective viscous layer thickness δ_c can be defined, which represents the place where the amplitude has decreased to 1% of the wall value. From (2.21), it can be found that:

$$\frac{\delta_c}{\sqrt{\frac{\nu}{\omega}}} = \frac{4.6\sqrt{R_\omega}}{1+(25+16R_\omega^2)^{\frac{1}{4}} cos\left(\frac{1}{2}tg^{-1}(\frac{4}{5}R_\omega)\right)}$$

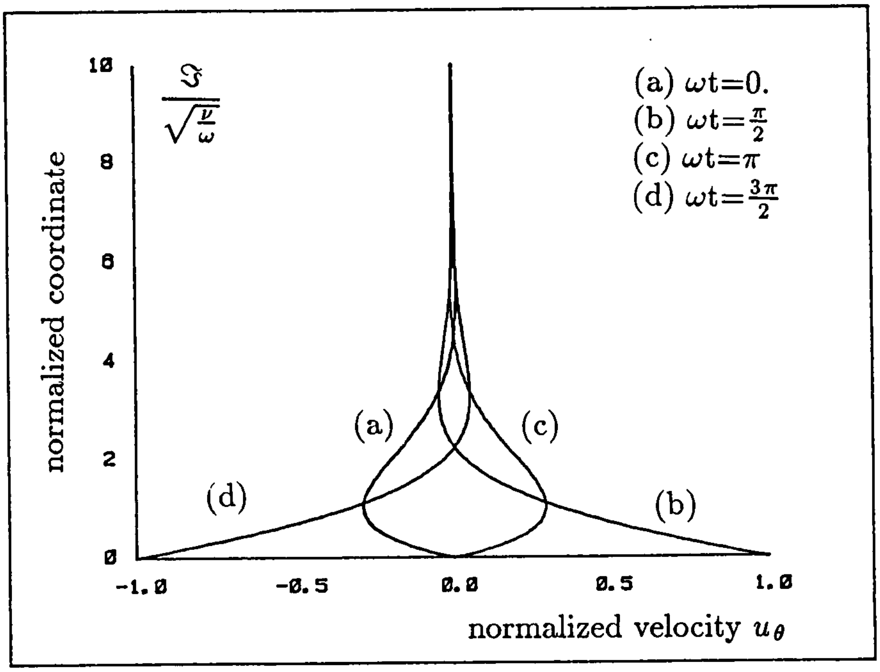

(a) Velocity profile development with time

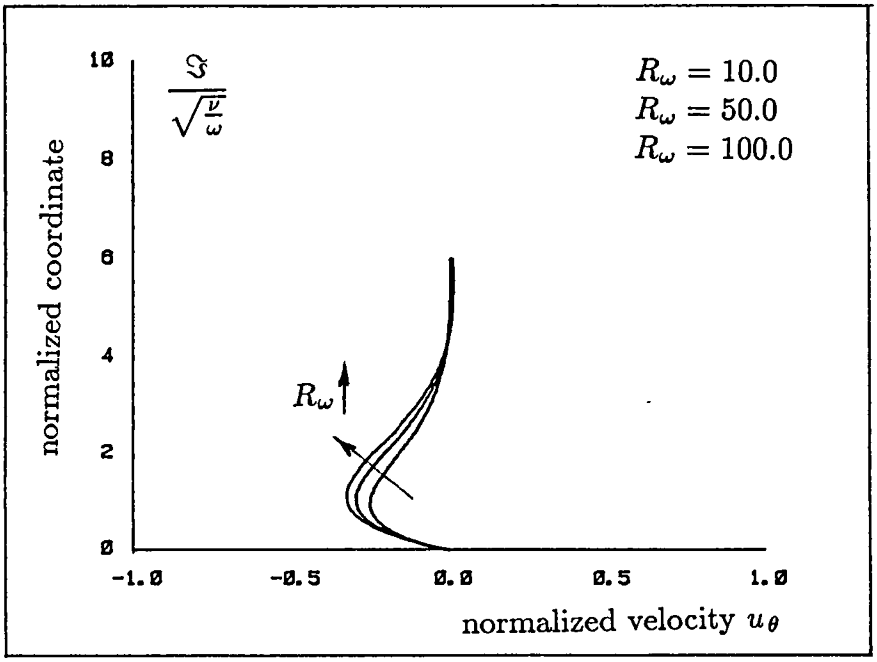

(b) Velocity profile for different R_ω

Fig. 2-2. Results of cylinder Stokes flowfield

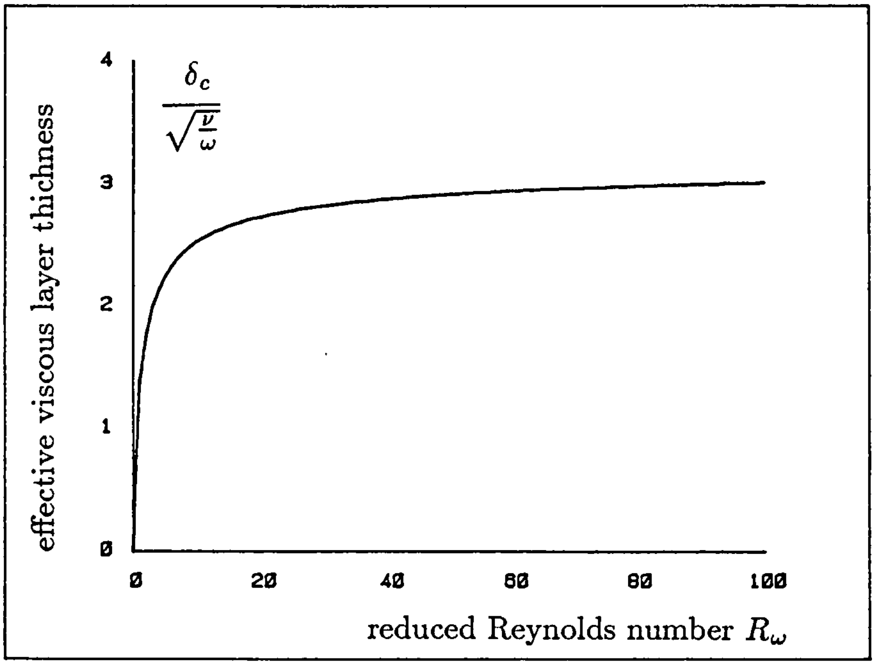

(c) Effective viscous layer thickness

Fig. 2-2. Continued

The results are shown in Figure 2-2(c). The effectively viscous region is larger if the reduced Reynolds numbers are higher.

§2.3 Potential Flow Modeling of Stationary Vortex Pair

So far, the analytical solutions have been obtained for the flow generated by the oscillating cylinder in a stationary medium. It has been seen that when the body oscillates in the medium, its boundary acts like a vorticity source to constantly feed vorticity into the flow field. However if the cylinder is placed in a uniform flow field, which is shown in Figure 1-2 as another branch, the physical process is more complicated. In that flow, besides the vorticity diffusion phenomena, convection becomes very important. The vorticity generated from the surface is carried downstream by the fluid elements, which consequently forms a vorticity region, and thus a vortex is finally formed behind the cylinder[27]. Experiments of flow around cylinders show that within a short time from starting, even for flows at high Reynolds number, there is a symmetrical vortex pair formed initially behind the cylinder; and as time increases the vortex pair grow in strength and size, finally the symmetry is broken down and a non-symmetric wake is formed. In order to understand this physical process, a simple potential model is used to predict the vortex pair path and its stability.

A. Stationary vortex pair path

In this model, a pair of symmetrical viscous vorties is replaced by two potential, point vortices, which have the same strength, initially have a symmetric position, but with opposite sign. From the image theory of potential flow, two image vortices exist inside the cylinder; and the other two vortices locate in the original point, but have opposite sign. The complete model is shown in Figure

2-3.

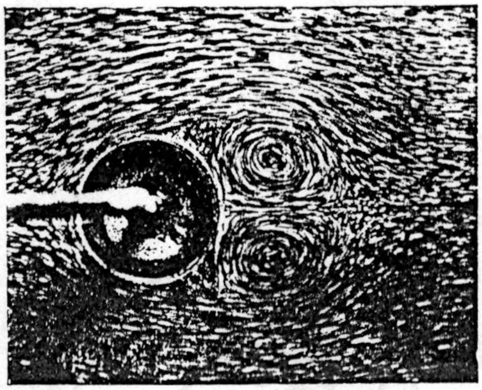

(a) Physical model

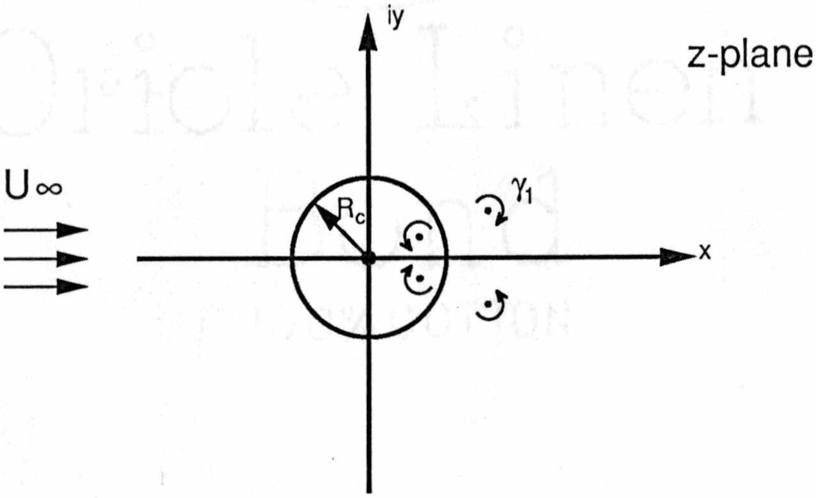

(b) Mathematical model

Fig. 2-3. Potential flow model of stationary vortex pair

The complex velocity potential for the flow is

$$W(Z) = Z + \frac{1}{Z} + i\gamma_1 Ln(\frac{Z - Z_1}{Z - \frac{Z_1}{||Z_1||^2}}) - i\gamma_2 Ln(\frac{Z - \bar{Z}_1}{Z - \frac{\bar{Z}_1}{||Z_1||^2}}) \tag{2.22}$$

where Z is the complex coordinate, γ_1 and γ_2 are the free vortex strengths which are equal in this model, Z_1 is the location of free vortex γ_1, $\bar{Z}_1$ is the complex conjugate of Z_1, which is the location of free vortex γ_2.

Completing some algebra operations, the stationary vortex pair path is derived as

$$sin\theta = \frac{1}{2}\frac{r^3 - 1}{r^2} \tag{2.23}$$

and the corresponding stationary vortex strength is

$$\gamma = \frac{(r^2 - 1)(r^4 - 1)}{r^5} \tag{2.24}$$

For the stationary vortex pair, if its strength changes, then from Equation (2.23) the path line can be seen in Figure 2-4, which is the zero velocity position where possibly the free vortices can stay.

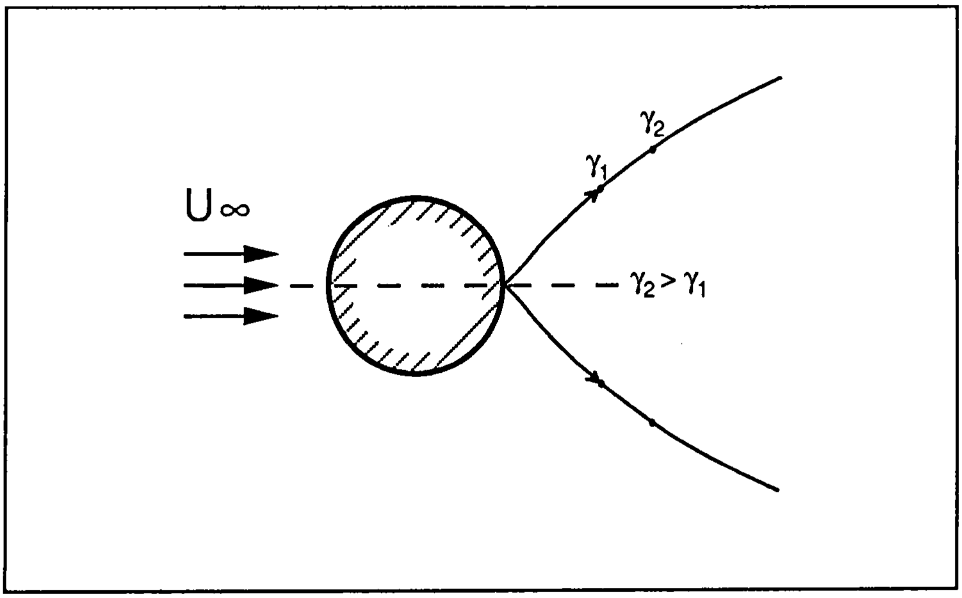

Fig. 2-4. Stationary vortex pair path

Physically, in starting flow, the size of the recirculating region grows and vorticity is collected as time increases. This is consistent with the above analytical results, in which the stationary points move out from the surface with the vortex strength increasing. The time development process is simulated by the change of the vortex strength. Some comparison of this result with numerical, viscous flow solution will be given in the next chapter.

B. Flow stability

As discussed above, under the potential flow model, a stationary point exists in the flowfield for a given free vortex strength; by changing the vortex strength, the stationary path lines have been obtained. This result shows that it is possible that the vortex pair can stay in the flow, in fact, it does exist from flow experiment. However the non-symmetric wake will be finally formed unless the Reynolds number of the flow is extremely low, e.g. 40. Therefore, the stability about the flow pattern is considered next.

There are different procedures to make the stability analysis. A method is used here in which a small vector displacement is introduced to one of the free vortices, then if the induced velocity on the other vortex is in the same direction as this displacement, we may say the system is not stable, otherwise it is stable. More exactly, what will be performed is simply to analyze the static stability.

Mathematically, from equation (2.22), the complex conjugate velocity is

$$\bar{V} = 1 - \frac{1}{Z^2} + i\gamma_1\left(\frac{1}{Z - Z_1} - \frac{1}{Z - \frac{Z_1}{||Z_1||^2}}\right) - i\gamma_2\left(\frac{1}{Z - Z_2} - \frac{1}{Z - \frac{Z_2}{||Z_2||^2}}\right) \quad (2.25)$$

in which $Z_2 = \bar{Z}_1$ and $\gamma_1 = \gamma_2 = \gamma$ at the initial time. Then by introducing a small perturbation Δ to the free vortex γ_1, the induced velocity is

$$\bar{V} = 1 - \frac{1}{(Z_1+\Delta)^2} + i\gamma\left(-\frac{\bar{Z}_1+\bar{\Delta}}{(Z_1+\Delta)(\bar{Z}_1+\bar{\Delta})-1} - \frac{1}{Z_1+\Delta-\bar{Z}_1} + \frac{Z_1}{(Z_1+\Delta)Z_1-1}\right) \tag{2.26}$$

After some algebra, finally, the induced velocity is

$$\begin{aligned} V = \frac{\varepsilon}{R^3}\{&2cos(\vartheta-3\varphi) + 2(R^2+1)sin(\vartheta) + \frac{sin(\vartheta-2\varphi)}{R^2-1} + \frac{2R^4cos(2\vartheta)sin\vartheta}{(R^4-1)(R^2-1)} \\ &-\frac{2R^6 sin\vartheta}{(R^4-1)(R^2-1)} - i[2sin(\vartheta-3\varphi) - \frac{cos(\vartheta-2\varphi)}{R^2-1} \\ &-\frac{2R^4cos(2\varphi)cos\vartheta}{(R^4-1)(R^2-1)} + \frac{2R^6cos\vartheta}{(R^4-1)(R^2-1)}]\} \end{aligned} \tag{2.27}$$

in which $Re^{i\varphi} = Z_1 = \bar{Z}_2$ and $\varepsilon e^{i\vartheta} = \Delta$. Then we take the inner product

$$\vec{V} \bullet \vec{\Delta} = \frac{(3R^2-2)\varepsilon^2 cos\varphi}{R^7}\{\frac{(R^2-1)(2R^6+4R^4+3R^2-2)}{2R^2(3R^2-2)cos\varphi}sin(2\vartheta) + cos(2\vartheta)\} \tag{2.28}$$

where ϑ can take any value. The criterion of stability is that if the inner product is positive, the system is not stable; otherwise it is stable. From the result of (2.28), it can be easily found that in some direction the system is stable, but in some other direction it is not stable. So we may conclude that the flow around a cylinder with a stationary vortex pair is not stable in general. That means the initial symmetry of the flow around a symmetric bluff body, like the cylinder, will finally break down. This is consistent to the formation of nonsymmetric flow in real situation.

To discuss the effectting factors on the stability, we introduce an influence function, which is

$$F_i = \frac{(R^2-1)(2R^6+4R^4+3R^2-2)}{2R^2(3R^2-2)cos\varphi}sin(2\vartheta) + cos(2\vartheta). \tag{2.29}$$

For any location of the free vortex, i.e., R and ϑ, the stability is detectable. One typical result is shown in Figure 2-5(a), in which $R = 1.5$ and $\vartheta = 30^0$. Obviously,

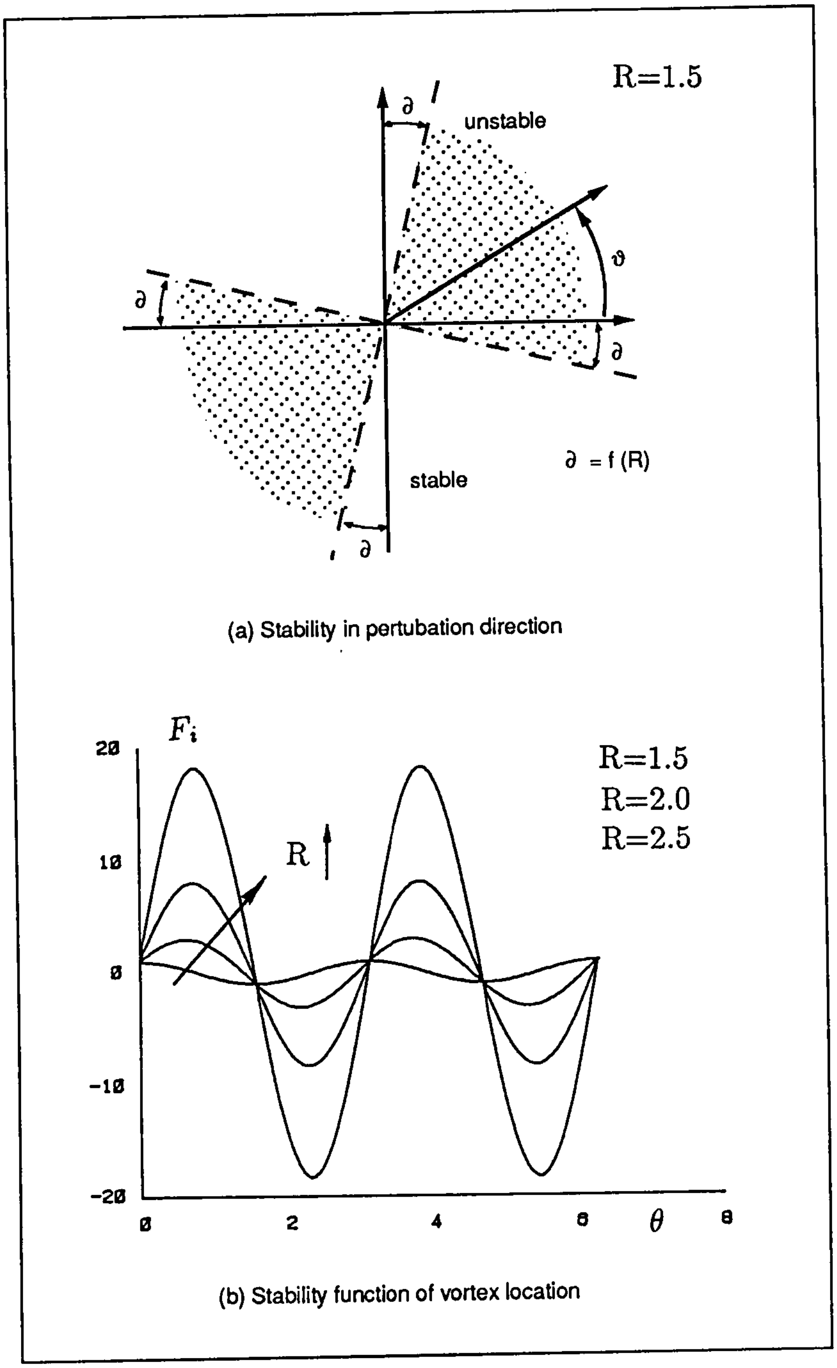

Fig. 2-5. Flow stability

the stability in various directions is a function of its location. The results of the influence function for different position R is shown in Figure 2-5(b). From the result, it can be seen that the farther away from the cylinder, the less stable it becomes.

One must keep in mind that the viscous effect plays a very important part in the stability, especially in the early stage of the formation of stationary vortex pair. More details about real flow stability and formation process of the nonsymmetricity needs to be addressed by the viscous flow theory. In fact, the vortex behind the cylinder results from viscosity; and its motion is controlled by the cylinder over which a viscous boundary condition is applied. The above simple potential flow model, however, offers a qualitative and instructive result. It serves in explainning the physics behind. The physical mechanism can be based on the fact that, when the vortex is far enough away from the cylinder, the viscous effect from the cylinder boundary is relatively low there.

C. Initial trajectory

It has been said in the above that the flow with a stationary vortex pair is generally not stable. The disturbance sources always exist in real life. So the flow development after receiving an arbitrary perturbation is extremely interesting. It is not practical to use such a simple potential flow model to predict the complete process. What follows is to show the initial free vortex trajectory after receiving the position perturbation in different directions.

From (2.25), the complex conjugate velocity of both vortices γ_1 and γ_2 are

$$\bar{V}_1 = 1 - \frac{1}{Z_1^2} + i\gamma\left(-\frac{\bar{Z}_1}{||Z_1||^2 - 1} - \frac{1}{Z_1 - Z_2} + \frac{\bar{Z}_2}{Z_1\bar{Z}_2 - 1}\right) \tag{2.30}$$

$$\bar{V}_2 = 1 - \frac{1}{Z_2^2} + i\gamma\left(\frac{\bar{Z}_2}{||Z_2||^2 - 1} - \frac{1}{Z_1 - Z_2} - \frac{\bar{Z}_1}{Z_2\bar{Z}_1 - 1}\right) \tag{2.31}$$

Set $Z_1 = r_1 e^{i\theta_1}$ and $Z_2 = r_2 e^{i\theta_2}$; it should be carefully noted that the positions Z_1 and Z_2 are different and follow their own trajectories after receiving a small perturbation. Then (2.30) and (2.31) can be recast by a velocity component in rectangular coordinate

$$V_{1x} = 1 - \frac{cos2\theta_1}{r_1^2} + \gamma\left(\frac{r_1 sin\theta_1}{r_1^2 - 1} - \frac{r_1 sin\theta_1 - r_2^2 sin\theta_2}{||Z_1 - Z_2||^2} + \frac{r_1 r_2^2 sin\theta_1 - r_2 sin\theta_2}{||Z_1\bar{Z}_2 - 1||^2}\right) \quad (2.32)$$

$$V_{1y} = -\frac{sin2\theta_1}{r_1^2} + \gamma\left(\frac{r_1 cos\theta_1}{r_1^2 - 1} + \frac{r_1 cos\theta_1 - r_2^2 cos\theta_2}{||Z_1 - Z_2||^2} - \frac{r_1 r_2^2 cos\theta_1 - r_2 cos\theta_2}{||Z_1\bar{Z}_2 - 1||^2}\right) \quad (2.33)$$

$$V_{2x} = 1 - \frac{cos2\theta_2}{r_2^2} + \gamma\left(\frac{r_2 sin\theta_2}{r_2^2 - 1} - \frac{r_1 sin\theta_1 - r_2^2 sin\theta_2}{||Z_1 - Z_2||^2} - \frac{r_2 r_1^2 sin\theta_2 - r_1 sin\theta_1}{||Z_2\bar{Z}_1 - 1||^2}\right) \quad (2.34)$$

$$V_{2y} = -\frac{sin2\theta_2}{r_2^2} + \gamma\left(-\frac{r_2 cos\theta_2}{r_2^2 - 1} + \frac{r_1 cos\theta_1 - r_2^2 cos\theta_2}{||Z_1 - Z_2||^2} - \frac{r_2 r_1^2 cos\theta_2 - r_1 cos\theta_1}{||Z_2\bar{Z}_1 - 1||^2}\right) \quad (2.35)$$

in which

$$||Z_1 - Z_2||^2 = r_1^2 + r_2^2 - 2r_1 r_2 cos(\theta_1 - \theta_2)$$

and

$$||Z_1\bar{Z}_2 - 1||^2 = ||Z_2\bar{Z}_1 - 1||^2 = r_1^2 r_2^2 + 1 - 2r_1 r_2 cos(\theta_2 - \theta_1).$$

By introducing a small disturbance on the initial position of one of the free vortices, say, γ_1, from the stationary point, then integrating the above equations numerically from that specific point, the trajectory can be predicted. However, as discussed above the flow has different stability in regards to the disturbance from different directions, thus, the vortex should have different responses to its trajectory.

Numerically, the trajectory integration is usually sensitive to error. In this work, a second-order Runge-Kutta method is used and the step length, that is the time interval, is determined by comparing the results with the step length and half step length. If the results obtained in the two cases agree adequately, the length is considered a reasonable one.

The results for the free vortices trajectories corresponding to position perturbations in three directions are shown in Figure 2-6. The three directions are $\theta = 0^0$, 90^0, and 180^0. All the results are obtained by assuming the initial position of $R = 1.5$, $\vartheta = 30^0$ and the displacement length be 0.0001.

The striking property shown in Figure 2-6 is that by changing the perturbation direction (e.g. $\theta = 0^0,\ 180^0$), the flow is changed totally. Originally these two free vortices have the same opportunity, but a small change in the perturbation direction can change their final fate. This is consistent to real phenomena, that is, it is impossible to predict which stationary vortex in the pair would be shed first.

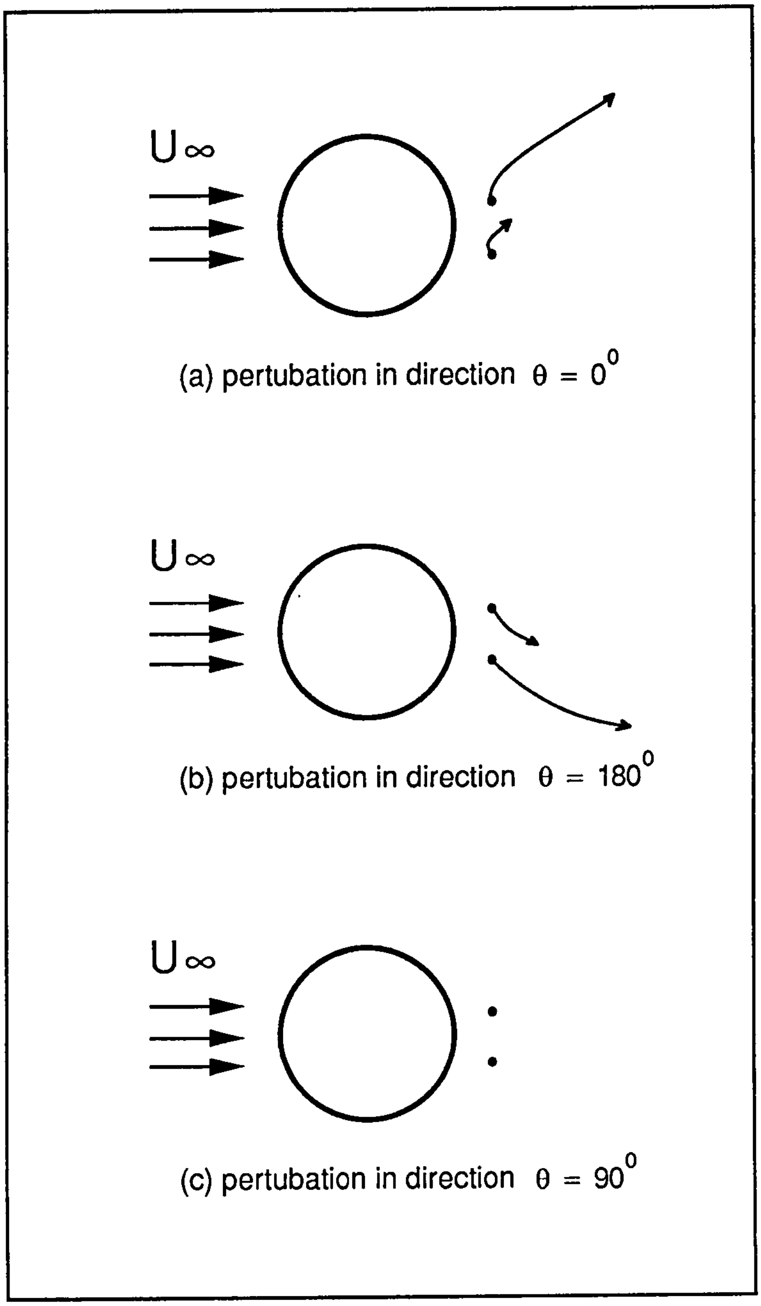

Figure 2-6. Initial trajectory

CHAPTER III

NUMERICAL APPROACHES

§3.1 Full Equation Formulation

In the last chapter, analytical solutions for the flow generated by an oscillating cylinder in a stationary medium have been discussed, which is one of the branches investigated in this study. Now, if there is a uniform freestream encountering such an oscillating cylinder, the convection terms in the governing equations become important. These terms are nonlinear. The equations must be solved by the computer with proper numerical procedures. The configuration of the physical problem of this branch of work is sketched in Figure 3-1. The circular cylinder of radius R_c has its center at the origin of the coordinate system, which is fixed. The cylinder stays stationary or performs a simple rotational oscillation about its axis. Different frequencies and amplitudes are treated.

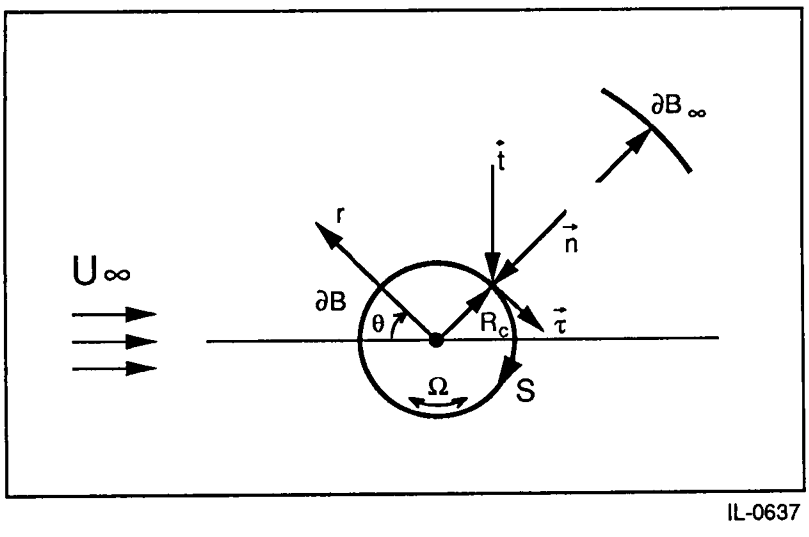

Fig. 3-1 Uniform flow over an oscillating cylinder and coordinate definition

To match the condition of our experiment to be discussed in chapter IV, the problem is treated as laminar, time-dependent and two-dimensional. The vorticity ζ, and the stream function ψ are used here instead of the primitive variables $\vec{v}$, p. The cylindrical coordinate system remains the same as defined in the last chapter. The governing equations in the form of vorticity-stream function are (see appendix A for the details)

$$\frac{\partial \zeta}{\partial t} + \nabla \cdot (\vec{v}\zeta) = \frac{2}{Re}\nabla^2 \zeta, \tag{3.1}$$

with

$$\nabla^2 \psi = \zeta, \tag{3.2}$$

where the stream function is defined by

$$u_r = -\frac{\partial \psi}{r \partial \theta}, \qquad u_\theta = \frac{\partial \psi}{\partial r}, \tag{3.3}$$

and $\vec{v}$ is the velocity vector, ∇ is the nabla operator and it is expressed in cylindrical coordinates (r, θ) by

$$\nabla = \frac{\partial}{\partial r}\vec{e}_r + \frac{\partial}{r \partial \theta}\vec{e}_\theta,$$

and

$$\nabla^2 = \frac{\partial^2}{\partial r^2} + \frac{1}{r}\frac{\partial}{\partial r} + \frac{1}{r^2}\frac{\partial^2}{\partial \theta^2}.$$

In what follows all variables, unless specified, will refer to nondimensional quantities where lengths are nondimensionalized with R_c, velocities with U_∞, time with R_c/U_∞, and the Reynolds number is based on the cylinder diameter($d = 2R_c$), the far field freestream velocity (U_∞) and kinetic viscosity (ν), which is expressed by the formula

$$Re = \frac{U_\infty d}{\nu}. \tag{3.4}$$

§3.2 Computational Procedure of Forces

One of the most important byproduct of the computation is the unsteady lift and drag coefficients. The hydrodynamic forces come from two factors: one is from the viscous shear stress, the other from the surface pressure. The advantage of utilizing the vorticity stream function formulation is that the number of variables is reduced, and the pressure does not appear explicitly. As a main contributor to the force, the pressure solution can be obtained from the numerical results for ψ and ζ.

To obtain a pressure solution, one can start at an arbitrary point with an arbitrary pressure level (constant of integration) and numerically integrate the discretized momentum equations in primitive variables, velocity components being obtained from the stream function solution[42]. However, in this work, the main concern is only with the calculation of lift and drag coefficients. That is, only the surface pressure difference along the body surface is needed. The surface pressure integration can be facilitated by using the vorticity solution directly.

Let $\vec{n}$ be the inward to the body normal vector, $\vec{k}$ be the normal to the plane of the flow, $\vec{\tau} = \vec{n} \times \vec{k}$ and s the curvilinear coordinate as shown in Figure 3-1. The conservation of momentum along $\vec{\tau}$ can be written

$$\frac{\partial p}{\partial s} = -\frac{1}{Re}\frac{\partial \zeta}{\partial n} + \frac{d\Omega}{dt}(\vec{r}\cdot\vec{n}) + \Omega^2(\vec{r}\cdot\vec{\tau}) \tag{3.5}$$

where Ω is the angular velocity of the cylinder. For the stationary cylinder, $\Omega = 0$.

Integrating the local stress $\vec{t} = p\vec{n} + Re^{-1}\zeta\vec{\tau}$ exerted by the fluid on the cylinder along the contour of body, the pressure force $\vec{F}_p$ and the viscous force $\vec{F}_\nu$ are obtained by integration by part,

$$\vec{F}_p = \int_{\partial\Gamma_0} p\vec{n}ds = -\vec{k} \times \int_{\partial\Gamma_0} \frac{\partial p}{\partial s}\vec{r}ds$$

$$= \frac{2}{Re}\int_{\partial\Gamma_0}\frac{\partial\zeta}{\partial n}\vec{k}\times\vec{r}ds \tag{3.6a}$$

$$\vec{F}_\nu = \frac{2}{Re}\int_{\partial\Gamma_0}\zeta\vec{\tau}ds \tag{3.6b}$$

In component form, the drag and lift coefficients can be obtained by integration over the body

$$C_d = \frac{2}{Re}\int_0^{2\pi}(\zeta - \frac{\partial\zeta}{\partial\xi})sin\theta d\theta \tag{3.7a}$$

$$C_l = \frac{2}{Re}\int_0^{2\pi}(\zeta - \frac{\partial\zeta}{\partial\xi})cos\theta d\theta \tag{3.7b}$$

It should be kept in mind that if a more accurate solution is required the Poisson form of the pressure equation needs to be solved, because the value of derivatives appearing in the above equations need to be found by finite difference approximation.

§3.3 Numerical Method

Numerical integration is performed on the time-dependent full Navier-Stokes equations in a finite difference form of Equations (3.1) and (3.2) to predict the flow development for $t > 0$, where t denotes the time since the flow starts. What follows in this section are the description of the numerical method.

A. Coordinate Transformation and Computational Grids

Now, the external flow is in an infinite domain, while numerical calculation is confined within a finite region. For moderate to high Reynolds number flows, the effective viscous-dominated regions are basically restricted near to, and downstream of, the body. Consequently, grids with unequal sizes in physical space are adapted in the numerical calculation. A coordinate transformation is performed analytically to produce unequally sized grids in the physical region, in which there are enough grid points near the cylinder to guarantee that the large gradient region is represntable by enough number of discrete grids, but the size of each grid is constant in the computational plane.

A transformation of exponential stretching in the radial direction is used. That is

$$r = e^{\xi}, \tag{3.8a}$$

$$\theta = \eta. \tag{3.8b}$$

The outer boundary of the computational domain is controlled by choosing the range of independent variable ξ. Then, the governing equations are converted by the above coordinate transformation

$$\frac{\partial^2 \psi}{\partial \xi^2} + \frac{\partial^2 \psi}{\partial \eta^2} = e^{2\xi}\zeta, \tag{3.9}$$

$$e^{2\xi}\frac{\partial \zeta}{\partial t} + \frac{\partial (U\zeta)}{\partial \xi} + \frac{\partial (V\zeta)}{\partial \eta} = \frac{2}{Re}\left(\frac{\partial^2 \zeta}{\partial \xi^2} + \frac{\partial^2 \zeta}{\partial \eta^2}\right) \tag{3.10}$$

where $U = -\frac{\partial \psi}{\partial \eta}$ and $V = \frac{\partial \psi}{\partial \xi}$.

As mentioned before, the computational region is always finite. We use one parameter ξ_∞ to define the outer boundary (∂B_∞) in physical plane which is adjustable depending on the problem. The ranges of ξ and η the independent variables are

$$0 \le \xi \le \xi_\infty, \qquad -\pi \le \eta \le \pi. \tag{3.11}$$

Numerically, (3.9) and (3.10) are solved on a rectangular finite difference grid of dimension I by J, where the grid spacing is constant and is given by

$$\Delta\xi = \frac{\xi_\infty}{I-1}, \qquad \Delta\eta = \frac{2\pi}{J-1} \tag{3.12}$$

An example for grids (21×41) obtained through this transformation is given in Figure 3-2. Obviously, the radial grid size in the physical plane is larger when the grid points are farther away from the cylinder. For simplicity the grid size in the circumferential direction are taken as equal. The subscripts are used to represent the independent variable coordinates. The first subscript i represents the radial direction from the body to the outer boundary when i changes from 1 to I, and j denotes the circumferential direction from $-\pi$ to π when j changes from 1 to J, in which $j = 1$ and $j = J$ are coincide with each other. This is more convenient to apply periodic condition in this direction. The values for ψ and ζ are discretized on grid points into ψ_{ij} and ζ_{ij}.

B. Finite difference approximation

The continuous flow region has been discretized into discontinuous grid points; and continuous functions have been discretized as an isolated value at the grid nodes. So it is necessary to find a proper approximation to the derivatives of the dependent variables in the differential equations. In this work, we use a Taylor expansion to obtain the finite difference approximation of the derivatives. Looking into the governing equation of (3.9) and (3.10), it can be found that the equation for vorticity has the parabolic nature in time, while the stream function is of elliptic type and independent of time, t. When solving them, the solutions should match in time with the satisfication of boundary conditions at the spatial boundaries. A second order central difference scheme is used for the approximation of any spatial derivatives, and one side differencing for time t is necessary in order to embody the parabolic nature of the differential equation of vorticity in the time direction. Usually, there are two kinds of difference for the time variable, i.e., explicit and implicit schemes. To guarantee numerical stability, an implicit scheme is adopted

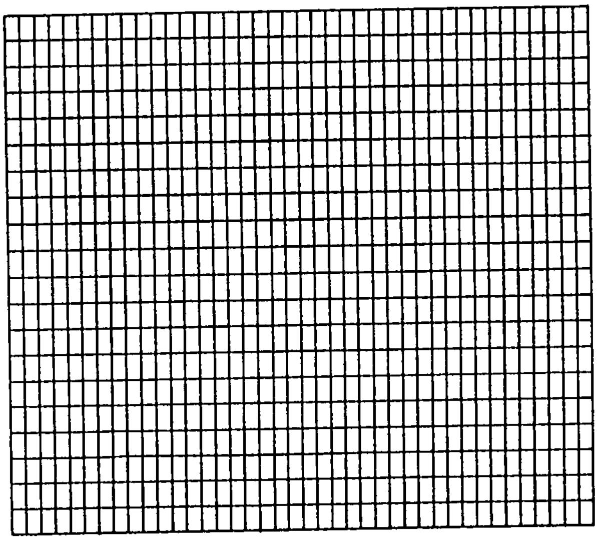

(a) grids in computational plane

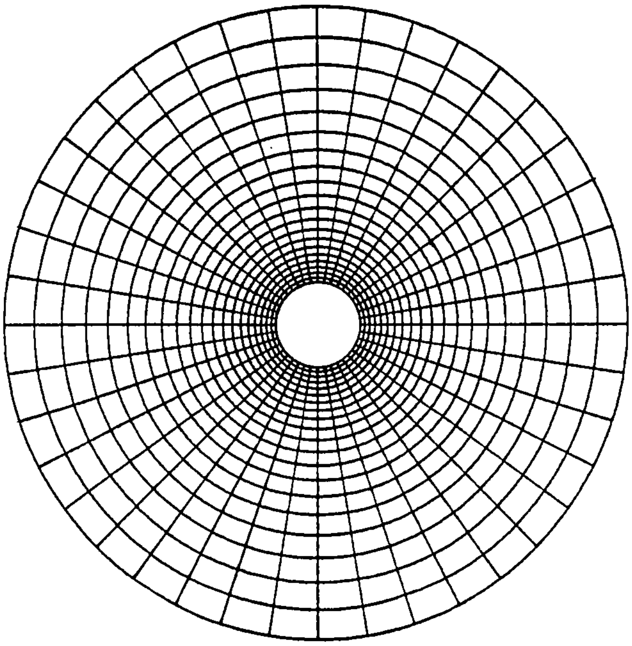

(b) grids in physical plane

Fig. 3-2. Mesh 21 $\times$ 41 with $\xi = 2.0$

in this study. Hence, $\frac{\partial \Xi}{\partial \chi}$, $\frac{\partial^2 \Xi}{\partial \chi^2}$ and $\frac{\partial \Xi}{\partial t}$, for example, are approximated at the grid point (i, j) by

$$\frac{\partial \Xi_{i,j}}{\partial \chi} = \frac{\Xi_{i+1,j} - \Xi_{i-1,j}}{2\Delta\chi},$$
$$\frac{\partial^2 \Xi_{i,j}}{\partial \chi^2} = \frac{\Xi_{i+1,j} - 2\Xi_{i,j} + \Xi_{i-1,j}}{\Delta\chi^2},$$
$$\frac{\partial \Xi_{i,j}}{\partial t} = \frac{\Xi(t+\Delta t)_{i,j} - \Xi(t)_{i,j}}{\Delta t}.$$

In which Ξ and χ represent any dependent and spatial independent variables for general purposes.

Thus, the governing differential equations (3.9), (3.10) can be approximated by the finite difference form;

$$\frac{\psi_{i+1.j}^{(n+1)} - 2\psi_{i,j}^{(n+1)} + \psi_{i-1,j}^{(n+1)}}{\Delta\xi^2} + \frac{\psi_{i,j+1}^{(n+1)} - 2\psi_{i,j}^{(n+1)} + \psi_{i,j-1}^{(n+1)}}{\Delta\eta^2} = e^{2\xi_{i,j}}\zeta \qquad (3.13)$$

$$e^{2\xi_{i,j}} \frac{\zeta_{i,j}^{(n+1)} - \zeta_{i,j}^{(n)}}{\Delta t} + \frac{(U\zeta)_{i+1,j}^{(n+1)} - (U\zeta)_{i-1,j}^{(n+1)}}{2\Delta\xi} \frac{(V\zeta)_{i,j+1}^{(n+1)} - (V\zeta)_{i,j-1}^{(n+1)}}{2\Delta\eta}$$
$$= \frac{2}{R_e}\left(\frac{\zeta_{i+1,j}^{(n+1)} - 2\zeta_{i,j}^{(n+1)} + \zeta_{i-1,j}^{(n+1)}}{\Delta\xi^2} + \frac{\zeta_{i,j+1}^{(n+1)} - 2\zeta_{i,j}^{(n+1)} + \zeta_{i,j-1}^{(n+1)}}{\Delta\eta^2}\right) \qquad (3.14)$$

in which the superscripts represent the time step, and superscript n represents time t, and n+1 represents the $t + \Delta t$. In this way, the continuous differential equations have been replaced by a discrete set of algebraic equations which are only valid at the grid points. In the following section, the calculation procedure for these discrete algebraic equations are described.

§3.4 Solution Procedure

In this section, ADI and SOR methods are introduced to solve the algebraic governing equations. Also the corresponding solution conditions, both the boundary and initial conditions, are discussed.

A. ADI and SOR

The vorticity equation is parabolic in time, and the stream function equation is elliptic (Poisson equation). To cope with the problem in hand, an alternating direction implicit (ADI) method is proposed to solve the vorticity equation, while the successive over-relaxation (SOR) is used to solve for the stream function equation. The ADI method can provide enough numerical stability because it still keeps the implicit nature of the scheme; a conventional implicit solution, which requires a larger computer storage, is avoided. For each time step, the two equations for stream function and vorticity are coupled and should be solved simultaneously. The whole process in numerical calculation can be described in general as: advancing the vorticity solution in time while ensuring that the stream function equation and the spatial boundary conditions are satisfied. However, because of the nonlinearity of the problem, as well as the unknown stream function that initially provides the boundary condition for vorticity at each time step, an iterative process is required to solve these two dependent variables.

The ADI method used to solve for the vorticity is of second order accurate in time, also in spatial variables and the scheme is unconditionally stable. In applying the ADI method, the time step in Equation (3.14) is split into two halfsteps, where an intermediate solution $\zeta_{i,j}^{(n+\frac{1}{2})}$ is obtained at time $t+\frac{1}{2}\Delta t$. Over the first halfstep from t to $t+\frac{1}{2}\Delta t$, η-direction derivatives are expressed implicitly, while ξ-direction derivatives are kept at their values at t. Over the second halfstep from $t+\frac{1}{2}\Delta t$ to $t+\Delta t$, η-direction derivatives retain their values at $t+\frac{1}{2}\Delta t$, while ξ-direction derivatives are expressed implicitly. While each halfstep is only first order accurate in time, the total procedure is second order accurate in time.

The vorticity equation written in ADI two-step method is replaced by, for the first halfstep implicitly in η direction,

$$a\frac{\zeta_{i,j}^{(n+\frac{1}{2})}-\zeta_{i,j}^{n}}{\frac{1}{2}\Delta t}+\frac{\partial\left(U_{i,j}^{(-)}\zeta^{(n+\frac{1}{2})}\right)}{\partial\eta}-\frac{2}{Re}\frac{\partial^2\zeta^{(n+\frac{1}{2})}}{\partial\eta^2}$$

$$=\frac{2}{Re}\frac{\partial^2\zeta^{n}}{\partial\xi^2}-\frac{\partial\left(V_{i,j}^{(-)}\zeta^{n}\right)}{\partial\xi} \tag{3.15a}$$

and for the second halftime in which implicitly in ξ direction,

$$a\frac{\zeta^{(n+1)}-\zeta^{(n+\frac{1}{2})}}{\frac{1}{2}\Delta t}+\frac{\partial\left(V_{i,j}^{(+)}\zeta^{n+1}\right)}{\partial\xi}-\frac{2}{Re}\frac{\partial^2\zeta^{(n+1)}}{\partial\xi^2}$$

$$=\frac{2}{Re}\frac{\partial^2\zeta^{(n+\frac{1}{2})}}{\partial\eta^2}-\frac{\partial\left(U_{i,j}^{(+)}\zeta^{(n+\frac{1}{2})}\right)}{\partial\eta} \tag{3.15b}$$

where $a=e^{2\zeta_{i,j}}$.

In Equations (3.15a) and (3.15b), U^-, V^-, U^+ and V^+ are intermediate approximations of U and V within one time step. The predictor value $\zeta_{i,j}^{(n+\frac{1}{2})}$ can be considered as an approximation of the exact solution at time $(n+\frac{1}{2})\Delta t$ if U^-, V^- and U^+, V^+ are suitable approximations. For example, if only first order accuracy in time is required, the simple expressions $U^+ = U^- = U^{(n)}$ and $V^+ = V^- = V^{(n)}$, where $U^{(n)} = U(\zeta^{(n)})$ and $V^{(n)} = V(\zeta^{(n)})$, can be used. The accuracy is of second order in the special case where U and V are constants[40].

For second-order accuracy in time with U, V nonconstant, the general form of approximation could be:

$$U^{\pm}=C_oU^{(n+1)}+(1-C_o-C_1)U^{(n)}+C_1U^{(n-1)} \tag{3.16a}$$

$$V^{\pm}=C_oV^{(n+1)}+(1-C_o-C_1)V^{(n)}+C_1V^{(n-1)} \tag{3.16b}$$

where C_o, C_1 are constants chosen depending on accuracy requirement. In this work, C_o and C_1 are simply taken as 0.5.

For solving the vorticity equation, the velocity components in the equations are computed from the known stream function by a second order central-difference to match the same accuracy as in ADI. That is

$$V_{i,j} = -\frac{\psi_{i+1,j} - \psi_{i-1,j}}{2\Delta\xi}, \tag{3.17a}$$

$$U_{i,j} = \frac{\psi_{i,j+1} - \psi_{i,j-1}}{2\Delta\eta}. \tag{3.17b}$$

Therefore, the Equations (3.15a) and (3.15b) can be simplified as the following short form

$$a_j\zeta_{i,j-1}^{(n+\frac{1}{2})} + b_j\zeta_{i,j}^{(n+\frac{1}{2})} + c_j\zeta_{i,j+1}^{(n+\frac{1}{2})} = d_j, \tag{3.18}$$

$$A_i\zeta_{i-1,j}^{(n+1)} + B_i\zeta_{i,j}^{(n+1)} + C_i\zeta_{i+1,j}^{(n+1)} = D_i, \tag{3.19}$$

where a_j, b_j, c_j, d_j, A_i, B_i, C_i and D_i are approximated by evaluating from previous iteration results. Thus for the interior grid points $2 < i < I-1$ and $1 < j < J$, each of these expressions creates an algebraic equation and all of them result in a tridiagonal system of equations, which are solved by using forward- and backward-substitution and matrix factorization, respectively (see appendix B).

The stream function equation, in the form of a Poisson equation, is replaced by the difference equation (3.13),

$$\frac{\psi_{i+1,j}^{n+1} - 2\psi_{i,j}^{n+1} + \psi_{i-1,j}^{n+1}}{\Delta\xi^2} + \frac{\psi_{i,j+1}^{n+1} - 2\psi_{i,j}^{n+1} + \psi_{i,j-1}^{n+1}}{\Delta\eta^2}$$

$$= e^{2\xi_{i,j}}\zeta_{i,j}^{n+1} \tag{3.20}$$

its truncation error is of the second order $\theta(h^2)$, where $h = \sqrt{\Delta\eta^2 + \Delta\xi^2}$. The vorticity is adopted from the updated time level, and it plays the role as an influence function (non-homogenient term) in the elliptic differential equation. Its algebraic nature has not created any instability to equation (3.20)[41]. The equation can be written in an approximate form:

$$\bar{\psi}_{i,j}^{n+1} = \frac{1}{2(1+\beta^2)}\{\psi_{i+1,j}^{n+1} + \psi_{i-1,j}^{n+1} + \beta^2(\psi_{i,j+1}^{n+1} + \psi_{i,j-1}^{n+1})\}$$

$$-2\Delta\xi^2 e^{2\xi_{i,j}}\zeta_{i,j}^{n+1} \tag{3.21}$$

where $\beta = \frac{\Delta\xi}{\Delta\eta}$ = grid size ratio, and the barred value is the newly iterated value. Equation (3.21) is the classical " Jacob method", also called the "method of simultaneous displacement". Alternatively, the newly-iterated values are used as soon as possible during the sweeping. Thus, (3.21) can be rewritten as,

$$\bar{\psi}_{i,j}^{n+1} = \frac{1}{2(1+\beta^2)}\{\psi_{i+1,j}^{n+1} + \bar{\psi}_{i-1,j}^{n+1} + \beta^2(\psi_{i,j+1}^{n+1} + \bar{\psi}_{i,j-1}^{n+1})\}$$

$$-2\Delta\xi^2 e^{2\xi_{i,j}}\zeta_{i,j}^{n+1} \tag{3.22}$$

which is called the "Gauss-Seidel method," a method of successive displacement. It only used half as much storage as in the Jacobi method, and it converges as fast as Jacobi's.

A further improvement of the rate of convergence upon iteration of (3.22) is the "point successive-over (or under) -relaxation method"(SOR). Introducing the relaxation parameter λ, $(0 < \lambda < 2)$, Equation (3.22) becomes

$$\bar{\psi}_{i,j}^{n+1} = \psi_{i,j}^{n+1} + \frac{\lambda}{2(1+\beta^2)}\{\psi_{i+1,j}^{n+1} + \bar{\psi}_{i-1,j}^{n+1} + \beta^2(\psi_{i,j+1}^{n+1} + \bar{\psi}_{i,j-1}^{n+1})\}$$

$$-2\Delta\xi^2 e^{2\xi_{i,j}}\zeta_{i,j}^{n+1} - 2(1+\beta^2)\psi_{i,j}^{n+1} \tag{3.23}$$

where $\lambda < 1$, under-relaxation

$\lambda = 1$, Gauss-Seidel

and

$\lambda > 1$, over-relaxation.

It must be kept in mind that the ψ-inner iteration is executed upon the (n+1) time level. Values at n and n-1 time levels are temporary constants during the iteration process, the barred and the unbarred values are the (k+1)th and kth iterated values, respectively. A good estimate of λ would reduce the rate of convergence drastically. Young[42] and Verga[43] have derived the optimum relaxation parameter of SOR for a rectangular domain in solving Dirichlet type boundary condition. Unfortunately, the gigantic matrices in the present work do not satisfy the assumptions of their method, and therefore, the relaxation parameter can only be determined by trial and error. As long as the time marching procedure converges within an acceptable computer time, it is considered that the chosen relaxation parameter is the one needed. With the iterative methods, a basic question is when the iteration should be stopped. One criterion may be defined in terms of the norm $||\psi_{i,j}^{(k+1)th} - \psi_{i,j}^{kth}||$ or the residue of the matrix. The former approach is used in the present work. Because the solution at this step is still an estimated value, the stop error should not be too low. The details will be discussed later.

Finally, it needs to be noted, in the whole process of finding solutions, that equations for vorticity (3.18), (3.19) and for stream function (3.23) are coupled together by the iteration process. However at the beginning of the iteration solution for each new time step $t + \Delta t$, the value of ψ and the wall conditions for ζ must be given. Also it should be pointed out that solving the vorticity equation is the major difficulty in the stream function-vorticity approach because of the nonlinearity and unknown boundary conditions. For each time step, advancing the vorticity and then solving for the stream function, it gives an update approximation which is used to repeat the solution process for the vorticity. The iteration process for both vorticity and stream function within one time step is repeated until successive iterations differ by a norm as if used in the inner iteration for the stream function solution alone. That is

$$||\zeta_{i,j}^{(m+1)th} - \zeta_{i,j}^{mth}|| < \varepsilon_{\nu}, \qquad ||\psi_{i,j}^{(m+1)th} - \psi_{i,j}^{mth}|| < \varepsilon_{s} \tag{3.24}$$

It should be noted that here the iteration is for the outer iteration. Even though the criterion is applied to the same variable ψ, it is totally different from that of the previous inner iteration. This criterion is used to check the successive errors of that variables in the outer iteration. Only when the conditions in (3.24) are satisfied, are the results considered as the converged solution. Following the same principle, another new time step can proceed until the expected time is arrived for the time-dependent problem in hand.

B. Initial flow development

In view of the fact that an impulsively started flow at $t = 0^+$ is basically still a potential flow[44], the inviscid flow field is assumed as the starting condition. For $t > 0$, a thin vortex sheet is formed on the body surface due to the adherence condition. The generated vorticity is then diffused rapidly into the flowfield, similar to that of the Rayleigh problem of a suddenly accelerated wall. However, a numerical attempt to advance the viscous solution from the inviscid initial condition will generally fail to capture the instantaneously developed viscous region, and thus it is an ill-posed numerical problem.

To overcome this difficulty, an asymptotic expansion around a small incipient time can be employed to advance the solution to a present time $t = t_0$, such that a sufficient number of grid points may fall into the larger gradient region. Then the solution of the time-dependent flow for $t > t_0$ could be advanced from this incipient condition by numerical means. The details about the solution time sequence will discussed later.

Consequently, at $t = 0^+$, the initial condition for the flow around a circular cylinder of radius 1 is:

$$u_\theta = \left(1 + \frac{1}{r^2}\right)\sin\theta \qquad \text{at } t = 0^+,$$

$$u_r = -\left(r - \frac{1}{r}\right)\cos\theta \qquad \text{at } t = 0^+. \tag{3.25}$$

The familiar no-slip and no-penetration conditions are imposed on the surface of the cylinder, or

$$u_r = u_\theta = 0 \quad \text{at} \quad r = 1$$

and the flow should merge smoothly into the undisturbed free stream at infinity.

For the early stages of the starting flow, the Reynolds number and Strouhal number are assumed to be the same order in the following analysis, say $\bar{\varepsilon}^{-1}$, or

$$\mathrm{Re} = 0(\bar{\varepsilon}^{-1}), \qquad St = 0(\bar{\varepsilon}^{-1}).$$

So an asymptotic expansion in powers of $\bar{\varepsilon}$ is then possible.

Introduce a stretch variable in the direction normal to the wall, or the radial direction in the present problem,

$$\overline{r} = \frac{r-1}{\bar{\varepsilon}}$$

and the familiar variable $\bar{\eta}$ for inner region of the flow,

$$\bar{\eta} = \frac{\overline{r}}{2\sqrt{t}}$$

So the inner and outer expansion in term of a stream function are made

$$\psi = \bar{\varepsilon}\psi_0(\bar{\eta},\theta,t) + \bar{\varepsilon}^2\psi_1(\bar{\eta},\theta,t) + \dots$$

$$\text{and} \quad \Psi = \Psi_0(r,\theta,t) + \bar{\varepsilon}\psi_1(r,\theta,t) + \dots$$

To match the inner and outer solutions at this level, an intermediate variable is introduced

$$\tilde{\eta} = \sqrt{\varepsilon}\eta$$

Finally a composition solution is obtained[44]

$$\begin{aligned}\psi = &\left(r - \frac{1}{r}\right)\sin\theta + 4\bar{\varepsilon}\sqrt{\frac{t}{\pi}}\left[-\frac{1}{r} + e^{-\bar{\eta}^2} - \sqrt{\pi}\bar{\eta}(1 - erf\bar{\eta})\right]\sin\theta \\ &+ 4\bar{\varepsilon}^2\frac{t}{\sqrt{\pi}}\left[-\frac{\sqrt{\pi}}{4}erf\bar{\eta} + \frac{3\sqrt{\pi}}{2}\bar{\eta}^2(1 - erf\bar{\eta}) - \frac{3}{2}\bar{\eta}e^{-\bar{\eta}^2}\right]\sin\theta \\ &+ 4\bar{\varepsilon}^2 t^{3/2}\int_0^{\bar{\eta}} f(\bar{\eta})d\bar{\eta}\cdot\sin 2\theta + 0(\bar{\varepsilon}^3)\end{aligned}$$

In which erf is the error function and

$$\begin{aligned}f(\bar{\eta}) = &\frac{1}{2}(2\bar{\eta}^2 - 1)erf^2\bar{\eta} + \frac{3}{\sqrt{\pi}}\bar{\eta}e^{-\bar{\eta}^2}erf\bar{\eta} + 1 \\ &- \frac{4}{3\pi}e^{-\bar{\eta}^2} + \frac{2}{\pi}e^{-2\bar{\eta}^2} - \left(1 + \frac{2}{3\pi}\right)(2\bar{\eta}^2 + 1) \quad . \\ &+ \frac{1}{\sqrt{\pi}}\left(1 + \frac{4}{3\pi}\right)\left[\frac{\sqrt{\pi}}{2}(2\bar{\eta}^2 + 1)erf\bar{\eta} + \bar{\eta}e^{-\bar{\eta}^2}\right]\end{aligned}$$

C. Boundary Conditions

Since the equation for the vorticity is of parabolic nature in time, its solution can be matched in the time direction with the initial condition discussed above. But as the vorticity equation and stream function are of elliptic type in the spatial variables, proper boundary conditions must be applied.

For the viscous flow, the solid body boundary conditions are no-slip and non-penetrateable at the surface and uniform flow at infinity. It should be addressed that the boundary condition must be transformed into the computational plane along with the governing equations. Due to the advantage of the chosen coordinate system, the various dependent variables have a periodic nature in the circumferential direction. Therefore, real boundary conditions are only necessary in the radial direction for any practical solution.

(a) Boundary condition for stream function

Owing to the pure rotational motion of the cylinder, at any moment the cylinder surface is always a stream surface. Any constants may be assigned to the value of stream function ψ on the surface. The conventional choice is $\psi = 0$ at the wall boundary $\zeta = 0$, which is in the same form for a stationary and moving cylinder. However the evaluation of ψ at the outer boundary ∂B_∞, which is controlled by choosing the parameters ξ_0, is one of the most interesting computational boundary value problems. We must somehow neglect the details of farther downstream flow and obtain realistic answers upstream. From the wind tunnel experience, if the "test section" is long enough, the downstream flow is not important[29]. In this work, a non-reflection boundary condition is applied to the downstream boundary of the computational region. But care is needed to ensure that catastrophic instabilities are not propagated upstream from the outer boundary and destroy the solution. On this point, what can be done is to check the solution by changing the size of the outer boundary. If the change of the size influences the solution within an acceptable value, the solution is considered to be realistic.

(b) Vorticity on boundaries

One of the problems in using the vorticity equation is that its boundary conditions are unknown. Yet they must somehow be derived from the known interior solutions, which could introduce errors if not treated correctly.

Physically, the diffusion of vorticity is the mechanism indicating the momentum loss in a viscous flow. Usually the greatest change of vorticity occurs near the boundary of a surrounded body. More precisely, the vorticity transport equation determines how vorticity is advected and diffused, but the total vorticity is conserved at interior points. At no-slip boundaries, vorticity is produced (either source or sink). It is the diffusion and subsequent advection of this wall-produced vorticity which actually drives the problem. So, should the wall vorticity be obtained by an incorrect means, the result will be either numerically unstable or beyond the physical reality.

Before the general theory for unsteady viscous flow is built, some concepts of steady flow had to be used. The absolute value of vorticity indicates the degree of local momentum. The positive or negative sign only designates the orientation of the pseudo-vectorial vorticity. A solid boundary, immersed in a viscous flow, is equivalent to having a distributed source of vorticity. Separation occurs near the point where the source and sink change orientations[45]. This concept is used in predicting the flow separation, which is discussed later.

The boundary condition of the vorticity is so important for the solution, that its treatment in the numerical solution should be extremely careful. Prior to considering wall-boundary, a simple discussion is given of the outer boundary of the solution region. The uniform flow far-upstream provides a zero vorticity condition there. At the downstream boundary, the vorticity can be evaluated from the stream function solution by using a one-sided finite difference.

On the wall-boundary, the vorticity is controlled by the no-slip condition. From the relationship between vorticity and stream function, the boundary vorticity is

$$\zeta\Big|_{\partial B} = \nabla^2\psi\Big|_{\partial B} \tag{3.26}$$

where ∂B represents the boundary of the body. The non-slip condition means that: on the body surface, the normal velocity is zero, and the tangential velocity equals the local velocity of the cylinder at the boundary for the present unsteady problem. Generally, there are two approaches to determine the vorticity on boundaries: one is the mirror-image technique directly from the stream function equation, the other is by the Taylor expansion. The later is used here. We expand $\psi_{w+1,j}$ by a Taylor series from the wall values, $\psi_{w,j}$

$$\psi_{w+1,j} = \psi_{w,,j} + \frac{\partial\psi}{\partial\xi}\Big|_{w,j}\Delta\xi + \frac{1}{2}\frac{\partial^2\psi}{\partial\xi^2}\Big|_{w,j}\Delta\xi^2 + 0(\Delta\xi^3)$$

where $\frac{\partial\psi}{\partial\xi}\Big|_{w,j}$ is the local velocity V_t of the cylinder surface, which is known from the given applied oscillation on the cylinder. Finally, the vorticity on the body boundary can be obtained as

$$\zeta_{w,j} = \frac{2\psi_{w,j}}{\delta\xi^2} - \frac{2V_t}{\delta\xi} \tag{3.27}$$

where w represents the cylinder surface. For the stationary cylinder case, equation (3.27) can be simplified as

$$\zeta_{w,j} = \frac{2\psi_{w+1,j}}{\delta\xi^2} \tag{3.28}$$

which will be used for the impulsively started flow calculations.

The first-order form of (3.28) was given as early as 1928 in the pioneering work of Thom[29] and has been used extensively since then. It is the safest form to use, and it often gives result essentially equal to higher order forms. Here we extend it to the flow with a moving boundary.

As described earlier, the boundary points always lie on the grids in this work. So does the finite difference quotients. Therefore, the subscript w in (3.27) and (3.28) can be replaced by subscript 1 as shown in Figure 3-3. The coincidence of grid points and the wall is very much of advantage, otherwise an extrapolation or interpolation is needed to apply boundary condition on the wall, which often results in great errors.

The basic solution conditions for the usual solution procedures have been introduced. However, since the ADI method is time-split, the time-split has effects

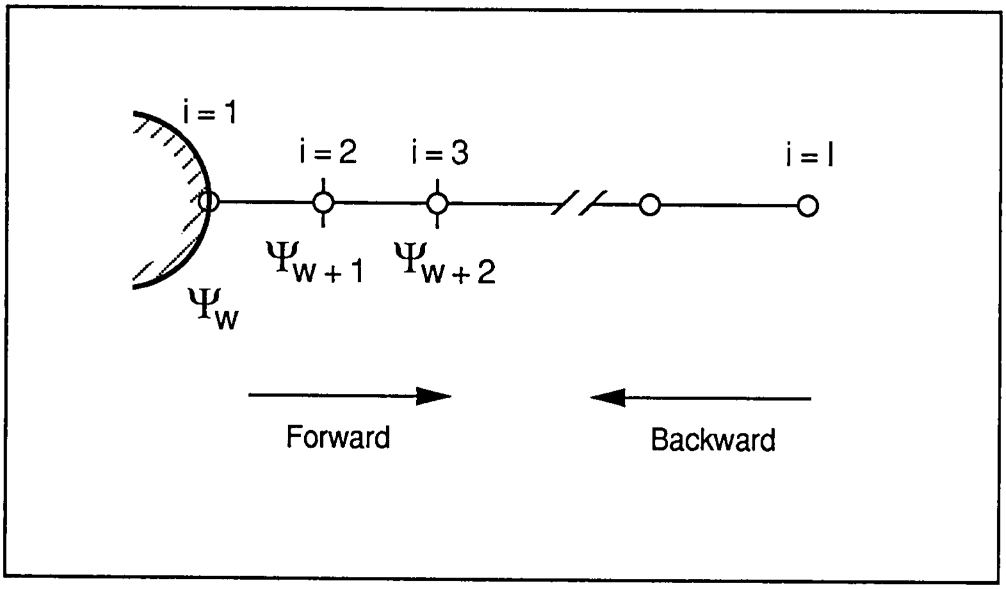

Fig. 3-3. Sketch of boundary grids

on the boundary conditions. In the following section, the time-split boundary condition is discussed.

(c) Time-split on boundary conditions

After getting each time-step boundary condition (3.27) or (3.28), we face a question of how to obtain the value of intermediate quantities on the boundary. Because in the ADI method, in which each time step is consistent with the original equation, an increase of the truncation error with respect to time appears for points adjacent to a boundary, if the exact time-varying boundary values are used to determine the provisional values on the boundary[40]. The usage of the boundary value $\zeta^{n+\frac{1}{2}}\big|_{\partial B} = \zeta(n + \frac{1}{2}\Delta t)\Big|_{\partial B}$ leads to a larger truncation error near the boundary. The best way to overcome this difficulty is to define a boundary value such that the combination of both time step yields second-order accuracy at points adjacent to the boundary as well as inner points. This can be accomplished if the value $\zeta^{(n+\frac{1}{2})}\big|_{\partial B}$ is deduced from the finite difference equations themselves. By using the two half-step equations (3.15a), (3.15b) and the no-slip boundary condition, there is

$$\zeta^{(n+\frac{1}{2})}\Big|_{\partial B} = \{\frac{1}{2}(\zeta^{n+1} + \zeta^{n}) - \frac{\Delta t}{Re}\frac{\partial^2(\zeta^{n+1} - \zeta^{n})}{\partial \eta^2}\}\Big|_{\partial B} \qquad (3.29)$$

This equation determines the value $\zeta^{(n+\frac{1}{2})}$ on ∂B because $\zeta^{(n+1)}$ and $\zeta^{(n)}$ are known on this boundary.

§3.5 Computer Program and Results

In this branch of the work, the study of the interaction between unsteady viscous flow and the surrounded body is emphasized. The numerical calculation is performed by following a practical starting flow process. A schematic of the solution time sequence is shown in Figure 3-4. The numerical solution of the flow is initialized from an analytic impulsively started flow solution. After the impulsively started flow gets well-developed, in which a non-symmetric wake with a natural vortex shedding frequency, i.e., Karman vortex street, developed, a computation for the oscillating boundary is started. The above stated well-developed flow around a stationary cylinder is used as its initial condition for the unsteady problem.

In fact, an impulsively started flow itself is a very interesting subject for study of the unsteady viscous flow. The basic mathematical formulation of flow with a steady or a unsteady boundary is the same except the difference in boundary condition. The computational process and the programming logic for both of them are described in a sequence below.

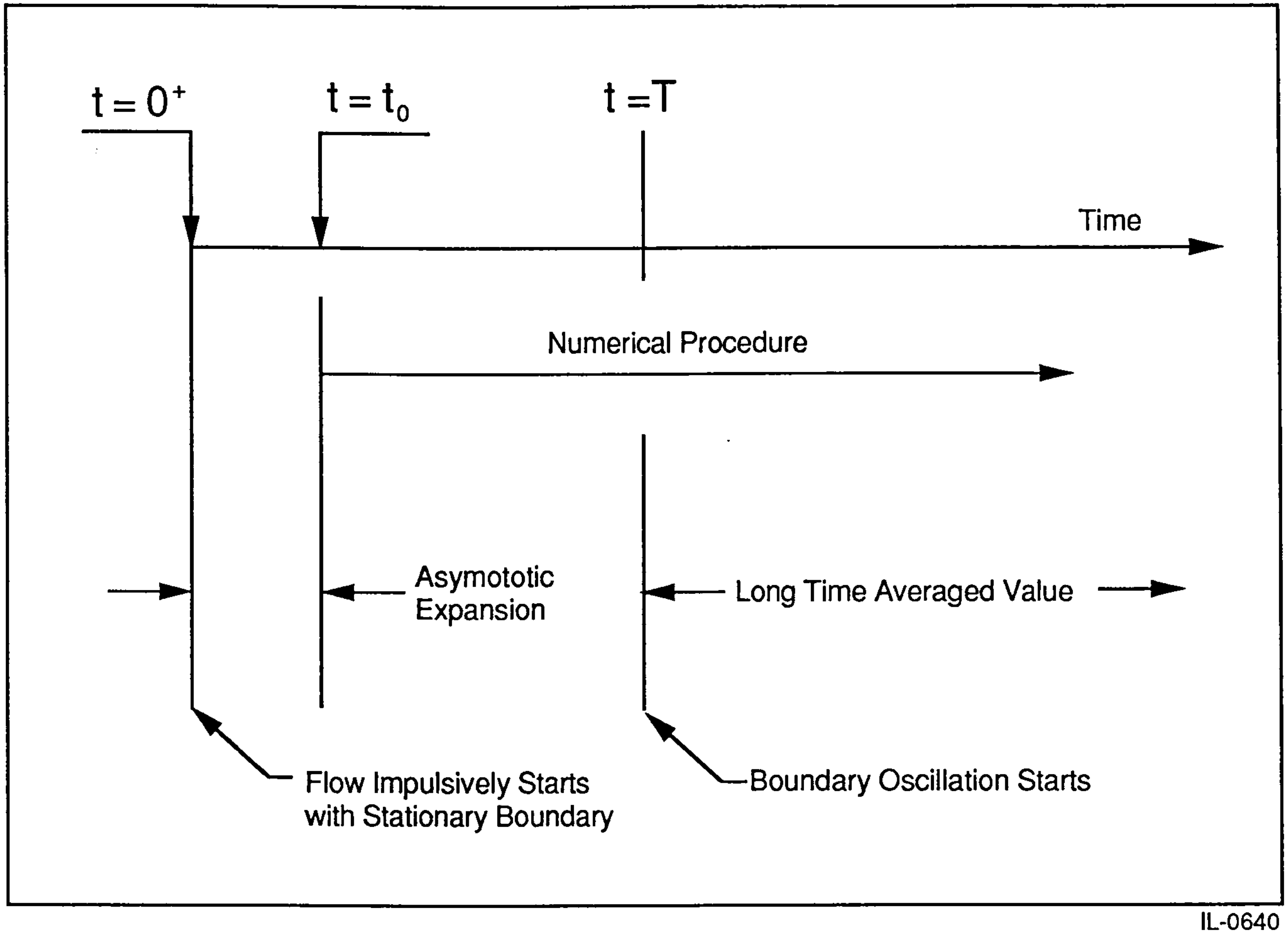

Fig. 3-4. Schematic of solution time sequence

A. Computer Program

In order to visualize the numerical calculation process more clearly, the flow diagram is shown in Figure 3-5, which is written in a form valid for the general unsteady flow problems. Step 1. Call system to assign one INPUT file and one OUTPUT file. It is more convenient to adjust the input parameters instead of changing the original program.

Step 2. Call subroutine INPUT. All required parameters in the calculation are stored in the INPUT, which includes the time interval, Reynolds number, Strouhal number, oscillation amplitude, Geometries in terms of grids, convergence parameters, maximum number of time steps and relaxation parameter. Naturally when the oscillation amplitude is taken as zero, the corresponding flow is that around a stationary cylinder.

Step 3. Because of the infinite flow region, a coordinate transformation is needed. Before starting to solve the problem, a subroutine COOR is used to generate the grids. In this program, a stretching in the radial direction is used and grids are created based on the number of grids given in step 2. After this, all physical quantities have been discretized on the grid points.

Step 4. Since the flow is initially at rest with a sudden starting, a subroutine INIT is provided to give an initial condition for the numerical calculation. The initial condition is obtained from a small time expansion solution to the exact Navier-Stokes equation. The initial time t_0 is usually taken very small, so that the order of approximation solution does not make a significant difference. In this program, the first order approximation is adopted. The discrete values of stream function and vorticity of the initial field on grid points are obtained directly from the analytical solution.

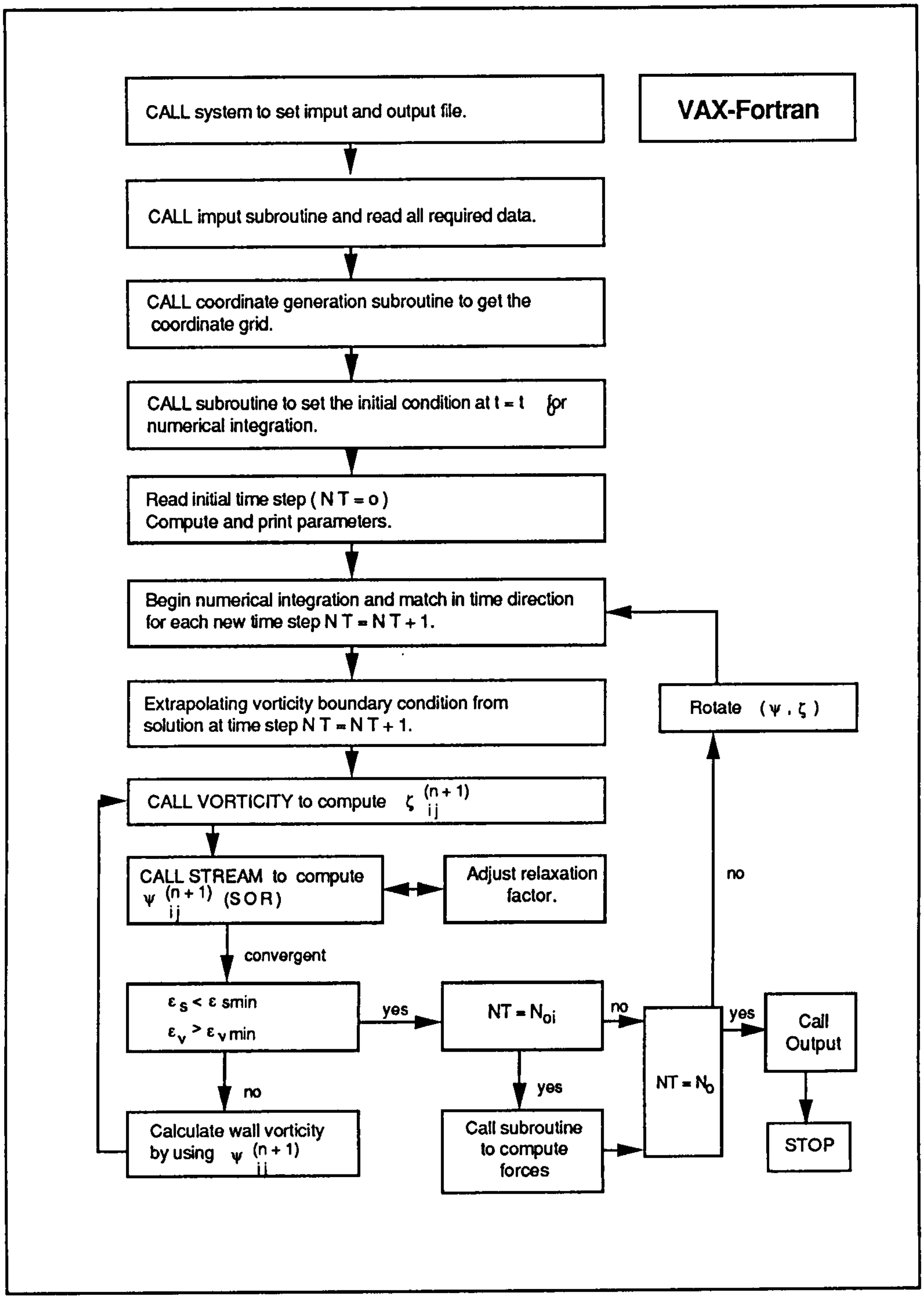

Fig. 3-5. Flow diagram of vorticity stream function method

Step 5. Compute the necessary constants, print out all constants and parameters. Then the time marching process is started by setting time accounting number $NT = 1$.

Step 6. For each new time step, the vorticity solution is designed to lead the iteration in this program. So the boundary vorticity needs to be guessed for the first circle of iteration. Here an extrapolation is used from the former two time steps.

Step 7. Call subroutine VORTEX to solve for ${\zeta_{i,j}}^{n+1}$ in the interior region by solving two tridiagonal equation systems in the two coordinate directions, which corresponds to the first half time step and second half time step respectively. Because the governing equation is parabolic in time, no iteration is needed in solving vorticity within every outer iteration.

Step 8. Call subroutine STREAM to compute ${\psi_{i,j}}^{n+1}$, at all interior points by the over-relaxation procedure. It is noted that only the ${\zeta_{i,j}}^{n+1}$ of the interior points come into the computation. The number $\varepsilon_i = 10^{-5}$ is given as the criterion value of convergence, and a maximum iteration time is set at 500. Should the iteration exceed this value, it is considered that the problem has not been properly arranged. Then the program will stop and give the detailed output. The situation has to be reconsidered from the very beginning. Within this step, the iteration is the inner iteration. The convergent results will join the outer iteration together with the solution of the vorticity.

Step 9. Call subroutine BOUN to compute all boundary vorticity from the updated interior stream function solution to continue the iteration process within one time step. In this subroutine, the boundary conditions for vorticity can be determined for the general cases as discussed in (3.27).

Step 10. After the computation of ${\psi_{i,j}}^{n+1}$ and ${\zeta_{i,j}}^{n+1}$ each time, it constitutes one time outer iteration. Also it is necessary to make the following checks in order to determine whether to advance a new time step or continue the iteration:

(i) Check the convergence. In solving the stream function and vorticity, two equations are coupled together by iteration. Two criteria are defined to two dependent variables, which are $\varepsilon_\nu = 10^{-5}$ and $\varepsilon_s = 10^{-5}$, respectively. The convergence is considered as within the time step, when the solution in successive iterations differs from that in the former iteration by the amount less than the above values. That is, in the mathematical form, the norms in (3.24) are taken as

$$Max|\psi_{i,j}^{k+1} - \psi_{i,j}^{k}| < \varepsilon_s$$

$$Max|\zeta_{i,j}^{k+1} - \zeta_{i,j}^{k}| < \varepsilon_\nu$$

here i $\in$ I and j $\in$ J, k is the kth outer iteration number. If this is satisfied, check the next item. Otherwise, continue the iteration from step 7 to step 10.

(ii) If the time step number NT is greater than the assigned maximum number, e.g., 100, output all the information. Otherwise, follow the next step. Here there are two items that need to be considered. One option is for the solution of the impulsively started flow. Usually the time of five natural periods is considered long enough for the starting flow development. Then the boundary conditions are changed into that with applied oscillation. The time marching is continued until the required time is arrived. All the details are shown in the results.

Step 11. Advance stream function and vorticity such that

$$(\psi, \zeta)_{i,j}^{n} \rightarrow (\psi, \zeta)_{i,j}^{n-1}$$

$$(\psi, \zeta)_{i,j}^{n+1} \rightarrow (\psi, \zeta)_{i,j}^{n}$$

for all i $\in$ I and j $\in$ J. Therefore the solution advances to a new time step $NT = NT + 1$. Then repeat the cycle described from step 6 to step 11.

B. Numerical results

Calculations were performed on a VAX-11/785 computer at the University of Tennessee Space Institute (UTSI). The over-relaxation factor for the stream function is chosen by trial-and-error, and finally the value of 1.65 was used in obtaining the results. The incipient time t_0 used in the analytical initial condition from starting was taken as 0.01. All the time is reduced time. Depending on the Reynolds number, the grid numbers and time-step length are chosen to guarantee numerical stability. Basically, the following limits need to be satisfied:

$$1. < \frac{U_\infty \Delta r}{\nu} < 10.$$

$$\frac{U_\infty \Delta t}{\Delta r} \approx 1. \sim 2.$$

Under the above requirements, the different grid numbers are used for different Reynolds number flows.

The numerical results for various flows are presented here, which include the impulsively started flow development process around a steady cylinder and the flow charateristics when with a rotationally oscillating boundary.

1. Solution of Impulsively Started Flow

The development of the flow induced by an impulsively started circular cylinder with time is a classic problem in fluid mechanics[46−53]. Although the geometry is simple, the phenomena appears to be complex. The theoretical work on this problem basically fall into two main classes. First, the flow for small times, before the appearance of the wake, may be studied using boundary layer theory. Blasius, etc., have considered this problem as the limiting case of infinite Reynolds number. Collins and Dennis[44] have extended the work to finite but still high values of

Reynolds number. The results, however, only indicate the flow structure for small times after starting. But for the flow with "any" values of the Reynolds number, the effective means for that highly non-linear problem should be the purely numerical solution, which is classified as the second one.

In this work, the solutions of the Navier-Stokes equations are performed for different Reynolds number flows. The properties of the development of the unsteady wake, e.g., the length of the pair of the standing eddies formed behind the cylinder, the separation angle which is a function of time for various values of Reynolds number, the formulation of the secondary vortices and the vorticity distribution along the body surface, will be presented in this part of numerical solution. The results are checked with the available experiment or numerical solution by others.

a. Flow separation

(i) First or major separation: Because of viscosity and adverse pressure gradient along the rear part of the cylinder, the main stream could not provide enough kinetic energy to the fluid near the body surface to downstream, a reverse stream is formed. For steady two-dimensional flow, the separation point is the zero skin-friction point on the surface. But for unsteady flow, it is still a controversial problem, even for two-dimensional flow. A simple criterion is adopted in this computation, which is the vorticity vanishing point at the surface. The computed separation time of flows with Reynolds numbers ranging from 150 to 550 are shown in Figure 3-6. The analytical solutions[44] are used to compare with this numerical result. They agree with each other reasonably well.

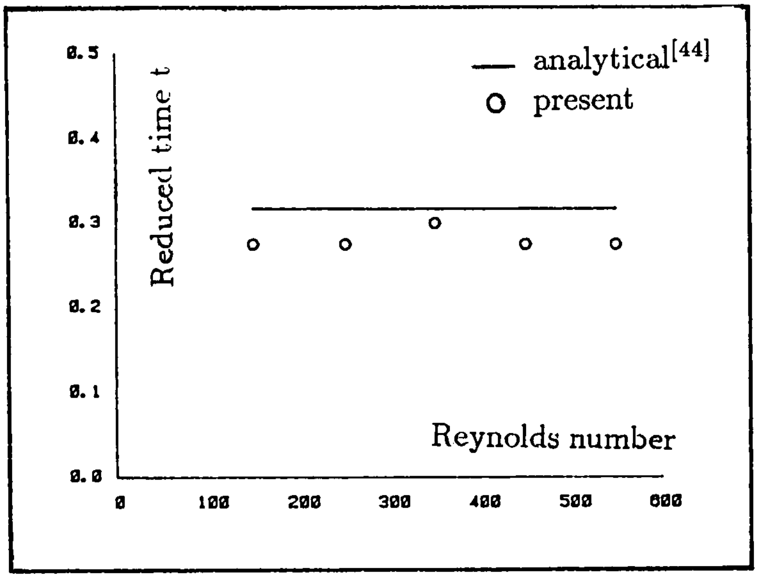

Fig. 3-6. Separation time vs. analytical results

(ii) Secondary separation: Besides the major separation, a secondary separation phenomena also appears during the flow development. The secondary eddy, which has a rotation opposite to that of the main eddy, is due to a second separation of the flow, i.e., a separation of the backflow itself from the cylinder wall. Of course, this occurs when the velocity in the recirculating zone is high enough, as in the first separation case. The computed results for flow with $Re = 550$ presented in Figure 3-7 is in good agreement with the available flow visualization photo.[27].

b. Vorticity distribution on the surface

The presence of these first and secondary separation phenomena can be detected from the distribution of strength of the vorticity over the surface of the cylinder. For flow without separation, the vorticity should keep the same sign on the surface, and for flow only with first separation, the vorticity is negative in the whole separated zone; it decreases from zero (at the rear stagnation point), reaches a minimum and regularly increase to take again a zero value at the point of separation S. Beyond S, the vorticity is positive and still increases up to the front stagnation point. The appearance of a bulge in the streamline pattern must rise to an alteration in the vorticity of distribution and the "birth" of a secondary eddy must be indicated by a positive vorticity in the separation zone. Figure 3-8 shows the results of the vorticity distribution sequence on the cylinder surface with time for the flow with Reynolds number 300.

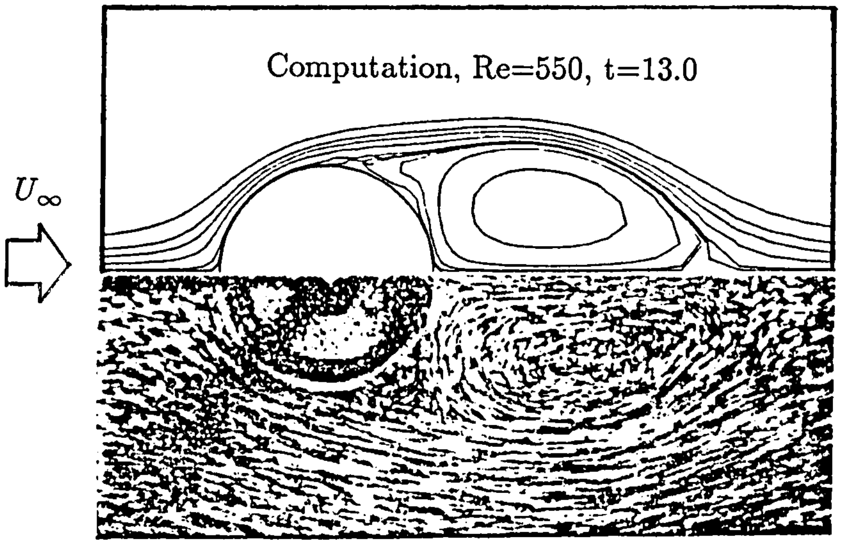

Flow visualization[27], Re $\approx$ 550

Fig. 3-7. Steady cylinder stationary wake

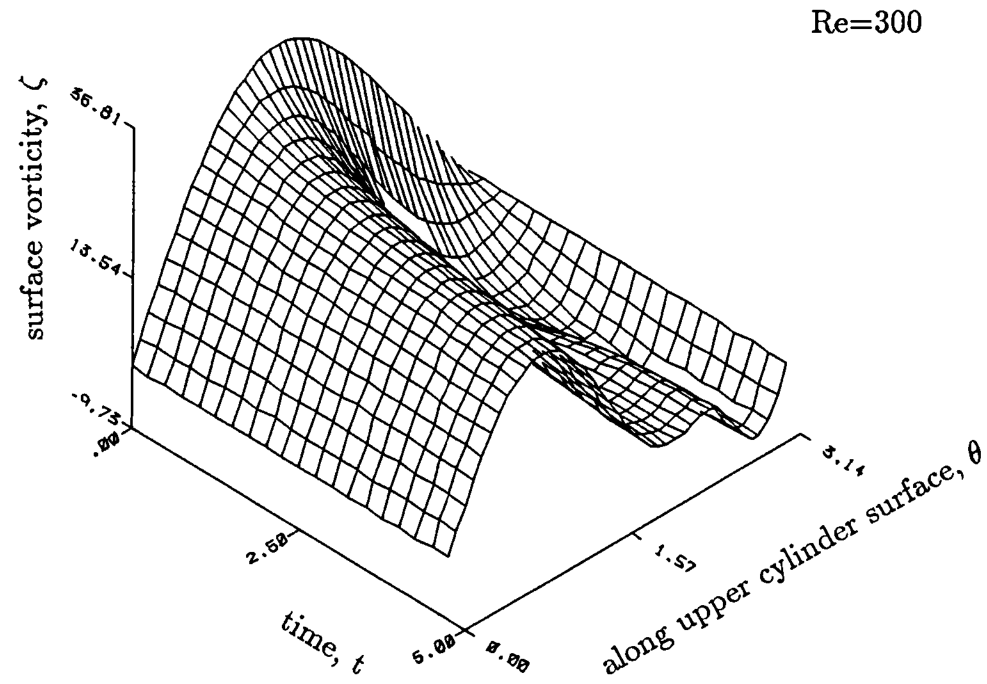

Fig. 3-8. Vorticity variation with time on surface

c. Exterior boundary of recirculating zone

For the problem in hand, the focus is on the flow detached from the wall. Our goal is to find the internal flow mechanism, which may respond to the excitation and the control of the energy associated with the detached vortex system in the flowfield. The exterior boundary of the detached zero streamline limits the main viscous region. Figure 3-9 shows the results of the exterior boundary on the started flow with Re = 300 and Re = 550 at different time level. Actually, the recirculating zone is a vortex flow. The zero velocity point in the region is referred to as its center. This center point was found from the stream function solution by a steepest gradient method. The computed results for vortex centers are shown in Figure 3-10 at different times. The analytical result of free vortex pathline from

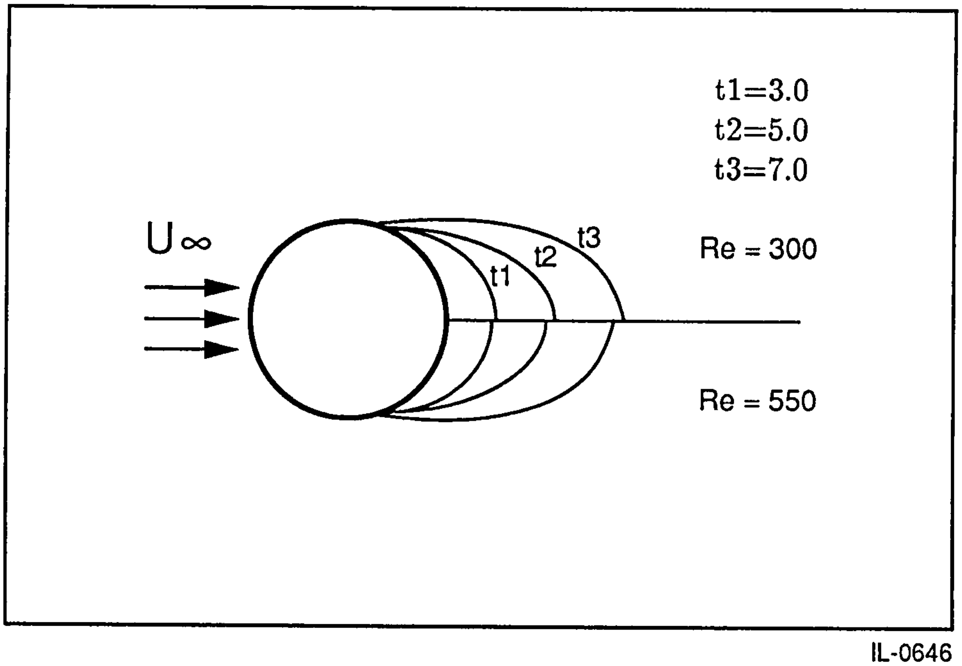

Fig. 3-9. Evolution of the closed wake shape

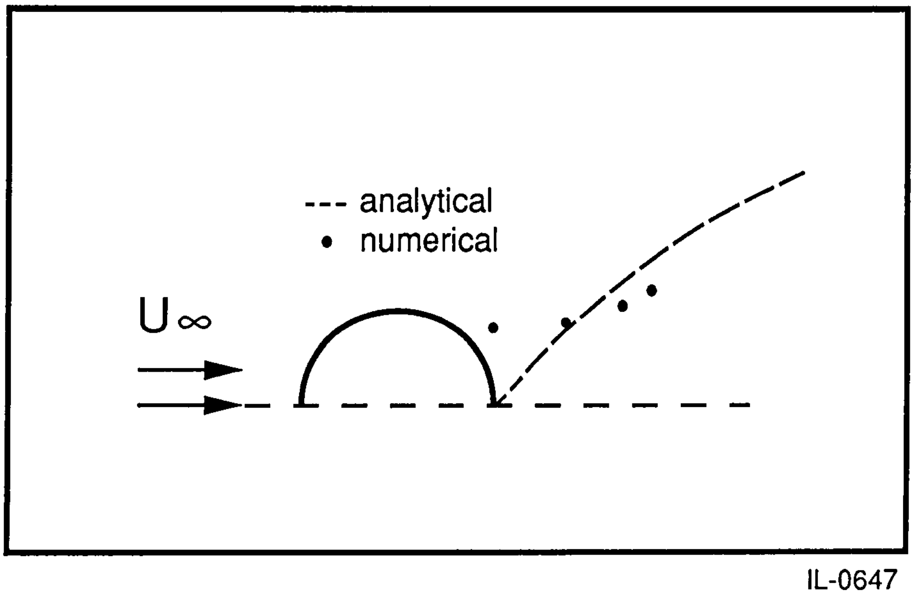

Fig. 3-10. Zero velocity points of closed wake

the potential flow model in chapter II are shown by a dashed line to compare with each other. It can be seen that: when the vortex center is very close to the wall, the two results have large deviation, which is attributed to the viscous effect. Finally, a sequence of the stream function and vorticity contour lines at several time stations for $Re = 300$ and $Re = 550$ are shown in Figure 3-11.

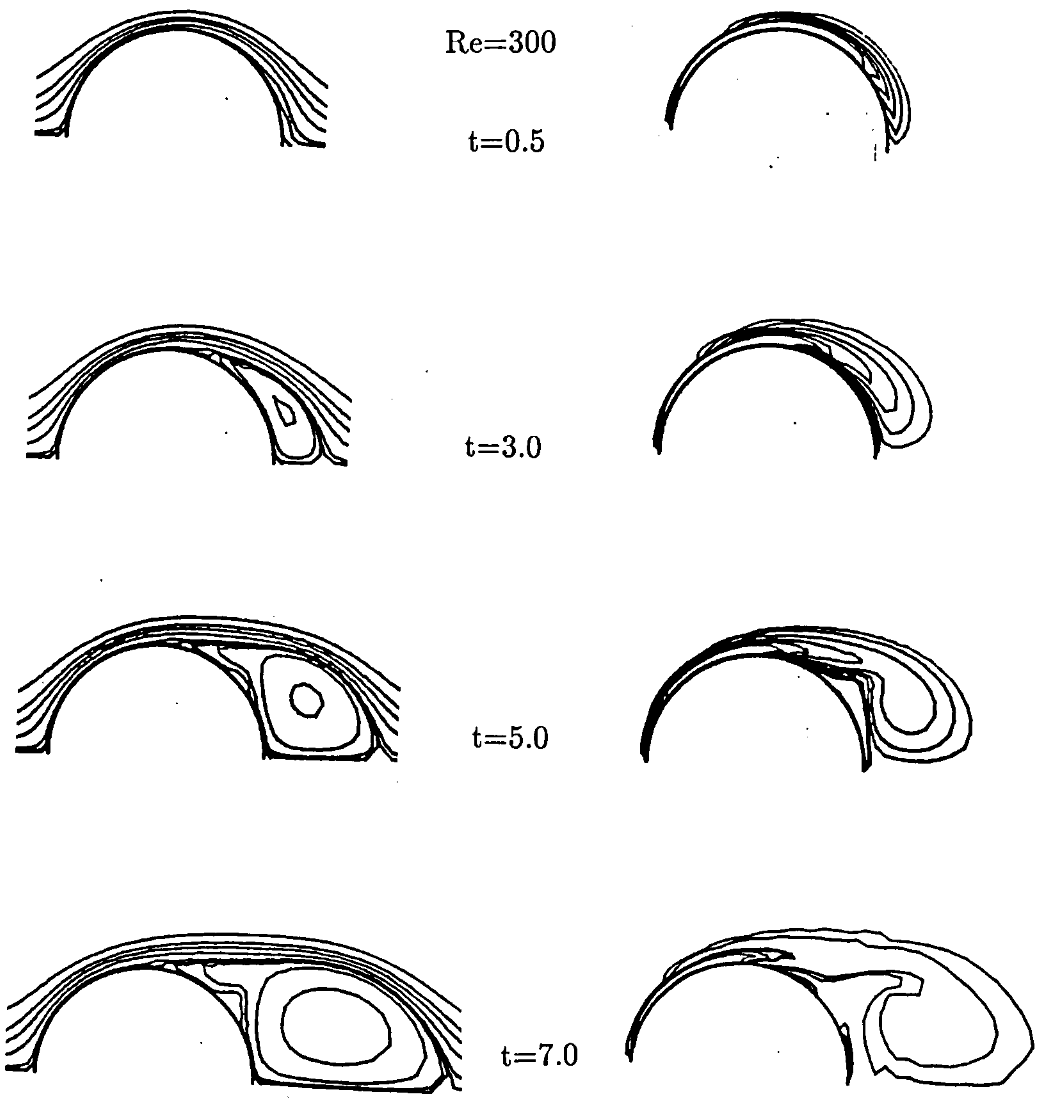

Fig. 3-11. Formation process of vortex behind cylinder

d. Non-symmetrical wake

As discussed above, once started, the flow separation develops further with time. Consequently, the closed wake grows in size as time increases. For very low Reynolds number flows, a steady solution is shown in Figure 3-12. A small symmetrical separation bubble exists behind the cylinder. Both experimentally and analytically, it has been shown that the stationary vortex pair is not stable as the Reynolds number increases. Finally, the unsteady but periodic Karman vortex street is formed in the wake.

Flow visualization[27], Re=19.6

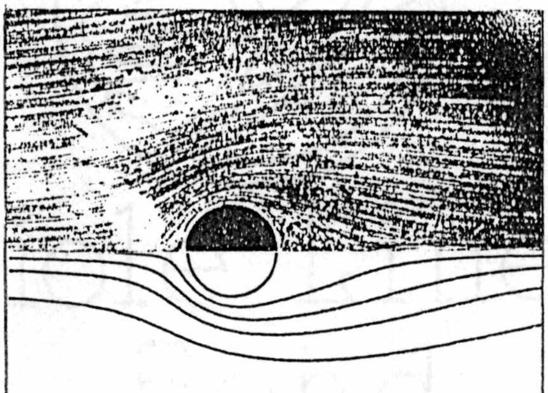

Computation, Re=20., developed

Fig. 3-12. Flow around a steady cylinder with a bubble

The mechanism and development process for the formation of an unsteady, non symmetrical vortex system is a challenging problem. In order to obtain the solution numerically, some authors introduce perturbation to the boundary condition to excite its natural unsteadiness, which comes from the nonlinearity of the problem itself. Some authors make use of the computational errors to excite the flow, the latter is more convenient for numerical calculation. The code developed here has the feature of capturing the inherent unsteadiness. The results shown below are obtained without any man-made perturbation in the calculation.

The vortex is shed alternately from the two sides of the cylinder; hence the lateral force on the cylinder exerted by the fluid oscillates with the same frequency. Numerically, the flow pattern appears to repeat itself between, say, NT_1 and NT_2. Then, the vortex shedding frequency can be determined from the following equation:

$$f_0 = \frac{U_\infty}{R_c \Delta t (NT_2 - NT_1)} \tag{3.30}$$

For the flow around a stationary cylinder, measurements show that the dimensionless frequency, which is called the Strouhal number,

$$S_t = \frac{f_0 d}{U_\infty} \tag{3.31}$$

depends uniquely on the Reynolds number[27]. Therefore the Strouhal number in (3.31) is given by the relation:

$$S_t = \frac{2}{\Delta t (NT_2 - NT_1)} \tag{3.32}$$

The period of vortex shedding, or more exactly the number $NT_2 - NT_1$, is obtained from the computed lateral force varying with time. The computed wake flow Strouhal numbers vs. experiments are shown in Figure 3-13. Typical computed flow streamline pattern around the steady cylinder is given in Figure 3-14.

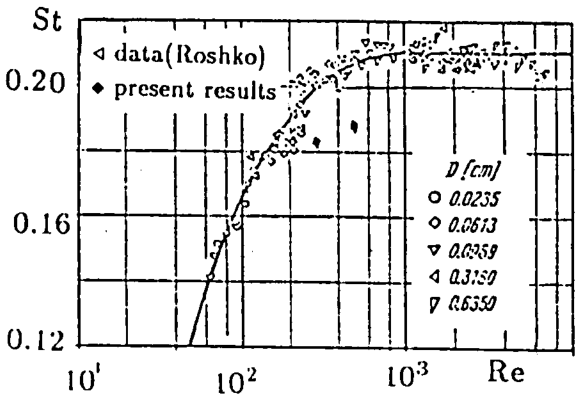

Fig. 3-13. Flow natural Strouhal number

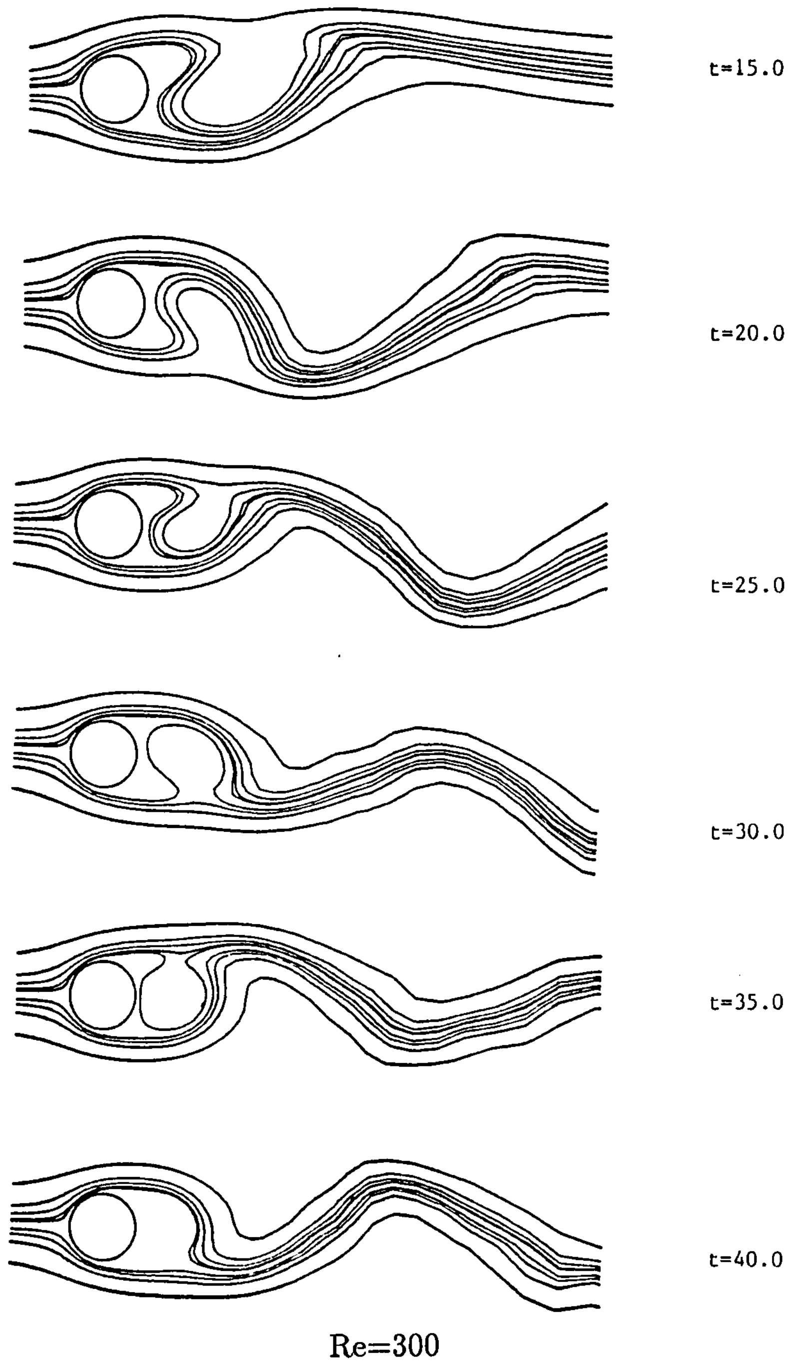

Fig. 3-14. Flow streamline pattern around a steady cylinder

2. Solution of Flows with rotatory oscillating boundary

As mentioned earlier, a forced harmonic rotational oscillation is applied on the cylinder. The unsteady motion of the boundary can be expressed

$$\theta = -\Theta_A cos(S_f(t-T)) \tag{3.33}$$

where θ is the angular displacement, Θ_A the amplitude and S_f is the forcing Strouhal number, which is defined as $S_f = \frac{f_f d}{U_\infty}$, and f_f is the forcing frequency. Finally, T is the time when the forced oscillation is applied. The velocity at the cylinder boundary is

$$V_T = S_f \Theta_A sin(S_f(t-T)) \tag{3.34}$$

the forced motion gives a zero velocity at the beginning. The forced oscillation is applied in such a way that any additional complication is avoided. If the initial forced oscillating velocity is not zero, another starting process is created. It is nothing new, but repeats the work involved in the initial condition.

There is an interaction between the flow and the boundary. Through the boundary condition, the vorticity distribution instantaneously responds to the boundary velocity. The surface friction, as well as the pressure distribution along the surface, is obviously a function of the motion of the cylinder. The hydrodynamic forces, which are the vector summation of the skin friction and pressure, depend on the forced oscillation of its boundary. Whether a positive or a negative contribution to the hydrodynamic forces on the body from its oscillation need to be dealt with in detail. The computed results are the effects of reduced frequency, amplitude and flow streamline pattern, the gross flow characteristics of the lift and drag coefficients.

a. Initial flow development under forced oscillation

In order to show the effect of forced oscillation on the oscillating wake flow, a sequence of studies has been conducted.

Even with a steady boundary, the flow is inherently unsteady if the wake flow contains a Karman street. When a forced oscillation is introduced into the problem through its oscillating boundary, these two frequencies will interact with each other. The flow developments under forced oscillations of its boundary are shown in Figure 3-15. Comparing these to the Karman vortices, it is obvious that the forced oscillation frequency has a strong effect on the vortex shedding from the cylinder. Basically when the forced frequency is lower than that of the natural one, the net effect counteracts the natural frequency. Thus, the period of vortex shedding increases. If it is higher than the natural frequency, the forced oscillation speeds up the vortex shedding.

b. Long time flow development under forced oscillation

After a sufficient time, the two frequency interactions reach an equilibrium. That is, the final flowfield appears to have a combined single frequency. The established flowfields under various forced oscillation frequencies are shown in Figure 3-16. The wake flows are greatly influenced by the forced oscillations. Due to viscous effect, there is a defect in the velocity profile at each wake station. The streamlines are divergent in the far wake. Figure 3-17 shows the typical results of flows with steady and unsteady boundary conditions.

c. Cylinder surface flow properties

To show the surface flow charateristics, the surface vorticity development

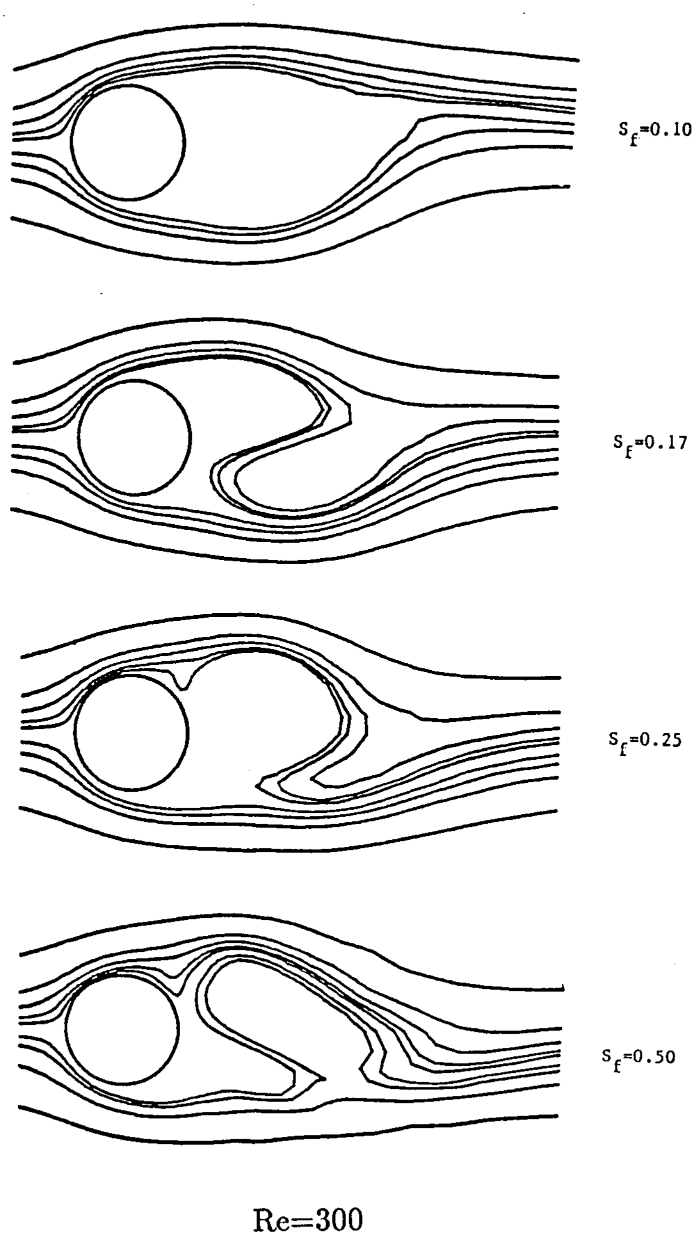

Fig. 3-15. Initial flow development under forced oscillation (T=10.)

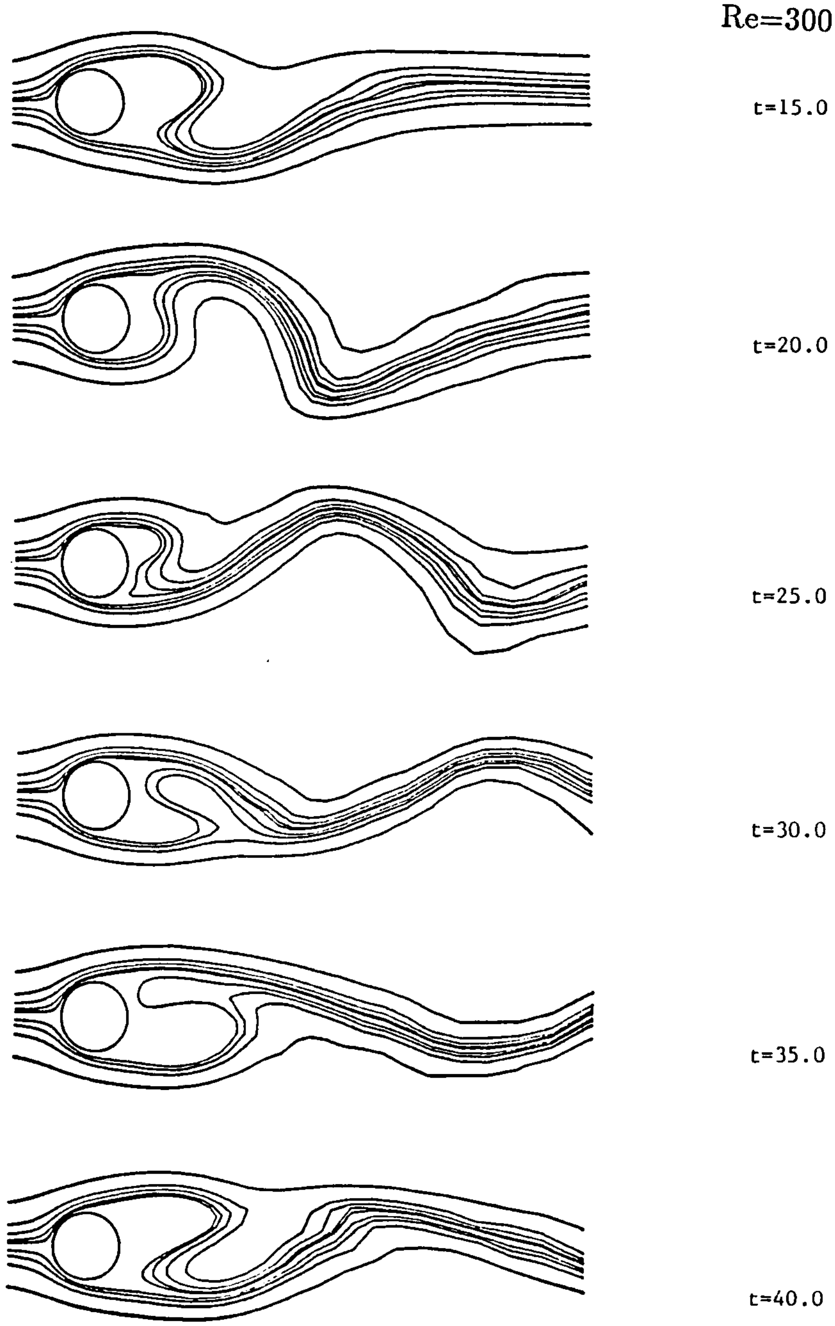

(a) flow with $S_f = 0.10$

Fig. 3-16. Flow streamline pattern under forced oscillation

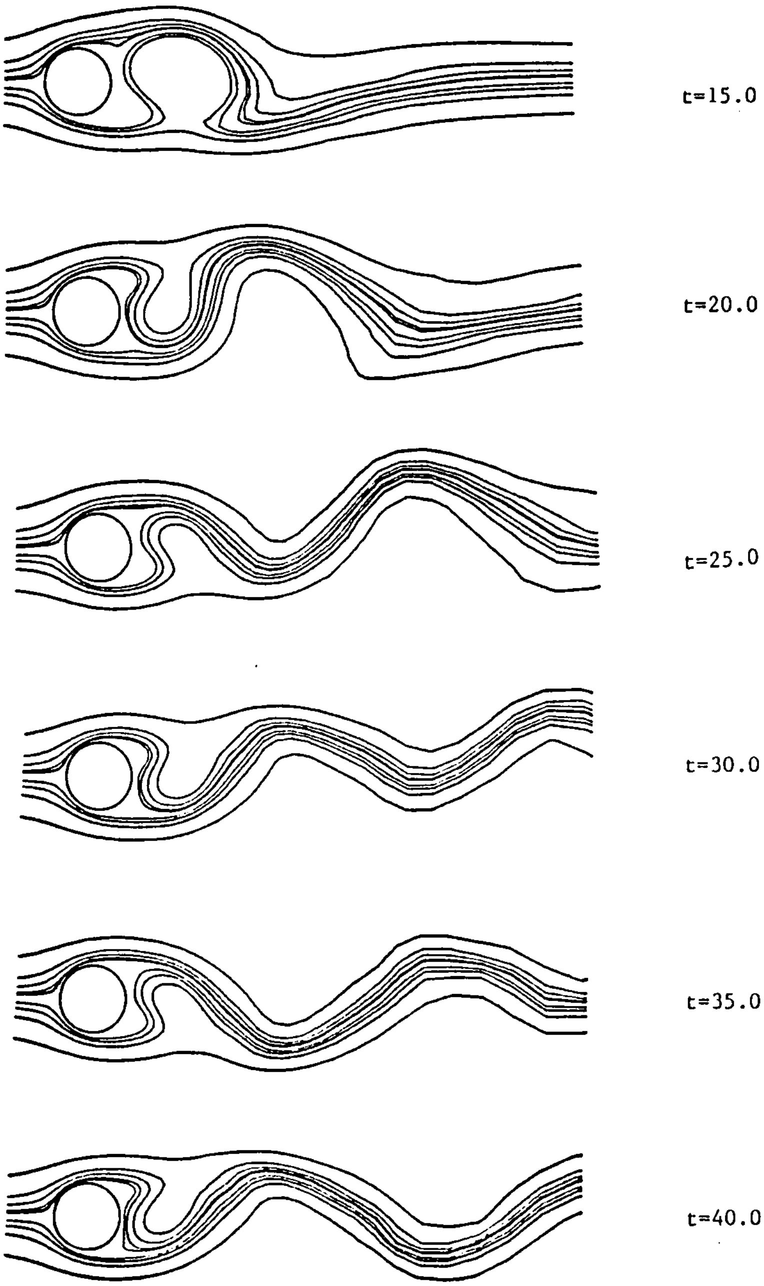

(b) flow with $S_f = 0.17$

Fig. 3-16. Continued

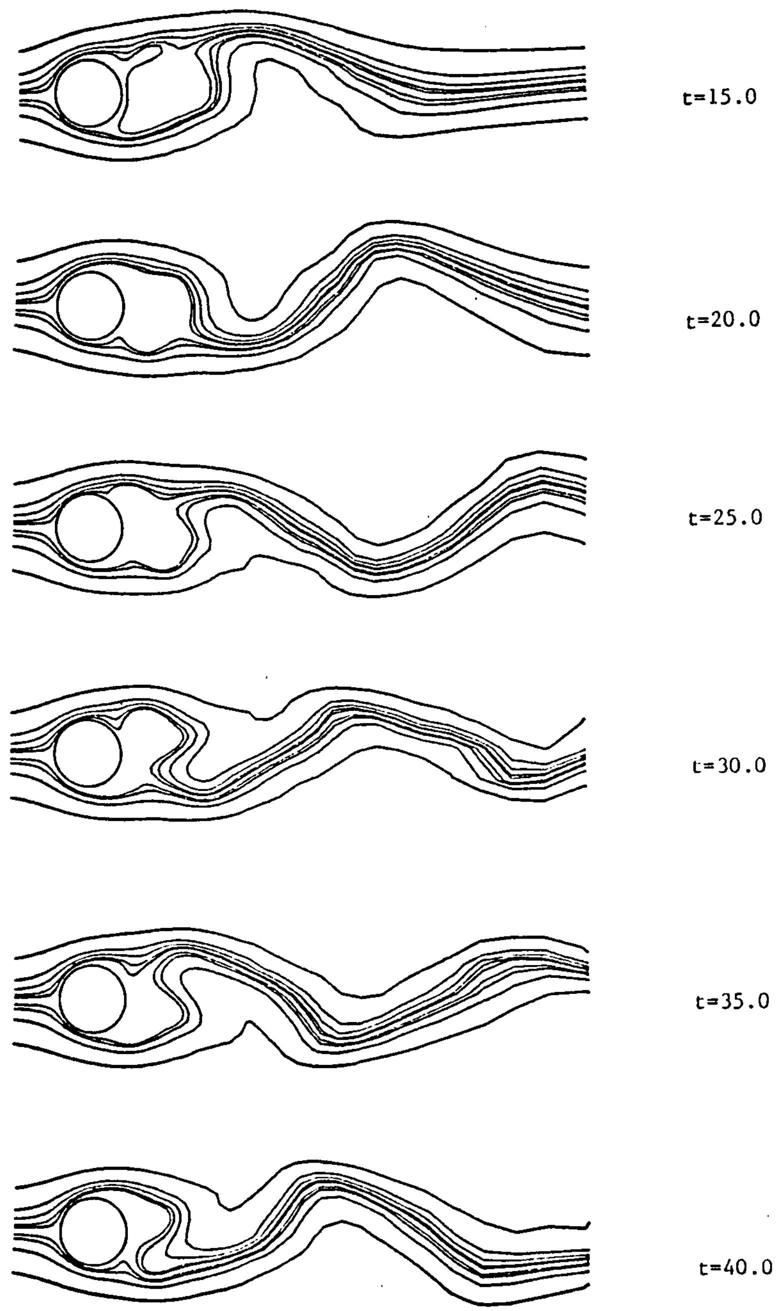

(c) flow with $S_f = 0.50$

Fig. 3-16. Continued

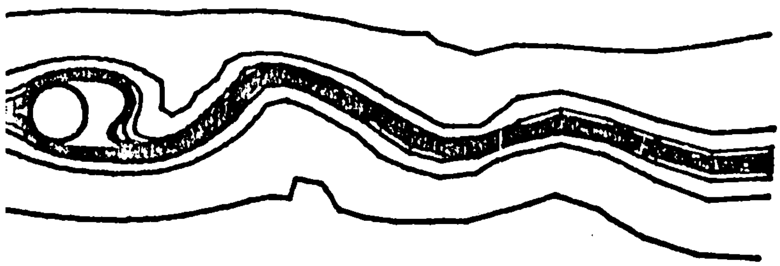

Re=300, developed

(a) wake flow around steady cylinder

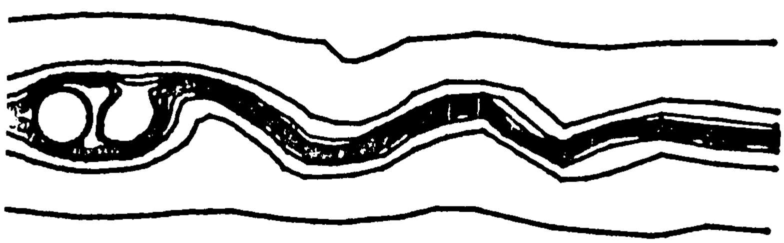

Re=300, S_f=0.178, developed

(b) wake flow around oscillating cylinder

Fig. 3-17. Wake comparison of both steady and oscillating cylinder after receiving a forced oscillation is shown in Figure 3-18.

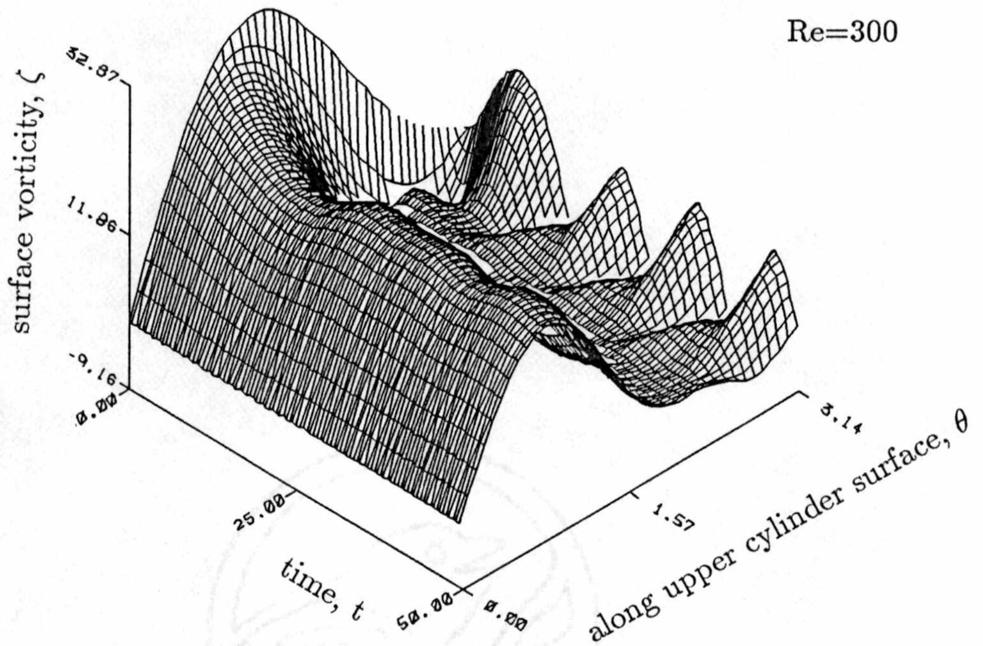

(a) Surface vorticity over steady cylinder

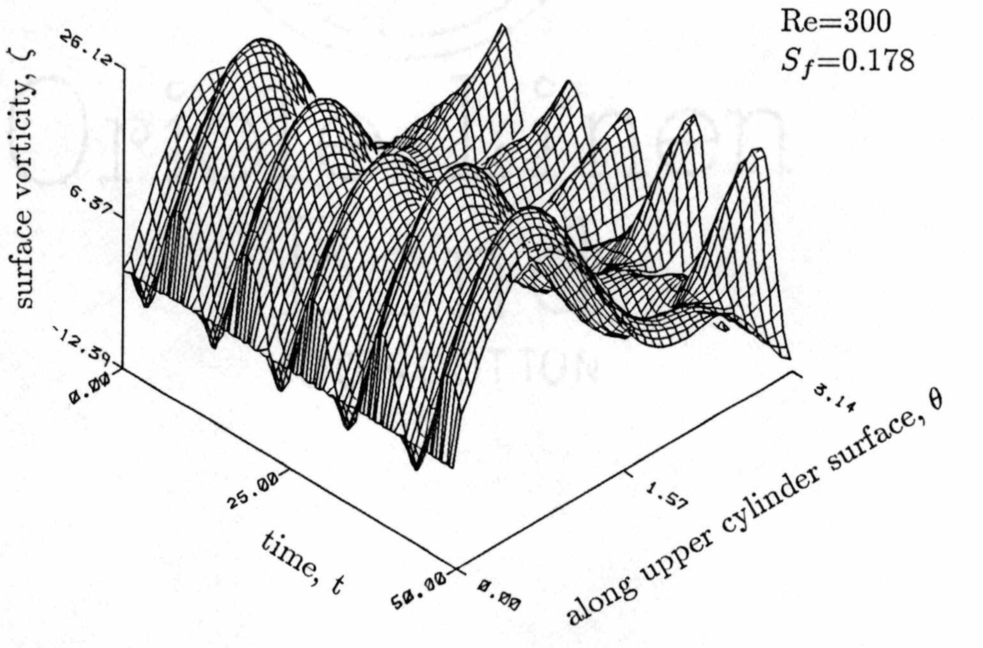

(b) Surface vorticity over oscillating cylinder

Fig. 3-18. Surface vorticity over cylinders

3. Hydrodynamic forces

Referring to § 3.4 and Figure 3-4, an impulsively started flow with an unsteady wake is used as the initial condition in solving the moving boundary case. A typical variation of lateral force, with forced Strouhal number of 0.19 and Reynolds number 300, is shown in Figure 3-19. Till time $t = T$, the forced oscillation is not applied on the cylinder and the flow has its natural frequency. After $t = T$, once the forcing is applied, the drag reacts to the forced oscillation on the body's boundary. The flow reaches an equilibrium with boundary in about three shedding periods (Fig. 19).

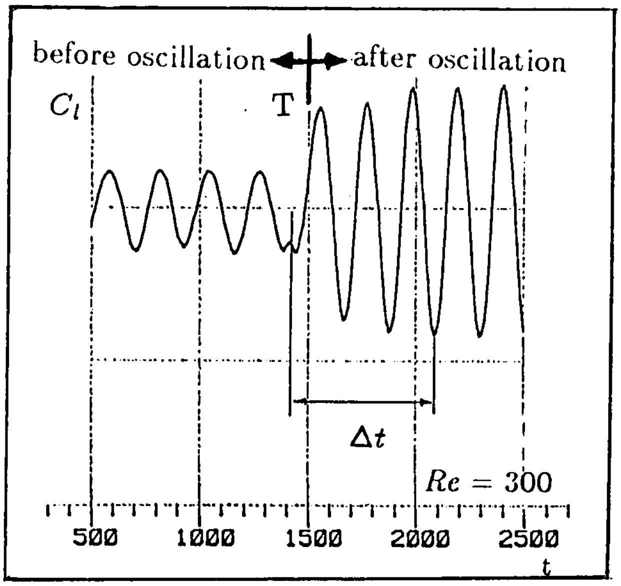

Fig. 3.19. Lateral force development with time

As can be seen from Figures 3-20 and 3-21, the force amplification effect is not uniform for the various forcing frequencies. The increase in lateral or axial forces is not directly proportional to the forcing frequency, even though more energy is imported onto the body for higher oscillation frequencies. It appears

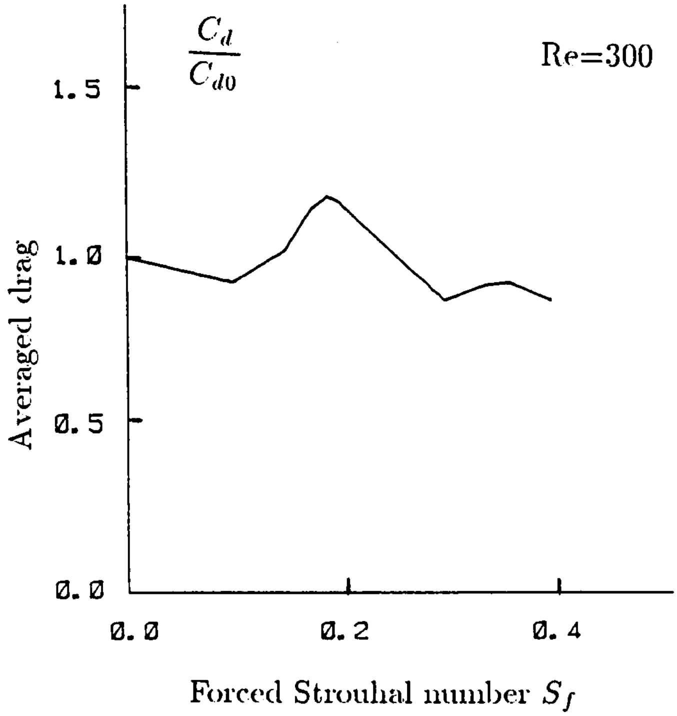

Fig. 3-20. Averaged drag with forced Strouhal number

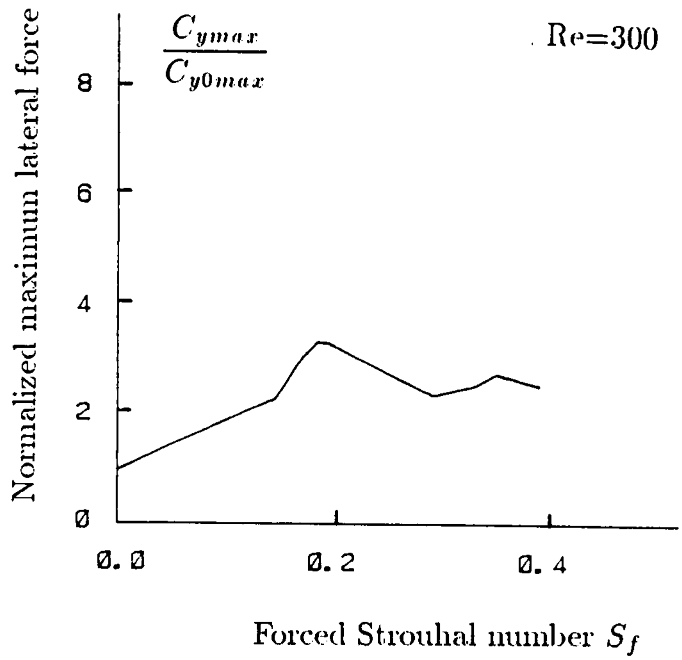

Fig. 3-21. Normalized maximum lateral force

that the maximum interaction happens at a frequency corresponding to the natural vortex shedding frequency of the flow. Also, some details can be gained from analysis of the cylinder drag under forcing conditions. The pressure drag, in addition to the skin friction drag, is of significance for the cylinder. If the pressure in the base flow region of the cylinder is lowered, then the overall cylinder drag will increase. Any changes in vortex shedding will certainly affect its base pressure and thus the drag. The forced oscillation now interacts with the natural unsteadiness of the flow and alter its vortex shedding. From this analysis, we learned that the preferred mode of interaction occurs at the natural shedding frequency. Under this condition, the vortex shedding and the wake organization is influenced by the forced oscillation. Drag varies with time and the forcing frequency is manifested in its trace. Time averaged variation of drag against the forcing Strouhal number is plotted in Figure 3-20. The peaks of the drag in Figure 3-20 are striking features of these results. The first peak occurs at oscillation frequency equal to the natural shedding frequency. The second peak, which is of lower amplitude, lies at twice that frequency.

Through a recent communication[66], we have learned that Prof. Hsiao's group has experimentally measured a 20% drag rise with acoustic flow, ($Re = 2 \times 10^4$), when the excitation frequency is that of the natural frequency of the cylinder. This is on the same order as we predicted in our analysis.

Finally, from the total energy point of view, the ratio of argumented flow energy to the total import energy is most important for practical application. It was not considered in this dissertation.

CHAPTER IV

EXPERIMENT APPROACHES

As indicated earlier, the present study consists of two parts. The theoretical part has been discussed in the former chapters; the visualization of the flows around an oscillating and stationary cylinder was conducted in the University of Tennessee Space Institute (UTSI) water tunnel. This facility is recognized for its flow uniformity.

Two flow visualization techniques were employed: a) Colored dye (food color in milk-alcohol mixture), and b) Laser induced fluorescence. A variable speed electric motor with a mechanical rotation system was designed to provide oscillations with desired amplitude and frequency. The cylinder model is designed to be long enough in the axial direction relative to its diameter to obtain approximate two-dimensionality. As discussed in the theoretical part, our goal in the experiment is to find the effect of the forced oscillation on the cylinder to the flowfield. The effecting factors mainly include the forced frequency and the amplitude.

§4.1 Water Tunnel Facility

The UTSI water tunnel is one of the largest in the United States. It was designed to provide excellent flow quality for flow visualization studies. The detailed description of this facility can be found in the UTSI report by Collins (1982)[54]. Some of the major features are discussed here.

The water tunnel is a closed circuit continuous flow facility. It lies in a horizontal plane and is powered by a 25 cm diameter two-bladed propeller which is located at the second bend downstream of the test section. The propeller is connected to a continuously variable speed transmission which allows the tunnel speed to be varied from 1.5 to 60 cm/sec. The fluctuations from the propeller are damped by the long return pipe leading to the stilling chamber. The motor is mounted on a vibration isolated mount and is flexibly connected to the propeller shaft. The length to diameter ratio of this pipe is about 75. The fluctuations in the test section due to the propeller are extremely small. The characteristics frequency of the empty tunnel is about twelve Hertz. The precaution was taken of avoiding test conditions with a characteristic frequency too close to this value. Test section dimensions are 30.5 cm high, 45.7 cm wide and 150 cm long (12 in x 18 in x 60 in). The test section walls are made of Plexiglas for versatility in observing and photographing the flow field. The test section is enclosed in a light-tight building with blackened inside walls for photographic purposes. The general layout of the water tunnel facility is shown on Figure 4-1.

The stilling chamber is a cylindrical shaped tank which is 1.55 m in diameter and 2.85 m long. There are four stainless steel screens and two aluminum honeycombs located in this chamber. The length to diameter ratio of the honeycomb is 6. It was designed to give a turbulence level of 0.1% in the test section. The nozzle is a bell mouth that continuously changes from a circular shape to a rectangular shape with a contraction ration of 13.5. In the first bend downstream of the test section, a portion of the main flow is bypassed through a filter to control the particle size in the tunnel to less than 10 microns.

The tunnel is controlled from a master control panel inside the building. All valves are operated by solenoids. The tunnel speed is measured with a digital meter on the control panel that indicates the rotational shaft speed. This meter was calibrated against tunnel flow velocity[55].

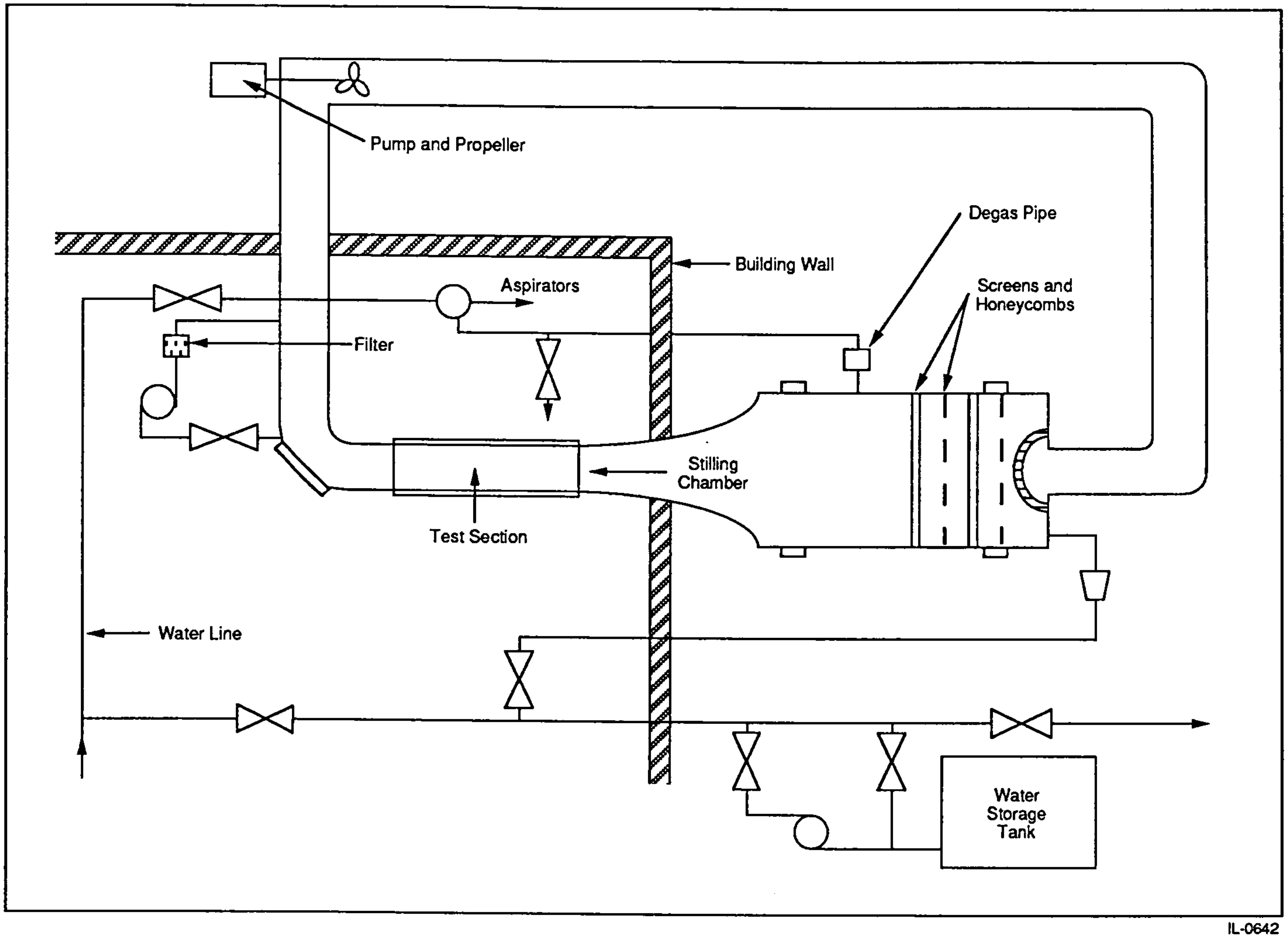

Fig. 4-1. UTSI water tunnel[54]

§4.2 Set-Up of Model and Working System

A. Model

In order to be convenient for mounting the test model in the test section of the water tunnel, the model was designed to be inserted into the water from the top of the test section. In the experiment, the laser beam is through the test section from the side wall. The cylinder was made from steel stock with a good axisymmetricity and without serious distortion during the test. To keep two-dimensionality geometrically, the cylinder model was designed to have the length which is nearly 20 times its diameter. The dimension of the cylinder is schematically shown in Figure 4-2.

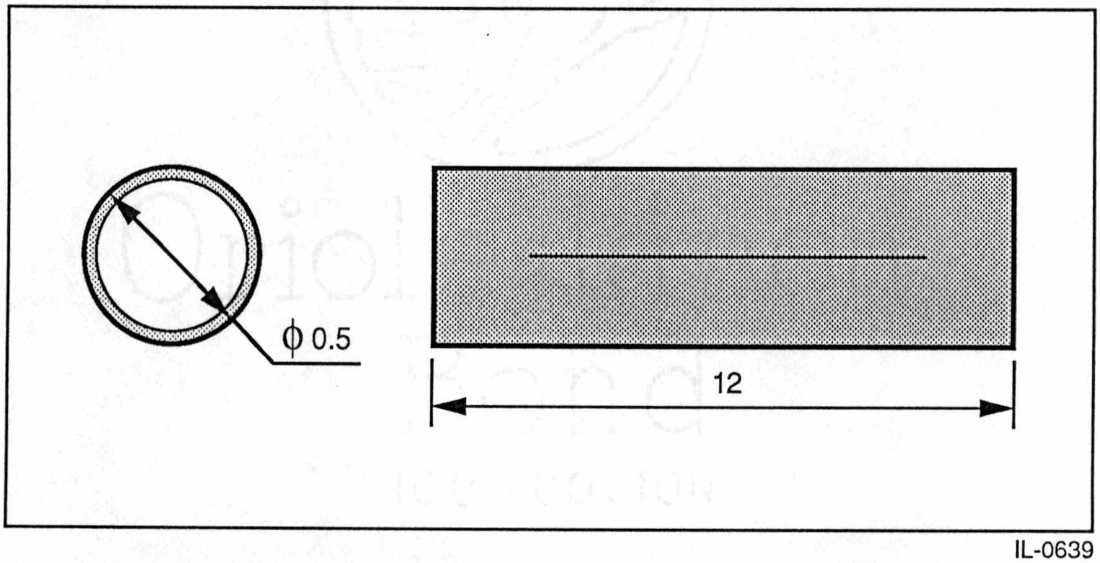

Fig. 4-2. Schematic of test model

For convenience of observation, there are four Mark lines marked on the cylinder surface along the axial direction by slightly painting. The mark lines are separated by 90^0. The model is supported by a top circular base-plate, to which a oscillation motion created by the driving system is delivered. There are three holes on the top circular base-plate, which have different distance R_A to its axial line.

The distance R_A can be used to adjust the oscillation amplitude. In conjunction with other parts, any desired amplitude can be produced by this setup.

B. Working system

The general arrangement of the whole equipment is shown in Figure 4-3. A variable speed electric motor is used as the power source, which has a speed from 10 to 1000 RPM. A vibrator is designed to transform the motor rotation into an oscillating motion of the cylinder model. This is shown in Figure 4-4.

From the planar mass-point kinetics, it can be proved that the vibrator performs a harmonic oscillation. Let r_a be the radius of the connection point on the driving wheel, then the relation for the amplitude is

$$\Theta_A = \frac{2\pi r_A}{R_A}.$$

By using different connection points on the driving wheel and the top circular base-plate, different amplitudes Θ_A can be obtained.

§4.3 Flow Visualization Techniques

Two kinds of flow visualization techniques were used in this work. It is cheaper for viewing three-dimensional effect in the flowfield to use the standard dye technique: The dye used was a mixture of alcohol, milk, and commercial food color in such a composition to ensure a specific gravity equal to that of water. A pointed dye source is placed upstream of the expected section of the model. When the dye comes out constantly from the source, it will follow the movement of the local fluid elements and show the flow pattern. In order to show a two-dimensional feature more clearly, the visualization techniques like the laser induced fluorescence is necessary. Three chemicals were used as laser light exciting agents. These are Rhodamine 6G, Rhodamine B and Fluorescein Sodium Salt. Once dissolved in

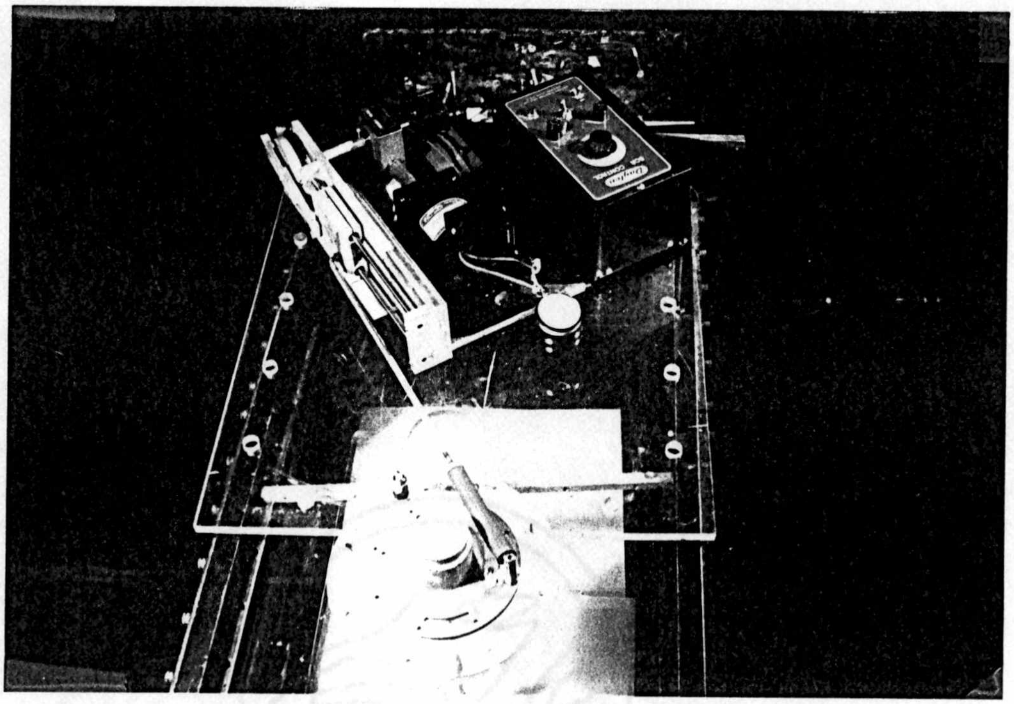

Fig. 4-3. Overwhole view of equipment

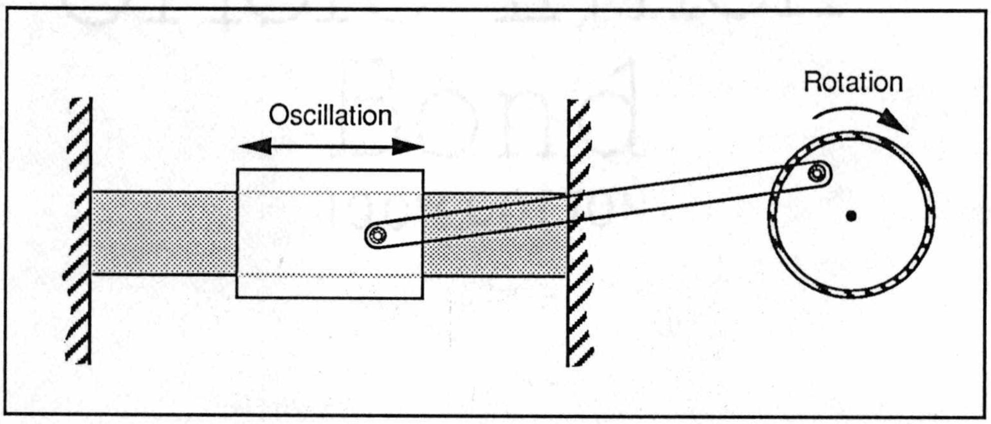

IL-0641

Fig. 4-4. Sketch of oscillation system

water, and under the excitation of a laser light sheet, they give yellow, red and green fluorescent colors respectively on the light sheet cutting a selected section of the flowfield. Dye was stored in a cylindrical can and injected into the flow field at controlled rates by a adjustable pressure system. Just by turning the pressure valve, a required dye rate can be obtained easily.

An Argon ion laser light source (LEXEL, model 95) with maximum power output of 10 watts was used for the laser fluorescence flow visualization. A 4mm cylindrical lens in front of the laser beam was used to spread the pointed laser light into a plane laser light sheet. Rotation of the cylindrical lens resulted in rotation of the light sheet plane. Combined translation and rotation of the light sheet plane provides visibility into the complete flow field at any desired orientation. This sheet of light excited the fluorescent dye to obtain a clear cross-section view. The results and analysis of the flow visualization are discussed in the following section.

§4.4 Results of Flow Visualization

A series of tests were conducted in order to study the effect of a rotary oscillation of cylinder on the flowfield. The vorticity within the flowfield comes from two sources. One is from the pressure gradient along the surface, another is from the unsteady motion of the boundary. The vortex shedding frequency varies with the frequency of body motion. Whether this produces more or less vorticity will depend on the resulting interaction of these two sources of vorticity. Similar to the theoretical treatment, the forced oscillation of the cylinder was applied after flow around the stationary cylinder with a natural frequency in its wake was well-established. Therefore, the effect can be measured by comparing the flow patterns with or without oscillation. In order to be consistent with the numerical calculation, the cylinder starts its oscillation from the maximum amplitude point. That means the perturbation velocity from the forced oscillation was zero at the start of the oscillation.

The cylinder performed a harmonic, rotary oscillation, $\theta = \Theta_A cos(2\pi f_f t)$, where f_f is the forced oscillation frequency of the cylinder. The experiment was conducted at the room temperature of $30^0 C$. The tunnel flow speed was 1.80 cm/s (0.71in/sec) The experiment Reynolds number based on the cylinder diameter was Re≈300. The frequencies was limited to near natural frequency(with $S_t \approx 0.18$, when $Re = 300$). The flow visualization was performed with two amplitudes and three frequencies in the water tunnel. These three frequencies are slightly lower, near, and slightly higher than its natural frequency.

Figure 4-5 shows the flow pattern when the cylinder stays stationary. There is a Karman vortex street in the wake. Figure 4-6 shows a set of flow patterns with the same amplitude but different Strouhal numbers. These Strouhal numbers are respectively 0.206, 0.179, 0.137. In order to find the amplitude effect, another set of experiments with different oscillation amplitude from the previous set but at the same Strouhal number and Reynolds were made. Figure 4-7 shows the results. It needs to be noted that the wake divergence angle observed in the photographs is not true because of the camera location. This is shown schematically in Figure 4-8. This camera angle causes a distortion in the perceived flowfield.

From the above visualization results, It is interesting to find that the forced oscillation frequency plays a key role in controlling the wake flow. The physical details will be discussed in next chapter.

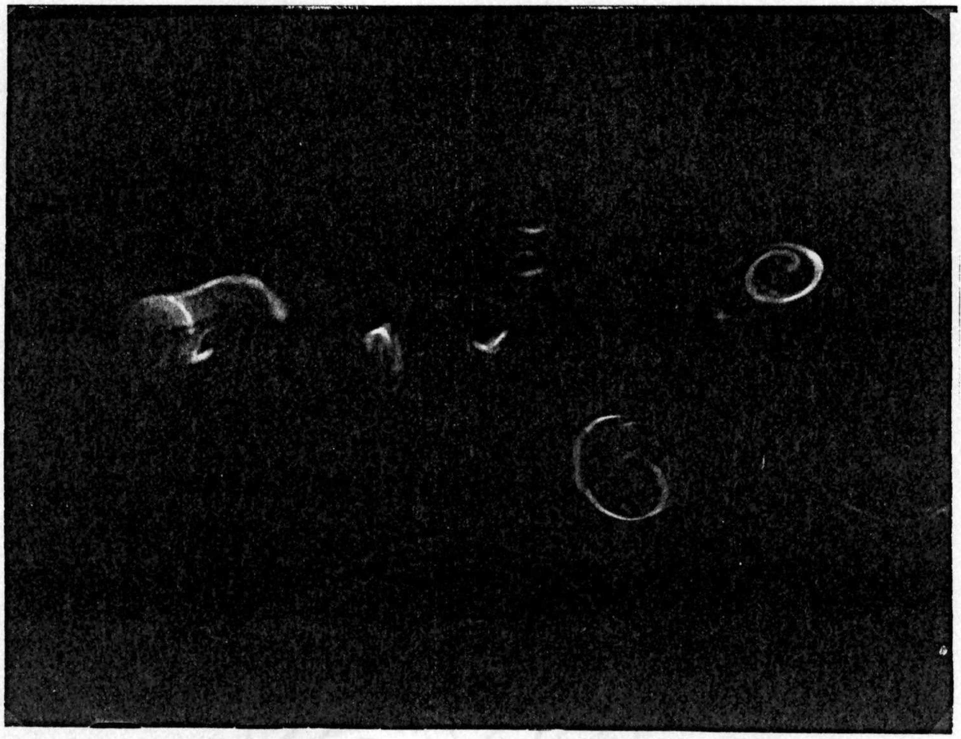

Fig. 4-5. Flow around a steady cylinder(Re=300)

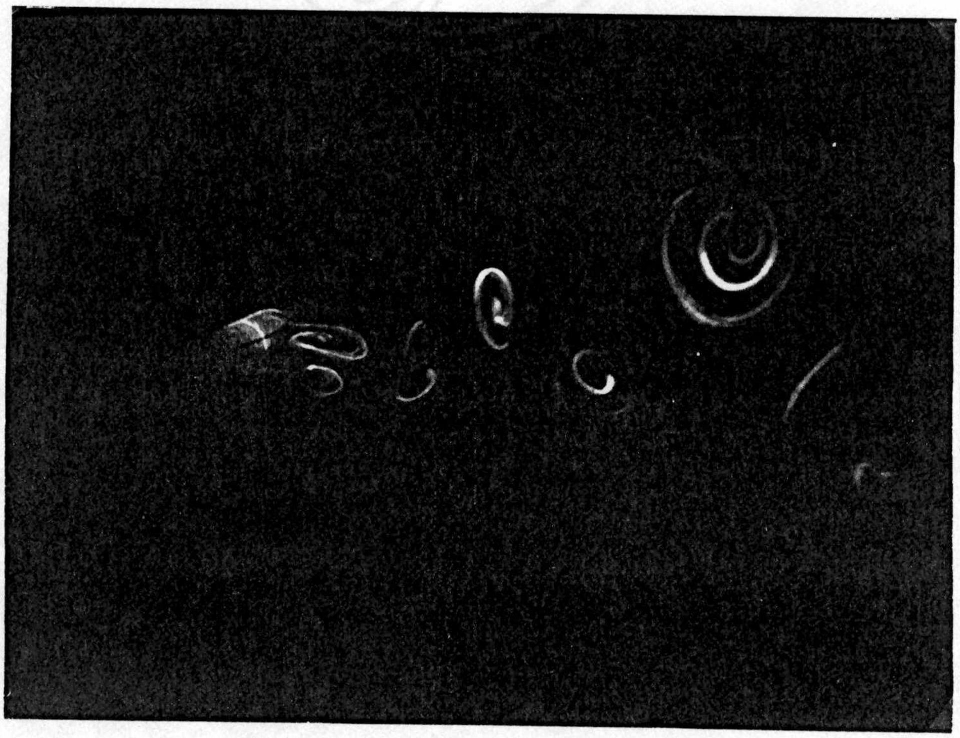

Fig. 4-6. Flow under oscillation(Θ_A=1.0, Re=300)

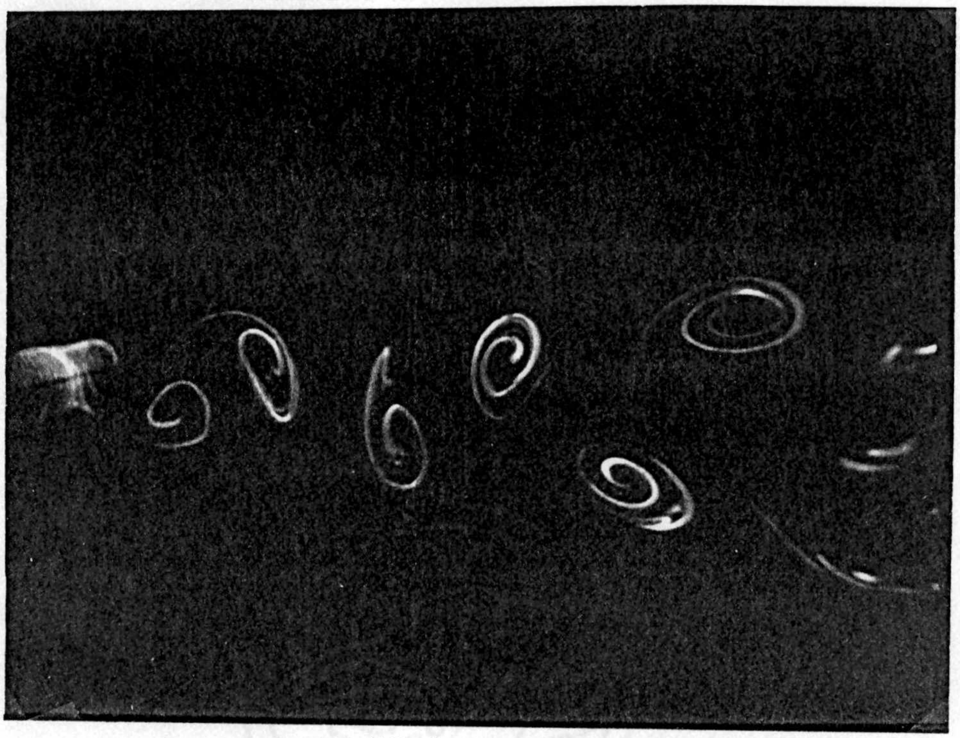

(b) $S_f = 0.179$

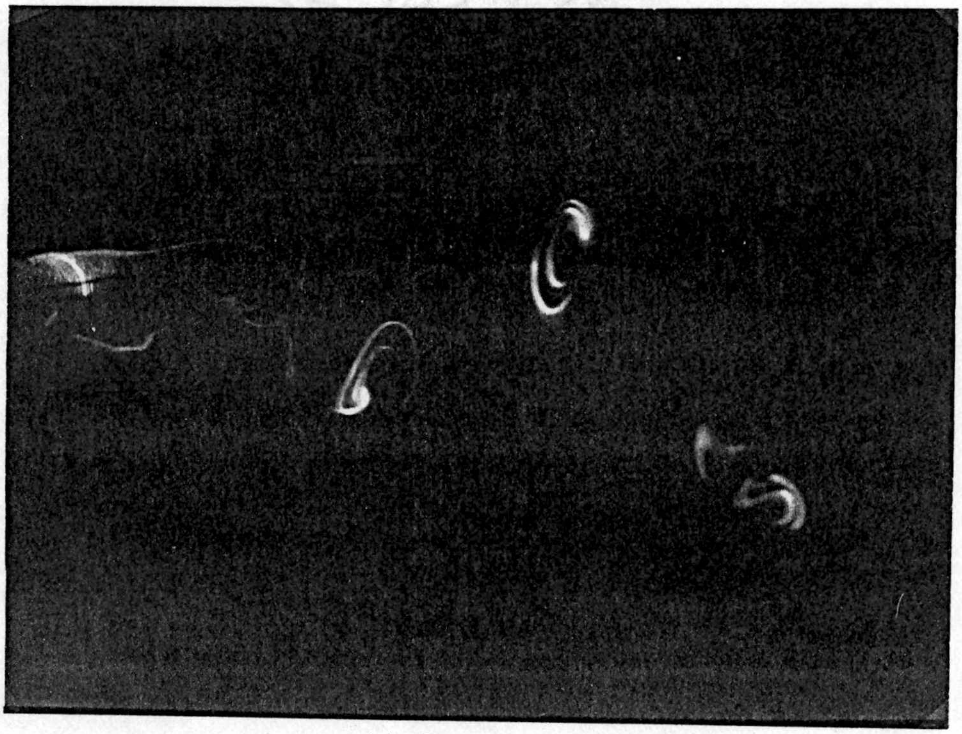

(c) $S_f = 0.137$

Fig. 4-6. Continued

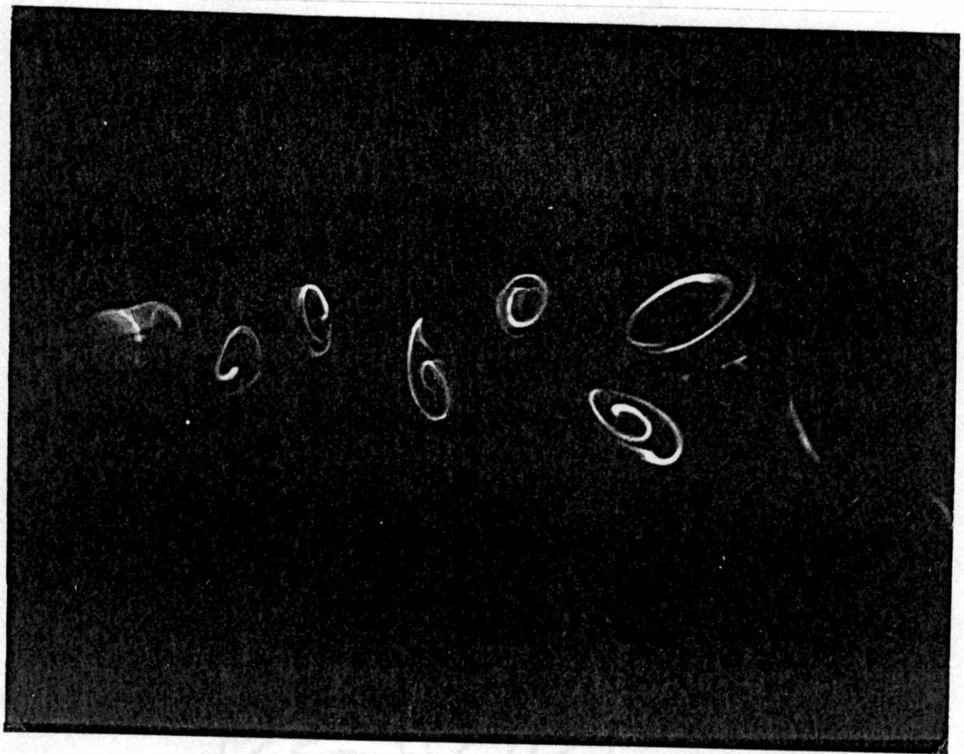

(a) $S_f = 0.206$

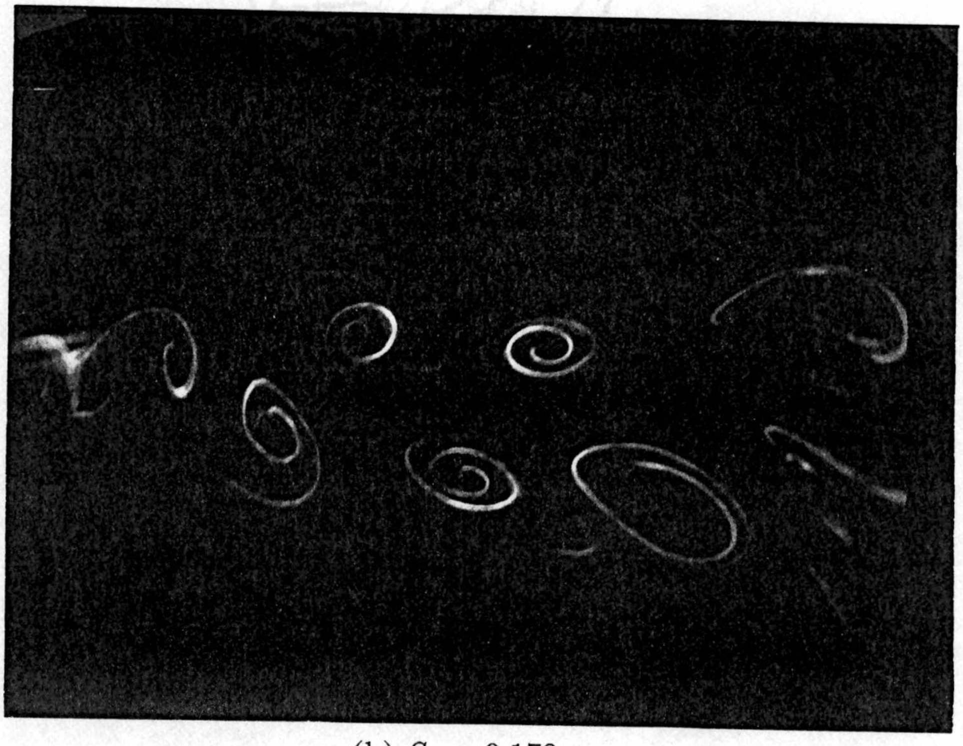

(b) $S_f = 0.179$

Fig. 4-7. Flow under oscillation(Θ_A=1.25, Re=300)

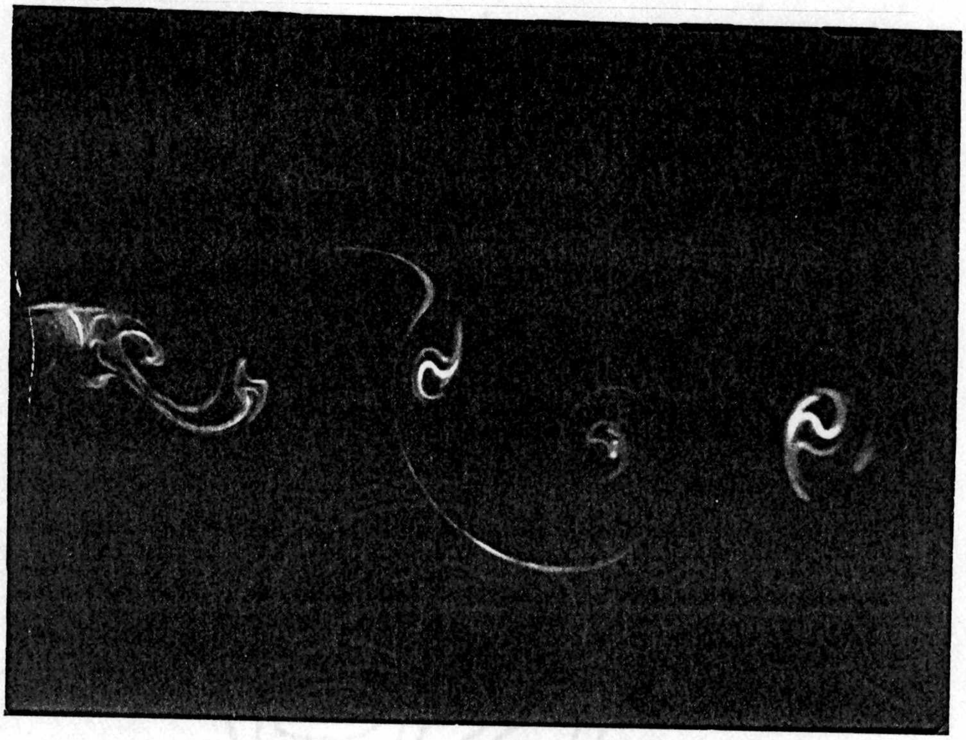

(c) $S_f = 0.137$

Fig. 4-7. Continued

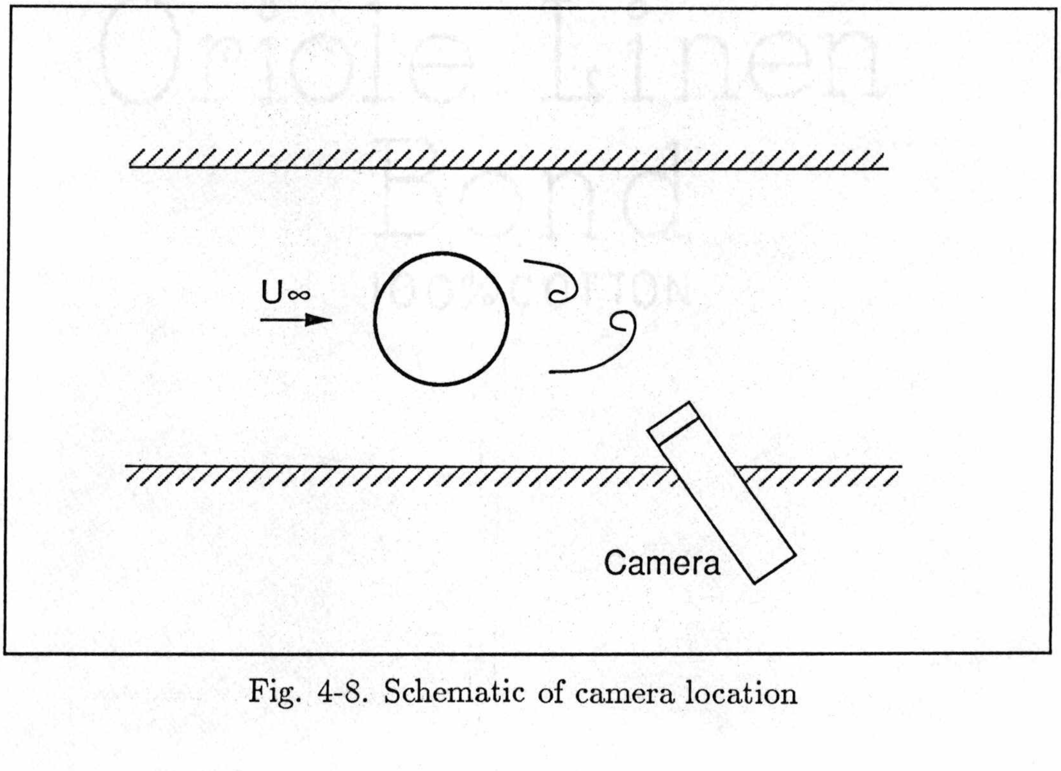

Fig. 4-8. Schematic of camera location

CHAPTER V

DISCUSSION OF FLOWFIELD

Analytical, numerical and experimental studies have been performed on the flows around an oscillating cylinder with or without a uniform stream. When no uniform stream is present, the flowfield is in oscillation and the solution is reduced to the classical result of oscillating flat-plate as the cylinder radius approaching to infinity. When in a uniform stream, the flows are fully separated. It has been shown both by the computation and by flow visualization that the wake behind a cylinder can be significantly modified by applying a rotary oscillation to the cylinder. The detailed mechanism is discussed below.

§5.1 Vorticity Generation

Seeking for high fluid dynamic force is the utilization of vortex or vorticity in the flowfield. The problem is how to generate vorticity, and then how to guide and control the vorticity to become more useful for the purpose of force generation. So the vorticity generation mechanism is discussed first.

The solid wall acts "like" a vorticity source. From the momentum equations, it can be shown that the production rate of the total vorticity in the flowfield is

$$\frac{d}{dt}\int_D \zeta ds = -\nu \int_{\partial D'} \frac{\partial \zeta}{\partial n} dl \tag{5.1}$$

The vorticity flux at the body surface is defined as[12]

$$\sigma = -\nu \frac{\partial \omega}{\partial n} \tag{5.2}$$

We see that the only source of vorticity for the flow is viscous diffusion from the solid surface.

The vorticity flux at the surface is determined by the vorticity gradient, which, in turn, is set up by the velocity field. However, the momentum equation along the surface provides a direct expression for the viscous vorticity flux on the cylinder surface,

$$\sigma = -\frac{\partial V_t}{\partial t} - \frac{1}{\rho}\frac{\partial p}{r\partial \theta} \tag{5.3}$$

The first term in the right hand side of this equation is directly responsible for the unsteadiness. The second term is the contribution of the vorticity flux from the pressure gradient along the cylinder surface. The pressure field is created and controlled by the whole flowfiled, in which part of the effect from unsteady motion on the boundary is also included. So this term, just as the problem itself, is nonlinear.

In the present work, the boundary performs a harmonic oscillation along its tangential surface. The time-averaged vorticity flux for steady and unsteady flow, with different forced reduced frequency S_f, are shown in Figure 5-1. It reveals that the vorticity flux is a weak function of the forced oscillation frequency. When the forced frequency is equal to the natural one, there is no change on the averaged vorticity flux. This means that, no additional vorticity is created from the moving boundary when it is in phase with the natural vortex shedding. If the forced frequency does not match the natural one, less vorticity is created from the boundary.

A time-average can be taken on the cylinder Stokes flow when there is no uniform stream. The averaged flow values are zero. In fact, we can directly take a time average on (5.3). When the cylinder performs a harmonic oscillation, the time-average of the first term is zero. The net effect comes from the second term. So it can be seen that the nonlinearity is the key factor of the physical excitation mechanism.

§5.2 Vortex Flow Control

The computed forces show that when the forced frequency is equal to the natural one, the amplifying effect appears in spite of the fact that no additional vorticity is fed into the flow. The corresponding visualization experiment also shows that the vortex wake behind the cylinder becomes better organized in that situation.

The time-averaged flowfield was also studied. The results of mean flows with different reduced frequencies S_f are shown in Figure 5-2. It is not surprising to find that when the rotary oscillation on the cylinder boundary has a frequency equal to the natural vortex shedding frequency, the mean flow has the smallest size of the mean wake and the vortex center is the closest to the cylinder. The averaged drag (Fig. 3-20) is a direct reflection of this result.

The maximum amplifying effect on the hydrodynamic forces on the cylinder occurs when the cylinder has a rotary oscillation with the reduced oscillation frequency equal to the natural one. The reason is that each vortex, before shedding into the far wake, keeps closer to the wall which results in the smallest size of mean flow separation region instead of more vorticity is created on the boundary.

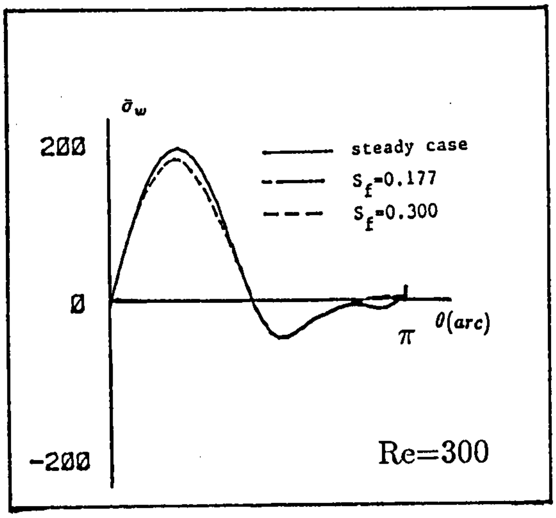

Fig. 5-1. Mean vorticity flux on wall

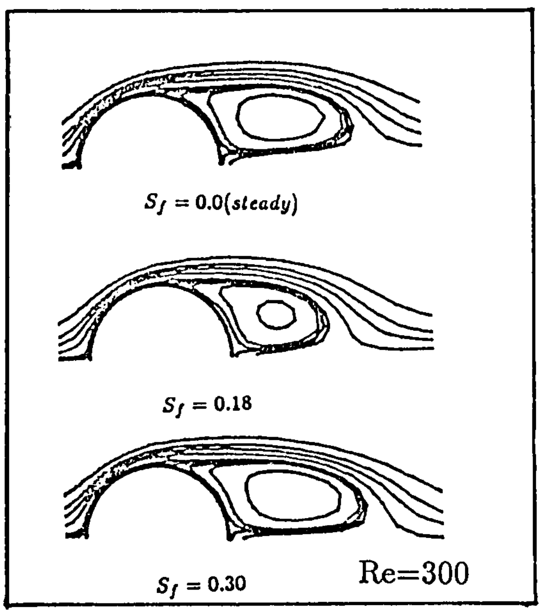

Fig. 5-2. Mean flow streamline pattern

CHAPTER VI

CONCLUSIONS AND RECOMMENDATIONS

The following conclusions are drawn from the present study.

• The cylinder Stokes problem, generated by an oscillating cylinder in a stationary medium, has the velocity profile in the radial direction that is damped in the same way as the classical Stokes problem; there is a layer of fluid with a depth to which viscosity makes itself felt that is proportional to $\sqrt{\nu}$ and the smaller the radius is, the thinner the layer will be (with a restriction $0(R_c)=0(1)$).

• When there is a uniform flow over a stationary cylinder, there exists a pair of zero velocity, symmetrical critical points behind the cylinder by using a potential flow approximation. The flow pattern with a vortex pair at these critical points is generally not stable and the initial trajectory of the vortices has different responses to different direction perturbations. Further work is needed, possibly by using the first order boundary layer approximation near the rear stagnation point, to develope a viscous stability theory.

• The separation region behind the cylinder can be significantly influenced by the rotational oscillation frequency and amplitude. This will, in turn, influence the spacing between shed vortices in the wake.

• For the nondimensionalized oscillation frequency of unity, representing resonance, the lateral force on the cylinder is doubled and the drag is increased by about 20% at an oscillation amplitude of 30^0.

• At higher frequencies of oscillation, subharmonic resonance takes place with amplifying effects lower than that for the natural resonance frequency.

• The vorticity within each shed vortex is the same as that of natural shedding. At the resonance state, the average separation point is moved downstream toward the rear stagnation point and with the aid of tangential motion of the body, the vortex is more compact in size. This effect results in closer spacing between the alternating shed vortices in the wake.

• The pathline for the wake flow obtained from the computations resemble the visualization of wake flow observed in the water tunnel.

The study carried out in this research is one simple physical model for understanding vorticity production and transport mechanisms by the unsteady motion on the body surface. The practical flow is much more complicated. Even for a simple geometry problem, what has been done in this dissertation is only in a preliminary step. For further work, this study should be expended to cover turbulent effect at high Reynolds number and the three-dimensionality.

BIBLIOGRAPHY

BIBLIOGRAPHY

1. Rebont, J. et al, "Recollement Dynamique Sur Vn Profil Daile En Movement De Tamis Influences Des Parameters Doscillation," AGARD, CP-227, 1977.

2. Wu, J. M., "Dawn of New Aerodynamics," Inter. Aviation, Vol.270, No. 8, pp 2-7, 1985.

3. Z. Y. Lu, "Study of Vortex Motion Induced by Oscillating Spoiler," Inter. Conference of Fluid Mech. in China, 1986.

4. Carr, L. W., McAlister, K. W. and McCroskey, W. J., "Analysis of the Development of Dynamic Stall Based on Oscillating Airfoil Experiments," NASA-TN-D-8382, 1977.

5. Cui, E. J., Private Communication, Aerodynamics Institute of Beijing, The People's Republic of China, May, 1986.

6. Wu, J. M., A. D. Vakili, "Aerodynamic Improvements by Discrete Wing Tip jets," AFWAL-TR-84-3009, Wright-Patterson AEB, Ohio, March, 1984.

7. Riley, N., "Streaming from a Cylinder due to an Acoustic Source," J. Fluid Mech., Vol. 180, 1987.

8. Lighthill, J., "Acoustic Streaming", J. of Sound and Vibration, Vol. 61, 1978.

9. Liu, C. F., "Control of Airfoil Performance by Local Excitation," Dissertation, Cheng Kung Univ., Taiwan, China, 1988.

10. Welsh, M. C., Stokes, A. N. and Paker, R. "Flow-resonant Sound Interaction in a Duct Containing a Plate," part I: semi-circular leading edge. J. Sound Vib. 95, 305, 1984.

11. Wygnanski, I. and Petersen, R. A., "Coherent Motion in Excited Free Shear Flows," AIAA Paper 85-0539, 1985.

12. Reynolds, W. C. and Carr, L. W., "Review of Unsteady, Driven, Separated Flows," AIAA-85-0527, 1985.

13. Luttges, M. W., Somps, C., Kliss, M. and Robinson, M. C., "Unsteady Separated Flows: Generation and Use by Insects," Workshop on Unsteady Separated Flow, Colorado, Aug. 1983.

14. Mcrosky, W. J., "Recent Developments in Dynamic Stall," Symposium on Unsteady Aerodynamics, ed. R. B. Kinney, Tucson 1975.

15. Lighthill, M. J., "On the Weis-Fough Mechanism of Lift Generation," J. Fluid Mech., Vol. 60, Part 1, 1973.

16. Herbst, W. B., "Future Fighter Technologies," J. of Aircraft, Vol. 17, No. 8, 1980.

17. Maskell, E. C. and Küchemann, D., "Controlled Separation in Aerodynamic Design," RAE-TM AERO. 463, 1956.

18. Nagib, H. M., Reisenthel, P. H. and Koga, D. J., "On the Dynamic Scaling of Forced Unsteady Separated Flows," AIAA paper 85-0553, 1985.

19. Reisenthel, P., Nagib, H. and Koga, D., "Control of Separated Flows Using Forced Unsteadiness," AIAA-85-0556, 1985.

20. Koga, D., Riesenthel, P. and Nagib, H., "Passive and Active Device-controlled Unsteady Separated Flow Fields," Workshop on Unsteady Separated flow, Colorado, Aug. 1983.

21. Maxworthy, H., "The Fluid Dynamics of Insect Flight," Ann. Rev. Fluid Mech., 1981.

22. Lighthill, J., Laminar Boundary Layers, (Ed, L. Rosenhead) Oxford, England: The Clarendon Press, Inc., 1963.

23. Lamb, H., Hydrodynamics, sixth edition, Dover Publications, New York, 1988.

24. Polhamus, E. C., "Predications of Vortex Lift Characteristics on a Leading Edge Suction Analogy," AIAA G9-1133, 1969.

25. Polhamus, E. C., "A Concept of the Vortex Lift of Sharp Edged Delta Wings Based on a Leading Edge Suction Analogy," NASA TND-3767, 1966.

26. Panton, R. L., Incompressible Flow, New York, 1984.

27. Schlichting, H., Boundary-Layer Theory, New York, McGraw-Hill Book Company, Inc., 1960.

28. Bloor, M. S., and J., H., Gerrard, "Measurements on Turbulence Vortices in a Cylinder Wake,"Pro. Soc., London Ser. A, Vol. 294, 1965.

29. Roache, P., Computational Fluid Dynamics, Albuquerque, New Mexico, Hermosa, 1976.

30. Li, C. P., "A Finite Difference Method for Solving Unsteady Viscous Flow Problems," AIAA J., Vol. 23, 1985.

31. Chilukuri, R., "Incompressible Laminar Flow Past a Transversely Vibrating Cylinder," ASME, Vol. 109, 1987.

32. Nagata, H., Hayashi, K. and Kawai, M., "Unsteady Flow Near a Circular Cylinder Oscillated Sinusoidally in Uniform Flow," JSME, Vol. 28, No. 246, 1985.

33. Eaton, B. E., "Analysis of Laminar Vortex Shedding behind a Circular Cylinder by Computer-aided Flow Visualization," J. Fluid Mech., Vol. 180, 1987.

34. Ingham, D., "Note on the Numerical Solution for Unsteady Viscous Flow Past a Circular Cylinder," J. Fluid Mech., Vol. 31, Part 4, 1968.

35. Lin, C. L., Pepper, D. W. and Lee, S. C., "Numerical Methods for Separated Flow Solutions Around a Circular Cylinder," AIAA J., Vol. 14, No. 7, 1977.

36. Hurlbut, S. E., M. L. Spaulding and F. M. White, "Numerical Solution for Laminar Two Dimensional Flow about a Cylinder Oscillating in a Uniform Stream," Transaction of the ASME, Vol. 104, 1982.

37. Jordan, S. K. and J. E. Fromm, "Oscillatory Drag, Lift, and Torque on a Circular Cylinder in a Uniform Flow," The Physics of Fluids, Vol. 15, No. 3, 1972.

38. Griffin, O. M., "Vibrations and Flow-Induced Forces Caused by Vortex Shedding," Symposium on Flow-Induced Vibrations, New Orleans, 1984.

39. Abramowitz, M. and I. A. Stegun, Handbook of Mathematical Functions with Formulars, Graphs, and Mathematical Tables, National Bureau of Standard Applied Mathematics Series 55, 1965.

40. Holt, M., Numerical Methods in Fluid Dynamics, Springer-Verlag Berlin Heidelberg, New York, 1977.

41. Chou, L. C., "On Numerical Studies of Time-Dependent Navier-Stokes Equations," Ph.D. dissertation, University of Tennessee, Knoxville, 1972.

42. Young, D. M., "The Numerical Solution of Elliptic and Parabolic Partial Differential Equations", Survey of Numerical Analysis, New York: Mcgraw-Hill Book Company, Inc., 1962.

43. Varga, R. S., "Matrix Iteration Analysis", Englewood Cliffs, New Jersey: Prentice-Hall, Inc., 1962.

44. Collins, W. and Dennis, G., "The Initial Flow Past an Impulsively Started Circular Cylinder," Quart. Journ. Mech. and Applied Math., Vol. XXVI, Pt. 1, 1973.

45. Prandtl, L., Essential of Fluid Dynamics, New York, Hafner Pub. Co., 1952.

46. Bearman, P. W., "Vortex Shedding From Oscillating Bluff Bodies," Ann. Rev. Fluid Mech., pp. 195–222, 1984.

47. Deffenbaugh, F. D. and Marshall, F. J., "Time Development of the Flow about an Impulsively Started Cylinder", AIAA Journal, Vol. 14, No.7, 1977.

48. Bouard, R. and Coutanceau, M., "The Early Stage of Development of the Wake behind an Impulsively Started Cylinder for $40 < Re < 10^4$", J. Fluid Mech., Vol. 101, Part 3, 1980.

49. Loc, T. P., "Numerical analysis of Unsteady Secondary Vortices Generated by an Impulsively Started Circular Cylinder", J. Fluid Mech., Vol. 100, Part 1, 1980.

50. Coutanceau, M. and Bouard, R., "Experimental Determination of the Main Features of the Viscous Flow in the Wake of a Circular Cylinder in Uniform Translation", Part 1, Steady flow, J. Fluid Mech., Vol. 79, 1977.

51. Coutanceau, M. and Bouard, R., "Experimental Determination of the Main Features of the Viscous Flow in the Wake of a Circular Cylinder in Uniform Translation," Part 2, Unsteady flow, J. Fluid Mech., Vol. 79, 1977.

52. Cantwell, B. and Coles, D., "An Experimental Study of entrainment and Transport in the Turbulent near Wake of Circular Cylinder," J. Fluid Mech., Vol. 136, 1983.

53. Taneda, S., "Visual Study of Unsteady Separated Flows around Bodies," Progress in Aerospace Sciences 17, 287-348, 1977.

54. Collins, F., "Description of the University of Tennessee Space Institute Water Tunnel," UTSI Report 82-1, 1982.

55. Yu, F. M., "Investigation of Non-symmetric Jets in Cross Flow," Ph.D. dissertation, University of Tennessee, Knoxville, 1986.

56. Kaneko, A. and Honji, H., “Double Structures of Steady Streaming in the Oscillatory Viscous Flow over a Wavy Wall”, J. Fluid Mech. 93, 727, 1979.

57. Lecointe, Y. and Piquet, J., “On the Use of Several Compact Methods for the Study of Unsteady Incompressible Viscous Flow Round a Circular Cylinder”, Computer and Fluids, Vol. 12, No. 4, pp. 225–280, 1984.

58. Spedding, G. R., Rayer, J. and Pennycuick, C. J., “Momentum and Energy in the Wake of a Pigeon in Slow Flight”, J. Exp. Bid, Vol. III, 1984.

59. Kawaguti, M., "Numerical Solutions of the Navier-Stokes Equations for the Flow in a Channel with a step", MRC TSR 574, Mathematics Research Center, Madison, Wisconsin, 1965.

60. Roshko, A., "On the Development of Turbulent Wakes from Vortex streets", NACA Rept., 1191,1954.

61. Wu, J. C. and Chen, H., "Unsteady Aerodynamics of Articulate Lifting Bodies", AIAA Paper 84-2184,1984.

62. Wu, J. C. and Gulcat, U., "Separate Treatment of Attached and Detached Flow Regions in General Viscous Flows", AIAA Paper 79-1451, 1979.

63. Ericsson, L. and Reding, J., “Unsteady Flow Concepts for Dynamic Stall Analysis”, J. Aircraft, Vol. 21, No. 8, 1984.

64. Morton, B. R., "The Generation and Decay of Vorticity", Geophys. Astrophys. Fluid Dynamics, Vol. 28, 1984.

65. Bhattacharjee, S., Scheelke, B. and Troutt, T. R., "Modification of Vortex Interactions in a Reattaching Separated Flow", AIAA Paper 85-0555, 1985.

66. Shaio, F. B., Private Communication, Institute of Aero. and Astronautics, Cheng Kung University, Taiwan, China, Nov. 1988.

APPENDICES

APPENDIX A

VORTICITY AND STREAM FUNCTION EQUATION

One kind of formulation of the Navier-Stokes equations makes use of the vorticity vector $\vec{\omega}$ as the dependent variables

$$\vec{\omega} = \nabla \times \vec{\vec{V}} \tag{$A-1$}$$

which satisfies the following equation:

$$\frac{\partial \vec{\omega}}{\partial t} + (\vec{\vec{v}} \cdot \nabla)\vec{\omega} - (\vec{\omega} \cdot \nabla)\vec{\vec{v}} = \nu \nabla^2 \vec{\omega} \tag{$A-2$}$$

where $\nu = \frac{\mu}{\rho}$. This equation is associated with an equation for a solenoidal stream-function vector $\vec{\psi}$ such that

$$\vec{\vec{v}} = \nabla \times \vec{\psi} \tag{$A-3$}$$

which automatically satisfies the incompressibility condition. The equation satisfied by $\vec{\psi}$ is derived by applying the curl operator to $(A-3)$ and using definition $(A-1)$ to obtain

$$\nabla^2 \vec{\psi} + \vec{\omega} = 0 \tag{$A-4$}$$

In the present work, we mainly treat the two dimensional flow around a cylinder, in which the procedure is not with loss of general properties for three dimensional flow following the above formulation.

For plane flow, the vorticity and stream-function become scalar functions, and $(A-2)$ and $(A-4)$ become the scalar equations.

$$\frac{\partial \omega}{\partial t} + (\vec{\vec{v}} \cdot \nabla)\omega = \nu \nabla^2 \omega, \tag{$A-5$}$$

$$\nabla^2 \psi + \omega = 0. \tag{$A-6$}$$

By choosing the stream-function vorticity formulation, an important feature has been obtained which is that the pressure is no longer explicit in the equations. So the pressure field can be solved separately from the velocity when the aerodynamic forces are interested.

Usually it is more convenient for computation by computer to use $(A-5)$ and $(A-6)$ in its conservation form. Easily by using continuity equation, $(A-5)$ becomes immediately

$$\frac{\partial \omega}{\partial t} + \nabla \cdot (\bar{\vec{v}}\omega) = \nu \nabla^2 \omega \qquad (A-7)$$

To non-dimensionalize the above governing equations, the following reference quantities are taken:

$$\zeta = \frac{R_c \omega}{U_\infty}$$
$$r = \frac{r'}{R_c}$$
$$\vec{v} = \frac{\bar{\vec{v}}}{U_\infty}$$
$$\psi = \frac{\bar{\psi}}{U_\infty R_c}$$
$$t = \bar{t}\frac{R_c}{U_\infty}$$

where R_c is the radius of cylinder, U_∞ is the free stream velocity.

Then the final non-dimensional equations are

$$\frac{\partial \zeta}{\partial \bar{t}} + \nabla \cdot (\vec{v}\zeta) = \frac{2}{Re}\nabla^2 \zeta, \qquad (A-8)$$

$$\nabla^2 \psi - \zeta = 0. \qquad (A-9)$$

where $Re = 2R_c U_\infty / \nu$.

APPENDIX B

SOLUTION OF TRIDIAGONAL ALGEBRA EQUATION

As discussed in chapter III, the discretized algebraic equation can be classified as of two kinds. They are represented in matrix form as follows:

$$\begin{bmatrix} b_1 & c_1 & & & & \\ a_2 & b_2 & c_2 & & & \\ & a_3 & b_3 & c_3 & & \\ & & & \ddots & & \\ & & & & a_L & b_L \end{bmatrix} \begin{bmatrix} x_1 \\ x_2 \\ x_3 \\ \vdots \\ x_L \end{bmatrix} = \begin{bmatrix} d_1 \\ d_2 \\ d_3 \\ \vdots \\ d_L \end{bmatrix} \qquad (B-1)$$

and

$$\begin{bmatrix} b_1 & c_1 & & & & a_1 \\ a_2 & b_2 & c_2 & & & \\ & a_3 & b_3 & c_3 & & \\ & & & \ddots & & \\ c_L & & & & a_L & b_L \end{bmatrix} \begin{bmatrix} x_1 \\ x_2 \\ x_3 \\ \vdots \\ x_L \end{bmatrix} = \begin{bmatrix} d_1 \\ d_2 \\ d_3 \\ \vdots \\ d_L \end{bmatrix} \qquad (B-2)$$

or $AX = D$ in abbreviated form.

To solve the above tridiagonal system of equations, a forward and backward substitution and matrix factorization methods have been used.

for (B-1), first compute

$$\beta_i = b_i - \frac{a_i c_{i-1}}{\beta_{i-1}} \qquad \text{with } \beta_i = b_1$$

and

$$r_i = \frac{d_i - a_1 r_{i-1}}{\beta_i} \qquad \text{with } r_1 = \frac{d_1}{b_1}.$$

The dependent variables x_i are then computed from

$$x_L = r_L$$

and

$$x_i = r_i - \frac{c_i x_{i+1}}{\beta_i} \qquad \text{with } 1 \le i \le L-1.$$

For $(B-2)$, a factorization method is used. Let $A = LU$ and

$$L = \begin{bmatrix} 1 & & & & & \\ \ell_2 & 1 & & & & \\ & \ell_3 & 1 & & & \\ & & \ddots & \ddots & & \\ & & & \ell_{L-1} & 1 & \\ \sigma_1 & \sigma_2 & \cdots & & \ell_L + \sigma_{L-1} & 1 \end{bmatrix}$$

$$U = \begin{bmatrix} \beta_a & c_1 & & & & \rho_1 \\ & \beta_2 & c_2 & & & \rho_2 \\ & & \beta_3 & c_3 & & \rho_3 \\ & & & \ddots & \ddots & \\ & & & & \beta_{L-1} & c_{L-1} + \rho_{L-1} \\ & & & & & \beta_L \end{bmatrix}$$

in which

$$\begin{cases} \beta_1 = b_1, \quad \sigma_1\beta_1 = c_L, \quad \rho_1 = a_1, \quad \delta_1 = d_1 \\ \ell_{i+1} = \frac{a_{i+1}}{\beta_i}, \quad \beta_{i+1} = b_{i+1} - \ell_{i+1}c_i, \quad \sigma_{i+1} = -\frac{c_i\sigma_i}{\beta_{i+1}} \\ \rho_{i+1} = -\ell_{i+1}\rho_i, \delta_{i+1} = d_{i+1} - \ell_{i+1}\delta_i \\ \qquad\qquad (i = 1, 2, \cdots L-2) \\ \ell_L = \frac{a_L}{\beta_{L-1}} \\ \beta_L = b_L - \sum_{i=1}^{L-2} \sigma_i\rho_i - (\ell_L + \sigma_{L-1})(c_{L-1} + \rho_{L-1}) \\ \delta_L = d_L - \sum_{i=1}^{L-2} \sigma_i\delta_i - (\ell_L + \sigma_{L-1})\delta_{L-1} \end{cases}$$

then

$$\begin{cases} \beta_i x_i + c_i x_{i+1} + \rho_i x_L = \delta_i \qquad (i = 1, 2, \cdots L-1) \\ \beta_L x_L = \delta_L \end{cases}$$

VITA

Jia-Da Mo was born Feb. 28, 1962, in Hunan, People's Republic of China. He attended elementary and high school in Hengyang, Hunan. He entered the Beijing Institute of Aeronautics and Astronautics(BIAA)* in October 1978 majoring in Aerospace Engineering with emphasize on aerodynamics. He received his Bachelor degree in 1982 and Master degree in 1984, respectively.

He was selected as the first graduate student from BIAA to enter the UTSI as a Research Assistant in January, 1986 under the established Academic Exchange Agreement between the two institutes. In May 1989, He completed his studies with the Doctor of Philosophy degree in Aerospace Engineering.

* Since 1988, the Institute has formally changed its name as The Beijing University of Aeronautics and Astronautics.